DEVELOPMENT AND PARAMETRIC STUDIES OF PULSED NITROGEN AND Q-SWITCHED Nd:GLASS LASERS AND SOME OF THEIR APPLICATIONS

N. SUBHASH

THESIS SUBMITTED
TO THE UNIVERSITY OF COCHIN
IN PARTIAL FULFILMENT OF THE REQUIREMENTS
FOR THE DEGREE OF
DOCTOR OF PHILOSOPHY

Laser Division, Department of Physics
University of Cochin

1981

D E D I C A T E D T O

M Y P A R E N T S

C E R T I F I C A T E.

Certified that this thesis is the report of the original work carried out by Mr. N. Subhash in the Department of Physics, University of Cochin, under my guidance and supervision and that no part thereof has been included in any other thesis submitted previously for the award of any Degree.

Cochin - 22
August 25, 1981.

Professor K. Sathianandan,
Supervising Teacher.

ACKNOWLEDGEMENTS.

The author has great pleasure in expressing his deep sense of gratitude to Professor K. Sathianandan, Head of the Department of Physics, whose profound interest and able guidance were his inspiration throughout the period of reasearch.

He is extremely grateful to all the members of the Faculty, Library, Laboratory and non teaching staff of the Department of Physics for their kind hearted co-operation during the course of his work.

The author owes his thanks to Mr. P.J. Sebastian, Mrs. Sudha C. Kartha, Mr. P. Radhakrishnan, Mr. K. Mohanachandran, Mr. U. Syama Prasad, Mr. S. Muralidharan Pillai, and Mr. K.P.Vijayakumar of the Department of Physics, for their good wishes and encouragement.

He is very much thankful to Dr. D.D. Bhawalkar and Mr. T.P. N. Nathan, Laser Section, Bhabha Atomic Research Centre, for many valuable discussions and suggestions. He is also thankful to Prof. C. Karunakaran, Director, Centre for Earth Science studies for making it possible for him to complete the work in time. He extends his thanks to all his colleagues in the Atmospheric Sciences Division, especially to Mr. V.N. Neelakantan who has assisted him in the preparation of Computer programs. He also feels grateful to the authorities of the Kerala University Computer Centre for having provided the necessary facilities.

A special note of gratitude goes to the staff of the Central Workshop Instrumentation and Services Laboratory of Cochin University for their assistance in the fabrication work.

Special thanks are due to Mr. M.K.Gopinatha Pillai, for typing the manuscript on a tight schedule. Finally the author takes this opportunity to thank the Indian National Science Academy, Department of Atomic Energy and the University Grants Commission for having awarded research fellowships during the course of his work.

C O N T E N T S.

			Page
CHAPTER I	..	INTRODUCTION	1
CHAPTER II	..	FABRICATION OF A COMPACT PORTABLE NITROGEN LASER	5
2.1	..	Introduction	5
2.2	..	Theoretical considerations for laser action.	7
2.21	..	Conditions for population inversion.	9
2.3	..	Electrical characteristics of Nitrogen Laser.	11
2.4	..	Details of laser fabrication.	13
2.41	..	Laser tube.	15
2.42	..	Gas Flow.	17
2.43	..	Spark gap.	19
2.44	..	Transmission lines as energy storage capacitors.	20
2.45	..	High voltage power supply.	21
2.46	..	E.M.Shielding of the laser.	23
2.5	..	Operation of the laser.	23
CHAPTER III	..	PARAMETRIC STUDIES OF NITROGEN LASER	26
3.1	..	Introduction.	26
3.2	..	Blumlein Circuit and E/P requirements.	27
3.3	..	Fabrication details of pulse forming networks.	29

			Page
3.4	..	Measurement of pulse width	29
3.5	..	Measurement of pulse energy and peak power output.	34
3.6	..	Variation of output energy with pressure.	34
3.7	..	Variation of maximum output peak power with square of voltage.	40
3.8	..	Variation of output peak power with voltage.	43
3.9	..	Variation of laser power with repetition rate.	43
3.10	..	Laser beam size and divergence.	43
3.11	..	Results and discussion.	46
CHAPTER IV	..	IDENTIFICATION OF NEW VIBRATIONAL BANDS IN THE NITROGEN LASER EMISSION SPECTRA.	48
4.1	..	Introduction.	48
4.2	..	Identification of vibrational bands.	49
4.3	..	Intensity variation of emission bands with pressure and voltage.	54
4.4	..	Results and discussion.	55
CHAPTER V	..	FABRICATION AND PARAMETRIC STUDIES OF PULSED, ELECTRO-OPTICALLY Q-SWITCHED AND DYE Q-SWITCHED Nd: GLASS LASERS.	67

		Page
5.1 ..	Introduction.	67
5.2 ..	Lasing considerations and selection of laser rod.	70
5.3 ..	Conventional mode glass laser oscillator.	74
5.31 ..	Pumping chamber.	74
5.32 ..	Laser support structure and mirror mounts.	80
5.33 ..	Flashlamp drive circuits.	81
5.4 ..	Alignment of the laser cavity.	89
5.5 ..	Performance evaluation.	89
5.51 ..	Estimation of the optical losses and pumping coefficient.	91
5.52 ..	Measurement of divergence.	95
5.6 ..	Electro-optically (E-O) Q-switched laser.	95
5.61 ..	Design of the E-O Q-switch.	100
5.62 ..	Measurement of the halfwave voltage and extinction ratio.	100
5.63 ..	Q-switching circuit.	102
5.64 ..	Rate generator and delay circuit.	106
5.65 ..	Alignment of the Q-switch inside the cavity.	109
5.66 ..	Optimisation of Q-switch delay and bias voltage.	110
5.67 ..	Measurement of output energy and pulse width.	110

Page.

5.7 .. Dye Q-switched Glass laser. 113

5.71 .. Design of a simple dye Q-switch. 115

5.72 .. Optimisation of Q-switch performance 115

5.8 .. Results. 119

CHAPTER VI .. THERMAL LENS EFFECT IN LSG 91H SILICATE LASER ROD PUMPED IN A DOUBLE CIRCULAR CAVITY. 124

6.1 .. Introduction. 124

6.2 .. Theory. 126

6.21 .. Thermally induced focal length. 126

6.22 .. The thermal time constant. 130

6.3 .. Experiment. 130

6.4 .. Results and Discussion. 134

CHAPTER VII .. LASER-INDUCED DAMAGE TO TRANSPARENT CONDUCTING SnO_2 FILMS AT 1062 nm. 142

7.1 .. Introduction. 142

7.2 .. Method of preparation of SnO_2 films. 146

7.3 .. Measurement of refractive index, thickness, transmittance and resistivity of the thin films. 147

7.4 .. Measurement of damage threshold. 149

7.5 .. Results and Discussions. 153

CHAPTER VIII .. CONCLUSIONS. 159

Page

APPENDIX A .. Computer program for the determination of rod focal length. 163

APPENDIX B .. Computer program for the determination of W_D in the single shot mode. 167

ILLUSTRATIONS.

		Page
Fig. 2.1	Potential energy diagram of the nitrogen molecule.	8
Fig. 2.2	The Blumlein discharge circuit.	8
Fig. 2.3	Nitrogen laser assembly.	12
Fig. 2.4	Voltage waveform across the cavity and laser output.	12
Fig. 2.5A	Double Blumlein Nitrogen laser system.	14
Fig. 2.5B	Laser cavity and transmission lines.	14
Fig. 2.6	Laser tube assembly.	16
Fig. 2.7A	Spark gap with perspex/Aluminium walls.	16
Fig. 2.7B	Spark gap with O-ring seals and Nylon/Aluminium walls.	16
Fig. 2.8	20 kV, 50 mA, DC Power supply.	22
Fig. 3.1	Photodiode circuit.	32
Fig. 3.2	Nitrogen laser pulse shapes at 70 torr N_2.	33
Fig. 3.3	Variation of pulse width with pressure for double Blumlein circuit laser.	32
Fig. 3.4A	Output energy/pulse and peak power variation with pressure for single Blumlein circuit	35
Fig. 3.4B	Output energy/pulse and peak power variation with pressure for double Blumlein circuit.	36
Fig. 3.4C	Output energy/pulse and peak power variation with pressure for double non-Blumlein circuit.	37
Fig. 3.5	Output peak power variation with square of charging voltage at optimum pressure (E/P value)	41

Page

Fig. 3.6A Output peak power dependence on charging voltage for single Blumlein circuit 41

Fig. 3.6B Output peak power dependence on charging voltage for double Blumlein circuit. 42

Fig. 3.6C Output peak power dependence on charging voltage for double non-Blumlein circuit. 42

Fig. 3.7A Variation of output intensity with repetition rate for double Blumlein circuit. 44

Fig. 3.7B Variation of output intensity with repetition rate for double non-Blumlein circuit. 44

Fig. 3.8 Output pulse energy dependence on repetition rate. 45

Fig. 4.1 Experimental setup for recording N_2 laser emission spectra. 50

Fig. 4.2 Record of the laser emission spectra. 52

Fig. 4.3 Slow speed scan of the 331.03 nm band. 52

Fig. 4.4 Record of the variation in intensity of the laser spectra with pressure at 12 kV. 52

Fig. 4.5A Intensity variation of 337.13 nm band with pressure. 56

Fig. 4.5B Intensity variation of 331.83 nm band with pressure. 56

Fig. 4.5C Intensity variation of 340.85 nm band with pressure. 57

Fig. 4.5D Intensity variation of 357.69 nm band with pressure. 57

Fig. 4.5E Intensity variation of 303.49 nm band with pressure. 58

Fig. 4.5F Intensity variation of 371.05 nm band with pressure. 58

Fig. 4.5G Intensity variation of 315.93 nm band with pressure. 59

Page

Fig. 4.6A Relative intensity variation of other prominent N_2 bands with pressure at 10 kV. 63

Fig. 4.6B Relative intensity variation of other prominent N_2 bands with pressure at 12 kV. 64

Fig. 5.1 Partial energy level diagram of Nd^{3+} in glass. 71

Fig. 5.2A Conventional pulsed glass laser layout. 71

Fig. 5.2B Conventional mode glass laser with double circular pumping chamber. 75

Fig. 5.2C Glass laser system control panel. 75

Fig. 5.3A Cross sectional view of the elliptical cylindrical pumping chamber. 77

Fig. 5.3B Laser rod holder assembly. 77

Fig. 5.4A Cross sectional view of the double circular close-coupled pumping chamber. 77

Fig. 5.4B Double circular chamber with the flashlamps and laser rod mounted. 75

Fig. 5.5 Mirror mount. 77

Fig. 5.6 Single flashlamp drive circuit along with trigger circuit. 82

Fig. 5.7 Double flashlamp drive circuit. 82

Fig. 5.8 Single flashlamp circuit output pulse shape. 88

Fig. 5.9 Double flashlamp circuit output pulse shape. 88

Fig. 5.10 Laser alignment setup. 90

Fig. 5.11 Output energy and pulse width measurement setup. 90

Page

Fig. 5.12A Conventional mode laser output structure when pumped using a single flashlamp. 92

Fig. 5.12B Conventional mode laser output structure when pumped using two flashlamps. 92

Fig. 5.13 Laser output energy variation with input energy for the elliptical cylindrical pump system. 93

Fig. 5.14 Laser pulse width (at base) variation with input energy for the elliptical cylindrical pump system. 93

Fig. 5.15 Laser output energy variation with input energy for the double circular pump system. 94

Fig. 5.16 Laser output pulse width (at base) variation with input energy for the double circular pump system. 94

Fig. 5.17 Small signal, single pass gain and gain coefficient as a function of input energy. 97

Fig. 5.18 E-O Q-switched Glass laser. 98

Fig. 5.19 E-O Q-switch assembly. 101

Fig. 5.20 Setup for the measurement of extinction ratio and half wave voltage. 101

Fig. 5.21 Modulator extinction ratio variation with bias voltage. 103

Fig. 5.22 Modulator transmittance versus bias voltage. 103

Fig. 5.23 Q-switch drive circuit. 105

Fig. 5.24 Spark gap assembly. 105

Page

Fig. 5.25 Rate generator and delay circuit. 107

Fig. 5.26 Output energy variation with Q-switching delay. 111

Fig. 5.27 Output energy variation with Q-switching voltage. 111

Fig. 5.28 Flashlamp input energy versus output energy. 112

Fig. 5.29 E-O Q-switched Glass laser output. 114

Fig. 5.30 E-O Q-switched laser pulse recorded at reduced sweep speed. 114

Fig. 5.31 Dye Q-switched laser - Optical layout. 112

Fig. 5.32 Dye Q-switched Glass Laser. 98

Fig. 5.33 Dye Q-switch - exploded view. 112

Fig. 5.34 Q-switched output energy versus lamp input for different dye transmissions. 117

Fig. 5.35A-C Dye Q-switched output pulses. 118

Fig. 6.1 Thermal transient measuring setup. 127

Fig. 6.2 Experimental setup for studying thermal effects. 131

Fig. 6.3 Pin hole locations on the laser rod cross section. 127

Figs.6.3A-I Probe beam intensity variation in the single shot mode. 131 - 133

Fig. 6.4A Induced focal length variation with time. 127

Fig. 6.4B Induced focal length variation with time. 136

Fig. 6.5 Intensity profile of the probe beam for different input energies. 138

Fig. 6.6 Induced focal length versus input energy under repetitively pulsed condition. 139

		Page
Fig. 6.7	Prism effect dependence on input energy.	139
Fig. 6.8	Lasing test results.	133
Fig. 7.1	Optical method for measuring R_s and R_p values.	148
Fig. 7.2	Schematic of the damage threshold energy measurement setup.	148
Fig. 7.3	Experimental setup for laser-induced damage threshold energy measurement.	151
Fig. 7.4	Damaged sites.	151

TABLES

		Page
Table 3.1	Nitrogen laser characteristics.	30
Table 3.2	Nitrogen laser discharge parameters.	39
Table 4.1A	Nitrogen laser spectra assignments.	61
Table 4.1B	Nitrogen laser spectra assignments.	62
Table 5.1	Lasing properties : Silicate laser glass LSG - 91H.	73
Table 5.2A	Optimisation of flashlamp discharge circuit parameters.	84
Table 5.2B	Optimisation of flashlamp discharge circuit parameters.	85
Table 5.3	Pumping coefficients and resonator losses.	96
Table 7.1	Threshold energy determination.	154
Table 7.2	Results of the present and previous work.	155

CHAPTER I

INTRODUCTION.

Lasers are very commonly used as a scientific tool in almost every branch of Physics, Chemistry, Engineering and Medical Science. Nitrogen Lasers are used as a high power pulsed ultra-violet source for a wide variety of applications like dye laser pumping, flash photolysis experiments, fluroescence studies, pollution detection and medicine. Nd: Glass lasers find application in material processing, study of non-linear effects, resonance phenomena, thermonuclear fusion, plasma experiments, interferometry, holography, range-finding and in general for scientific research requiring high power densities.

Laser engineering is an area in which developments in the existing design concepts and technology appear at an alarming rate. Now-a-days, emphasis has shifted from innovation to cost reduction and system improvement. To a major extent, these studies are aimed at attaining larger power densities, higher system efficiency and identification of new lasing media and new lasing wavelengths. Todate researchers have put to use all the different forms of matter as lasing material. Laser action was observed for the first time in a gaseous system - the He-Ne system. This was followed by a variety of solid-state and gas laser systems. Various organic dyes dissolved in suitable solvents were found to lase when pumped optically. Broad band emission characteristics of these dye molecules made wavelength tuning possible using optical devices. Laser action was also observed in certain p-n junctions of semiconductor materials and some of these

systems are also tunable. The recent addition to this list was the observation of laser action from certain laser produced plasmas.

The purpose of this investigation was to examine the design and fabrication techniques of pulsed Nitrogen lasers and high power Nd: Glass lasers. Attempt was also made to put the systems developed into certain related experiments.

In order to attain higher power levels and to make a laser system achieve more efficiency, improvements in the existing design and engineering concepts are essential. This can only be achieved through a basic understanding of the lasing phenomenon and system considerations. Taking these factors into consideration a transversely excited portable Nitrogen laser was designed and built. The electrical and optical characteristics of this laser was studied with a view to improve the system efficiency.

Until recently, only a few investigations were carried out to analyse the various other bands that may be present in the Nitrogen laser emission spectra. This type of study is equally promising and useful as the search for new laser media. A similar study was attempted and many new transitions hitherto unreported have been identified. The importance of this type of investigation may be understood from the fact that the newly identified lines can fill up the need for coherent sources at these wavelengths because one can enhance the emission intensity of these lines by providing suitable discharge and amplification conditions.

Solid-state lasers are a different class of lasers and their design concepts and fabrication technology are quite different from that of gas laser systems. The prime purpose of this study was to develop a Nd: Glass laser system which is good enough for usual laboratory use and which can be operated reliably and with high efficiency in the conventional pulsed and Q-switched modes. System flexibility and the possibilities for further modification and expansion were considered when the laser was designed and built. The lasing characteristics were studied to evaluate the system performance in conventional pulsed, E-O Q-switched and Dye Q-switched modes.

For reproducible operation of any solid-state laser system, it is imperative to know the thermal time constant of the rod and to adjust the frequency of pumping so that the time interval between successive pump pulses is slightly greater than the thermal time constant of the laser rod. An attempt was made to measure this thermal time constant and the associated lens effect of Hoya LSG 91H Silicate laser glass pumped in a double circular cavity in the single shot and repetitively pulsed modes by passing a He-Ne laser probe beam through the rod and observing the probe beam behaviour during and after the flashlamp pulse.

In large apperture Pockel cells of high power laser amplifiers and in the E-O modulators of oscillators and pulse shapers of laser systems transparent conducting films are used as electrodes to attain better field uniformity and to facilitate the use of thin E-O crystals. Usually, RF sputter deposited films which have low absorption losses

are used in these shutters. As these films are not always within the reach of a laser technologist who builds his own E-O modulators, simple Chemical Vapour Deposited conducting films can come in handy, at times. But no data on the laser damage thresholds of these films are available. This is one of the factors for these films not finding application in E-O modulators, the other being the relatively high absorption losses. To make some headway in this regard, transparent conducting SnO_2 films prepared by Chemical Vapour Deposition technique were damage tested at 1062 nm using 15 ns laser pulses. The tests conducted goes on to prove that these SnO_2 films can become strong contenders for sputter deposited films in low cost E-O modulators.

CHAPTER II.

FABRICATION OF A COMPACT PORTABLE NITROGEN LASER.

2.1 INTRODUCTION.

The Nitrogen Laser which operates at 337.1 nm was first developed by Heard[1] in 1963. The spectral line at 337.1 nm corresponds to the superradiant transition $C^3\Pi_u$ to $B^3\Pi_g$ in the second positive system of nitrogen molecule and this line readily lases in the pressure range 30-100 Torr in an electrical discharge.

Since Heard's experiment a large number of variations in design have been reported[2-11] for improving the output power and conversion efficiency. Conventional longitudinal excitation was used in the earlier experiments. Later, Leonard[2] and Gerry[3] utilised transverse excitation of the gas resulting in very high output powers. This was due to the large electric field to pressure (E/P) values possible in such systems. Gerry developed a theorectical model for this laser and explained that the excitation mechanism is due to direct electron impact of the triplet states $C^3\Pi_u$ and $B^3\Pi_g$. Later, a more efficient system was built by Shipman[4]. He maintained a travelling wave excitation inside the gas. Here, the discharge strikes at one end of the channel and propagates towards the other end with the velocity of light. His system consisted of a flat plate transmission line connected to six dielectric switches by co-axil cable delay lines which initiate a travelling wave discharge. This laser gave a peak output power of 2.5 MW. Using a thinner dielectric material for the transmission line Goller et al.[5] obtained a peak power of

2.8 MW with a similar design.

The next important modification in design was made by Basting et al[6]. in 1972. They used a single spark gap instead of multiple spark gaps and thus eliminated the jitter inherent in the multiple spark gap arrangements. Moreover, they used a double parallel plate transmission line which gave half the impedance of a single line. When operated at 20kV , they obtained a peak power of 1.2 MW in pulses of duration 4 ns FWHM (full width at half intensity maximum) for an active discharge length of 30 cm. A very simple N_2 laser was built by Small and Ashari[7] in 1972 which gave 20kW peak power at 20kV charging potential. For the first time, in 1974, a pre-ionization technique was used by Levatter and Lin[8] in a set up similar to the one used by Basting et al.

Many new versions were developed to make the laser a compact and efficient laboratory tool. Schwab and Hollinger[9] used rolled up transmission lines using Mylar sheets and enclosed the whole assembly in a metal cabinet. At 12 kV this laser gave 1.2 MW peak power. Discrete ceramic capacitors were used by Nagata and Kimura[10] and Sam[11] as the storage element and obtained 1 MW in a 7 ns pulse for a cavity length of 50 cm and 170 kW in a 5.5 ns pulse for a cavity length of 15 cm for their respective systems.

Many Transversely Excited Atmospheric (TEA) Nitrogen lasers have been reported by Bergmann,[12,13] Hasson et al[14]., Herden[15], Patel[16] and Cubeddu et al[17]. with pulse widths in the nanosecond and sub-nanosecond regimes and output peak powers of a few MW's. Recently, ultraminiature TEA lasers have been built by Hasson et al[18]. and a

sealed off miniature TEA laser giving 150 kW in 0.3 to 1 ns pulses was developed by Von Bergmann[19]. Also of importance was the emergence of a TEA laser[20] which operates with gases like N_2, XeF, F & Ar, HF, CO, CO_2 and N_2O giving outputs in the UV, visible and IR. With nitrogen, the above laser gave 0.5 MW peak power.

Intense electron beams have been used [21-24] in recent years for the excitation of N_2 gas. Inert gases like argon which helps in excitation energy transfer were tried as additives to N_2 gas. With electron beam pumping energies upto 250 mJ have been obtained.[25]

2.2 THEORETICAL CONSIDERATIONS FOR LASER ACTION.

Necessitated by the need for understanding the short pulse widths, high power outputs and E/P requirements, the basic mechanism of laser action in nitrogen molecule was studied extensively by many workers[1-4]. The study of the spectral composition[26-29] of the laser output has identified a large number of rotational lines present in the various vibrational bands of the nitrogen molecule. The most noteworthy in this direction being the recent high resolution spectroscopic analysis by Petit et al.[29]

The potential energy diagram of the nitrogen molecule is shown in Fig. 2.1. $C^3\Pi_u \rightarrow B^3\Pi_g$ is the second positive system and $B^3\Pi_g \rightarrow A^3\Sigma_u^+$ is the first positive system. The first positive system consists of various bands from 0.745 μm to 1.235 μm. In the second positive system (0-0)337.1 nm, (0-1)357.7 nm, (0-2)380.5 nm and (1-0)315.9 nm vibrational bands are observed along with other bands of lesser intensity. Among the various bands, the (0-0) band

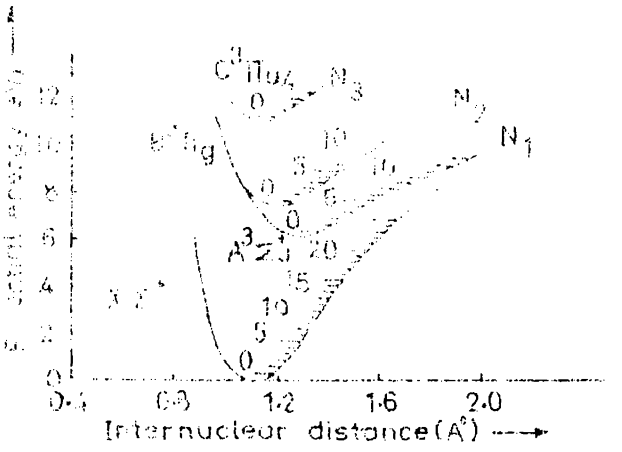

FIG. 2.1 POTENTIAL ENERGY DIAGRAM OF THE NITROGEN MOLECULE

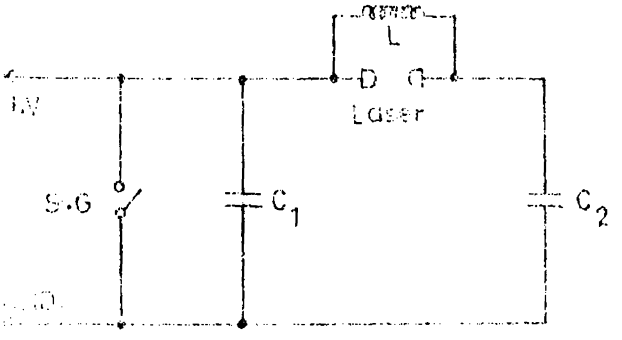

.2 THE CIRCUIT DIAGRAM

is the most intense one and it can easily be obtained in an electrical discharge in nitrogen.

2.21 CONDITIONS FOR POPULATION INVERSION.

For laser action one usually requires a metastable upper level and a fast decaying lower level. The radiative lifetime of C-state is 40 ns, that of B-state is 5-8 ns and that of A-state is 1-2 sec. Hence, a continuous laser action between C and B states is impossible in a nitrogen molecule. But if we can pump the C-level in a time less than its lifetime, a transient population inversion and pulsed laser action is possible. The rate equations for the three levels can be written as

$$\frac{dN_3}{dt} = X_{13}\, N_1 + X_{23}\, N_2 - (Y_{31} + Y_{32} + T_{31}^{-1} + T_{32}^{-1})\, N_3 - R_{32}\, i(N_3 - g_3\, N_2/g_2) \qquad : 2.1$$

$$\frac{dN_2}{dt} = X_{12}\, N_1 + (T_{32}^{-1} + Y_{32})N_3 - (T_{21}^{-1} + Y_{21} + X_{23})N_2 - R_{32}\, i(N_3 - g_3\, N_2/g_2) \qquad : 2.2$$

$$\frac{dN_1}{dt} = -(X_{12} + X_{13})\, N_1 + (T_{21}^{-1} + Y_{21})\, N_2 + (T_{31}^{-1} + Y_{31})\, N_3 \qquad : 2.3$$

where N_1, N_2 and N_3 are the population densities of $X^1\Sigma_g^+$, $B^3\Pi_g$ and $C^3\Pi_u$ states,

X_{ij} is the collisional excitation rates with electrons from level i to j ($i < j$),

Y_{ji} is the collisional de-excitation rate from j to i,

T_{ji} is the radiative lifetime for the transitions from j to i,

$R_{ji}i$ is the induced emission rate and

g_3 and g_2 are the statistical weights of the upper and lower levels respectively.

Using the above equations with certain approximations, Godard[30] has shown that for constant pumping rates with $N_3 \gg N_2$, the population inversion can exist only for a time,

$$t < \frac{1}{(Y_{32} + T_{32}^{-1})} \qquad -- \quad 2.4$$

From 2.4 it is clear that if we neglect Y_{32} inversion can exist only for about 40 ns. But for an electron density $Ne > 6 \times 10^{14} cm^{-3}$, $Y_{32} > T_{32}^{-1}$ and hence, the inversion time is still reduced. So in the actual case, the population inversion can last only for about 10-20 ns. This necessitates the requirement of a very fast method of exciting nitrogen molecules because inversion will cease to exist after 10-20 ns.

The Franck - Condon factors[31] for the C^3 (v=0) and B^3(v=0) states are 0.55 and 0.06 respectively. These factors govern the relative excitation rates to these states as well as their relative optical transition probabilities. The fact that the Franck - Condon factor between X^1(v=0) and C^3(v=0) is about 10 times greater than that between X^1 (v=0) and B^3(v=0) states is perhaps the basic reason why N_2 is a laser at all.

Another important parameter that govern the excitation of $C^3\Pi_u$ state is the electron temparature. The ionization and excitation of the gas is almost entirely due to collisions with electrons in the discharge. It is not due to any molecular collisions or ion recombinations, because of the very fast (few to 10 ns) nature of the electrical as well as the optical properties of the laser.

2.3 ELECTRICAL CHARACTERISTICS OF NITROGEN LASER.

The engineering of high peak power Nitrogen lasers center principally on the problem of achieving excitation of the gas in a few tens of nanoseconds. This dictates the use of very low impedance pulse circuits. In transversely excited N_2 lasers, the direction of electrical discharge is perpendicular to the laser axis. The main advantage of transverse excitation is that with moderate voltage, it is possible to operate at higher gas pressures, resulting in higher gain, uniform discharge and high output power. Usually, nitrogen gas flowing through the laser tube is excited by a Blumlein Circuit[32] as shown in Fig.2.2. The pulse forming network consists of two parallel plate transmission lines located at both sides of the laser tube as shown in Fig. 2.3 and charged to a high voltage by a D.C. power supply. When one of the transmission lines is short circuited at its end by a spark gap, a transient voltage occurs across the laser cavity, creating a powerful discharge between the electrodes. It is assumed that after the spark gap is fired a travelling wave occurs in the transmission line adjacent to it and this initiates the gas discharge and generates a second travelling wave in the transmission line on the other side of the channel. The superposition of these two travelling waves develops a complex voltage wave from across the electrodes that sustains the discharge.

Schwab and Hollinger[9] have used a 100 MHz Kerr - cell measuring system for studying the voltage variation across the laser electrodes. The time evolution of the voltage across the channel and the corresponding laser emission are shown in Fig. 2.4. This very low rates

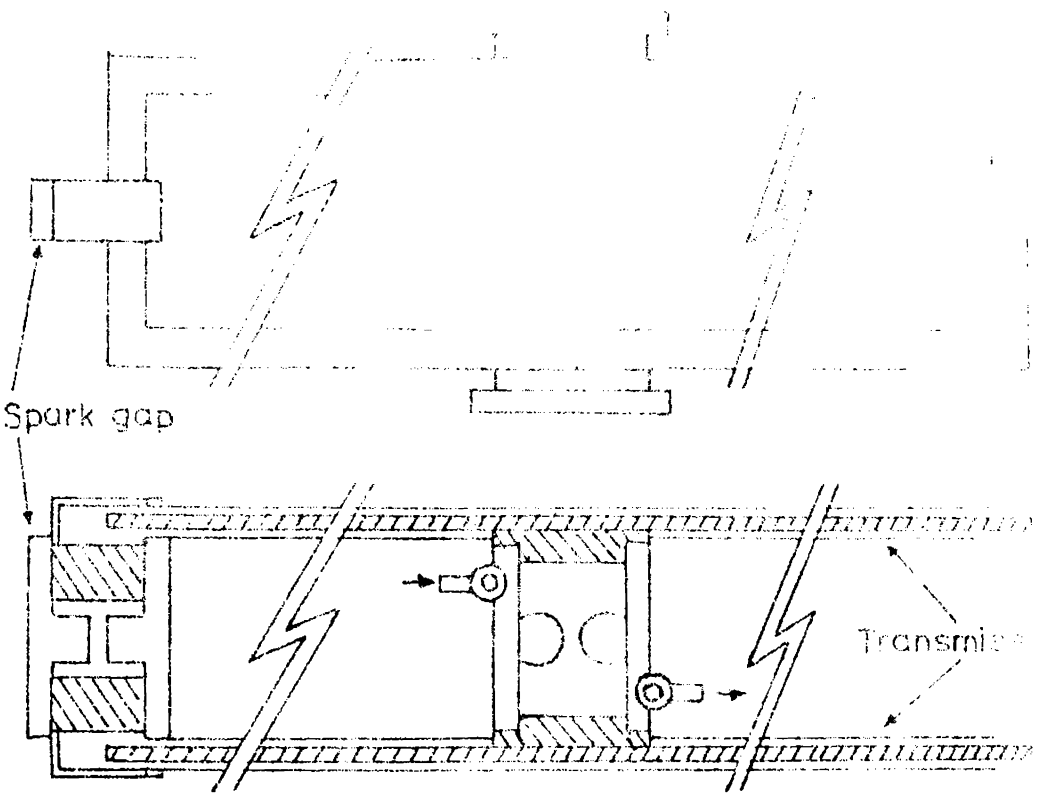
Spark gap

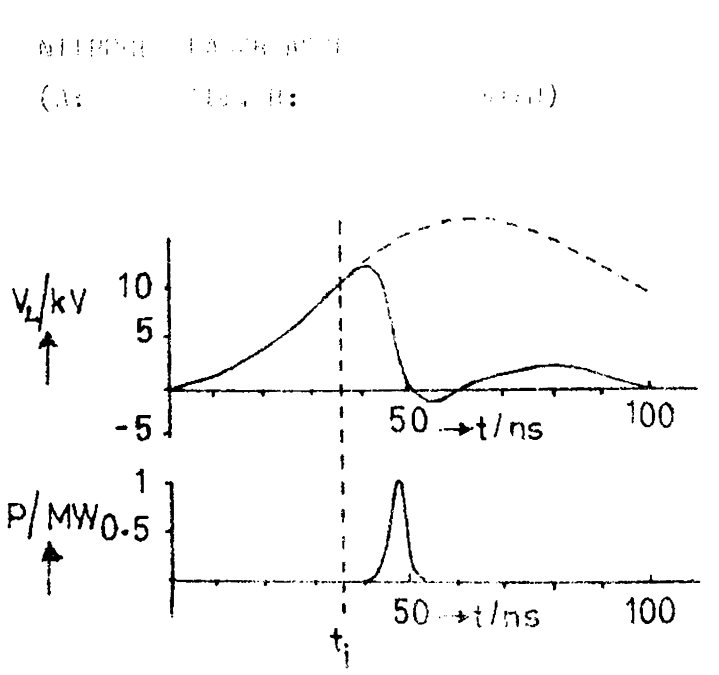
V_L/kV
10
5
-5
50
t/ns
100
P/MW
1
0.5
50
t/ns
100
t_i

of voltage variation can be attributed to the large inductance associated with the spark gap and is given by $T = L/Z$, where Z is the characteristic impedance of the line. Hence, to obtain a rise-time of 2 ns with $Z = 0.316$, L should be less than 0.4 nH, a value unrealizable using a single spark gap. So it is the circuit inductance that is responsible for the observed large time constants. For low impedance Blumlien generators used with N_2 lasers, the propagation time on the transmission line is of the order of 5 to 15 ns/meter. Hence, considering risetimes of about 25 ns inherent to many reported N_2 lasers, the travelling wave concept is no more valid. Enhancement in output power reported for such systems is not due to the time match between the laser light and the tapered arrival of the voltage at the electrode, but must rather be explained by the different impedances between the short circuit and the particular starting points of the discharge. In order to attain high output powers and lesser power variation from pulse to pulse, it is advantageous to have the discharge start at the rear end of the channel. This goal can very well be achieved by using a tapered electrode gap, as in the present design.

2.4 DETAILS OF LASER FABRICATION.

The double Blumlein Nitrogen laser fabricated is shown in Fig. 2.5A. The laser cavity is located at the centre of the two transmission lines which are arranged one above and the other below the cavity as in Fig. 2.5B. The spark gap is soldered on to one side of the transmission lines. A detailed description of the various constituents is given below.

FIG. 2.5A DOUBLE BLUMLEIN NITROGEN LASER SYSTEM

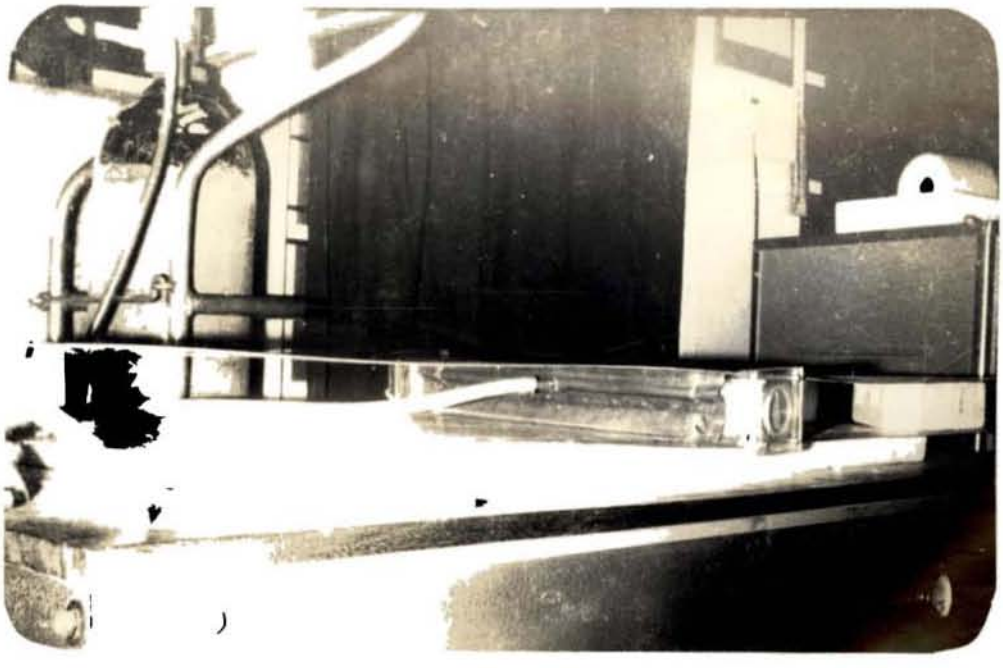

FIG. 2.5B LASER CAVITY AND TRANSMISSION LINES

2.41 LASER TUBE.

The major engineering considerations[33] in the design of the laser tube is that the materials used for it should withstand the deleterious effects of heating, UV radiation, high voltage, and high peak current discharge while maintaining vacuum tightness. The discharge channels for pulsed Nitrogen lasers fall into two distinct design classes. Channels in which the electrical discharge is tightly confined between the closely spaced side walls (about 1.3 mm apart). Such systems are capable of low to moderate output powers, typically, 50 KW at 100 pps (pulses/sec) with very low nitrogen flow rates. Channels in which the discharge is not confined by the side walls are capable of high output powers. Due to the long diffusion time to the walls, thermal energy and long lived excited states are removed slowly from the active region. Peak power, therefore, begins to drop off at repetition rates of 20 to 30 pps , with moderate nitrogen flow rates. It should be understood that slightly higher inductances can appreciably reduce the rate of current variation, thereby favouring arc formation and output degradation. So in order to reduce the inductance of the laser tube, it is advisable to have the insulating walls kept sufficiently close - but not too close to reduce the electrical power loading capability of the tube.

The laser tube, shown in Fig. 2.6, is constructed of brass plates separated by Perspex walls. The tube is held together by screws threaded into the Perspex and sealed vacuum tight with teflon tape and a suitable adhesive (Araldite). The laser tube has inner dimensions of length 50 cm, width 3 cm and height 4 cm. The electrodes are machined from aluminium

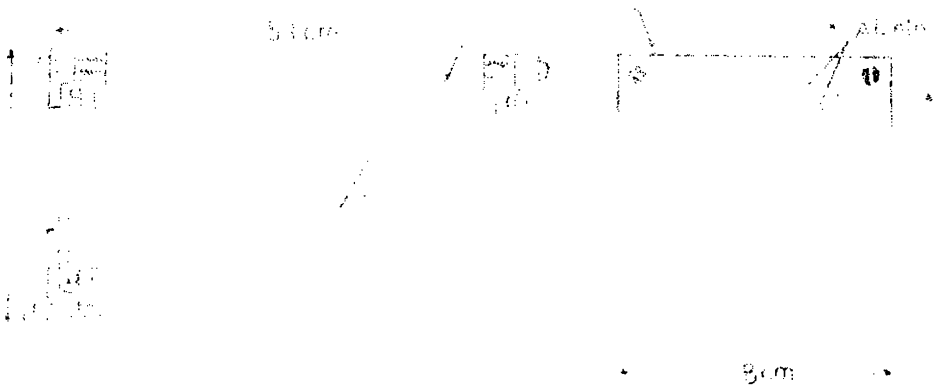

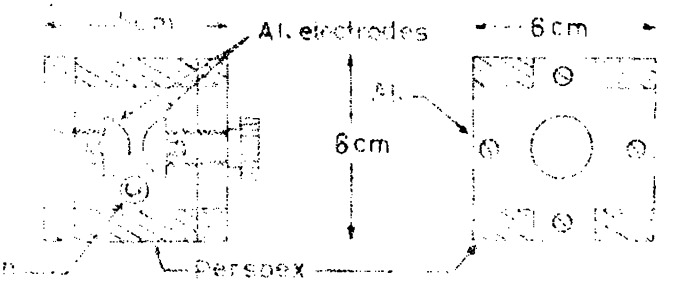
Al. electrodes
6cm
6cm
Al.
Persdex

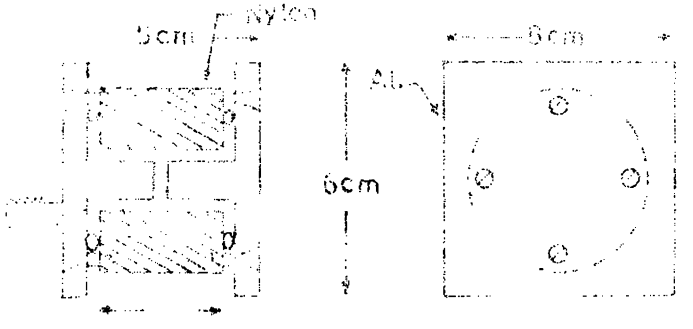
Nylon
6cm
6cm
Al.

rods of $\frac{1}{2}$ inch dia. to the shape shown in Fig. 2.6, and are screwed on to the brass plates from beneath. The electrodes have a length of 40 cm and the separation between them is 10.5 mm at the rear side and 11.5 mm at the front side. This tapering of the electrode gap was found to be good enough to make the electrical discharge start from the rear end of the channel. The electrodes were finely polished and buffed before they were fitted inside the channel. The field uniformity thus attained helped to prevent arcing and confined the discharge to a region between the electrodes, completely away from the walls, depending on the operating pressure.

A 90 % reflecting aluminium coated mirror and a quartz window, both 6 cm dia. and having a surface accuracy better than $\lambda/5$ at 632.8 nm are sealed with O-rings, one at each end of the laser tube. It is important that both the window and the mirror be aligned parallel to one another and perpendicular to the lasing axis. The alignment is done with a He-Ne laser beam by slightly varying the compression on the O-rings. Final alignment is done when the laser is in operation. The laser tube of the type shown in Fig. 2.6 has given satisfactory performance for many hours of operation at repetition rates in the range 1 - 50 Hz.

2.42 GAS FLOW.

Very great importance has to be given to the gas flow system when a Nitrogen laser is designed for operation at high repetition rates. The residual ionization of the previous discharge has to be uniformly distributed with proper density throughout the discharge volume so as to act as seeds for the next discharge.

Too few ions in the cavity will increase the breakdown voltage while too many ions will reduce it. The best discharge condition can be achieved by flowing the gas in a direction transverse to the optical axis as shown in Fig. 2.5B and 2.6.

In the present design N_2 gas is flown in and taken out through two 38 cm long brass tubes, fitted on to the grooves milled on brass side plates by brazing. The ends of these tubes are closed to prevent the gas from leaking out and each tube is provided with an inlet/outlet for flowing the gas. For maintaining a uniform transverse gas flow 9 - 10 holes are drilled from the other side of the brass plates in such a way that they do not face each other when fitted into the cavity. As can be seen from Fig. 2.6, the gas manifold on one side of the cavity is above the electrode while that on the other side is below the electrode.

Commercial purity N_2 gas enters the gas manifold via a needle valve from a nitrogen cylinder and is pumped out of the cavity by a 200 litres per minute rotary pump. When the laser is operated at low repetition rates (1-10 pps), the pump is throttled so that all the residual ionization is not pumped away during the time between discharges. The pressure and the flow rates of nitrogen gas are controlled by a gas regulator and a needle valve. The operating pressure which ranges from 30 to 150 torr is read on a manometer. The flow rate chosen depends on the repetition rate at which the laser is operated.

2.43 THE SPARK GAP.

The present laser system works on a two electrodes spark gap. The gap is pressurisable with nitrogen upto about 4 kg/cm^2, depending on the voltage applied on the transmission line and the repetition rate. In the present system two spark gaps were tried (Fig. 2.7A and 2.7B). The main consideration in the design of a spark gap is to minimise its inductance to a few nano henries which helps in attaining a high over-voltage across the cavity. This is done by minimising the physical dimensions of the spark gap. Moreover, the materials chosen should be able to withstand high gas pressures and heating associated with high repetition rate and long term operation.

The spark gap shown in Fig. 2.7A was used in the above laser for about two years with approximately 1 - 2 hours of operation per day. To test the reliability, it was operated for 6 hours continiously at a repetition rate of about 25 pps (ie. for 0.5 million shots approx.) without any failure or appreciable heating. Eventhough it has given the above stated performance, on certain occassions, it failed to withstand high pressures. In order to overcome this problem, the spark gap shown in Fig.2.7B was designed, eliminating the use of teflon tapes and Araldite for sealing the joints. In this design, a nylon rod was used instead of Perspex sheets for making the side walls and pressure tightness was achieved by using O-ring seals. In both the designs, the electrodes had a separation of about 1.5 mm and were made using aluminium. These electrodes were fitted on aluminium side plates

and the thick copper strips screwed on to these side plates were soldered on to the copper clad sheets (transmission lines).

2. 44 TRANSMISSION LINES AS ENERGY STORAGE CAPACITORS.

For carrying out the experimental study detailed in Chapter 3, three sets of transmission lines were fabricated and used in the above laser system. All these transmission lines were made of double side copper claded fibre-glass epoxy laminates (Grade CFG 6/2DS, supplied by M/s Formica India Ltd). Copper was etched out, using the standard techniques, from the portion where the laser tube is to be fixed and also from the bottom and top edges of the sheet, to avoid flash over. To make it more failure resistant and to facilitate operation even during humid weather, all the sharp edges were rounded off and the entire length of the edges were covered with Araldite.

Copper foils soldered on the etched out central portion were screwed on to the brass side plates of the laser tube (Fig. 2.5B). A resistance of about 20 k was connected across the laser tube for providing a charging path to the capacitor (transmission line) on the other side of the tube. The characteristic impedance Z, the capacitance C and the propagation delay time T of a flat plate transmission line are given by

$$Z = Z_o \, S/\sqrt{E}L \qquad \text{(Ohm)} \quad \text{--- 2.5}$$

$$C = 1.11 \; E \; L1/4S\Pi \qquad \text{(pF)} \quad \text{--- 2.6}$$

and $$T = 2 \; 1 \sqrt{E}/C \qquad \text{(Sec)} \quad \text{--- 2.7}$$

where Z_o - characteristic impedance of free space (377 Ω)

S - thickness of the dielectric

L - width of the transmission line

l - length of the transmission line

ε - dielectric constant of the material

and c - the velocity of light

For two transmissions lines in parallel, the characteristic impedance is half and the capacitance is twice the value for a single line, calculated using 2.5 and 2.6. For a double parallel plate transmission line, with S = 0.16 cm, L = 44 cm, l = 77 cm and ε=4.7; Z=0.316 Ohm, C=17.59 nF and T=11.12 ns. Thus this line has a propagation delay time of 14.45 ns/m and can store an energy of 1.27 Joules at 12 kV.

2.45 HIGH VOLTAGE POWER SUPPLY.

For charging the transmission lines a 20 KV, 50 mA high voltage D.C. power supply was built, the essential features of which are shown in Fig. 2.8. The transmission lines are charged through 200 k, 1600 Watt wire-wound resistor in about 0.3 sec. This charging time was sufficient for operation upto 50 pps. High voltage upto 20 kVDC was derived by rectifying the output of a 20 kV, 50 mA, oil-cooled step-up transformer. A chain of 36 diodes (DR 150) were used for half-wave rectification. Each diode had a PIV of 2.5 kV and a current carrying capacity of 1 ampere. These diodes were soldered on a P.C. board with a 0.01 uF, 2000 V Capacitor and a 750 k resistor across each, for equal division of voltage across the diodes and for surge protection.

The whole P.C. board assembly was enclosed in a perspex box and the output leads were taken out. The current limiting resistors were enclosed in a separate box. All the power supply components

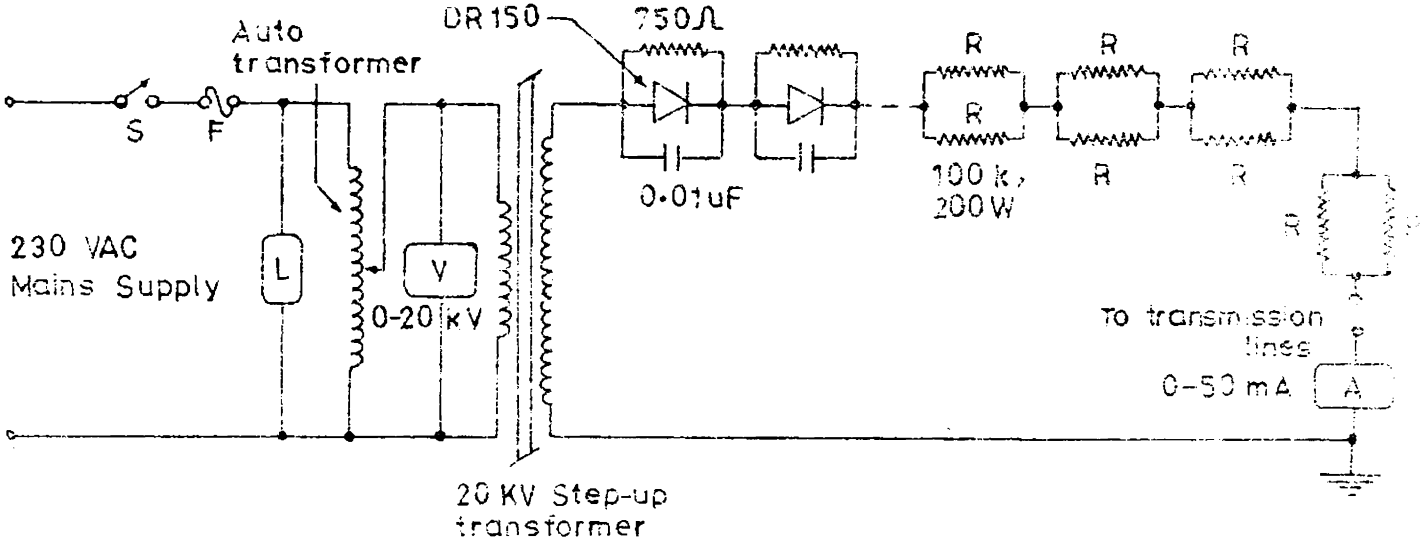
Auto
transformer
DR 150
750Ω
R
R
R
R
R
R
S
F
0·01uF
100 K,
200 W
230 VAC
Mains Supply
L
V
0-20 KV
To transmission
lines
0-50 mA
A
20 KV Step-up
transformer

along with the nitrogen cylinder were kept beneath the laser table on which the laser cavity and transmission lines were mounted. This made the whole instrument portable, on wheels.

2. 46 E.M SHIELDING OF THE LASER.

The high voltage discharges associated with the operation generated a large amount of R.F. noise which caused disturbances in oscilloscopes and other detection instruments kept in the near vicinity. To overcome this problem, the whole laser assembly including the power supply, transmission lines, laser cavity and spark gap was enclosed in shields made using M.S. sheets and were separately earthed. This eliminated the electro magnetic interferance considerably and was very much helpful during the pulse shape studies.

2.5 OPERATION OF THE LASER.

The rotary pump is switched on and the laser tube is pumped out and checked for any leaks in the gas flow system. Now, N_2 gas is fed in from the cylinder and the flow rate is adjusted. Using a needle valve the operating pressure is set on the manometer. The spark gap is pressurised to about 1-2 kg/cm^2 and the transmission lines are charged by gradually increasing the voltage using the auto-transformer in the primary side of the step-up transformer. Initially the laser starts lasing with a low repetition rate. By controlling the pressure inside the spark gap using a needle valve, the repetition rate of the laser is set to any desired value for a particular charging voltage.

This laser was operated with nitrogen in the pressure range 30 to 150 Torr. On using air instead of nitrogen the output power

was reduced to about 20 %. The repetition rate was variable from a few pps to 50 pps. This laser gave a maximum output peak power of 255 kW in 5 ns FWHM pulses, when operated at a repetition rate of 7 pps. The charging voltage was 11 kV and the operating pressure of N_2 was 120 Torr. The maximum efficiency obtained was 0.12 %.

REFERENCES.

1. H.G. Heard, Nature, 200, 667 (1963)
2. D.A. Leonard, Appl. Phys. Lett., 7, 4 (1965)
3. E.T. Gerry, Appl. Phys., Lett., 7, 6 (1965)
4. J.D. Shipman, Jr., Appl. Phys., Lett., 10, 3 (1967)
5. M. Geller et al., Appl. Opt., 7, 2232 (1968)
6. D. Basting et al., Opto Electronics, 4, 43 (1972)
7. J.G. Small and R. Ashari, Rev. Sci. Instrum., 43, 1205 (1972)
8. J.I. Levatter and Shao Chin Lin, Appl. Phys.Lett., **25**, 703 (1974)
9. A.J. Schwab and F.W. Hollinger, IEEE J.Quantum Electron, Q.E.-12, 183 (1976)
10. I. Nagata and Y. Kimura, J.Phys. E, 6, 1193 (1973)
11. C.L. Sam, Appl. Phys. Lett., 29, 505 (1976)
12. E.E. Bergmann, Rev. Sci. Instrum., 48, 545 (1977)
13. E.E. Bergmann, App. Phys. Lett., 31, 661 (1977)
14. V. Hasson et al., Appl. Phys. Lett., 28, 17 (1976)
15. Herden, Phys. Lett., 54 A, 96 (1975)
16. B.S. Patel, Rev. Sci. Instrum., 49, 1361 (1978)
17. R. Cubeddu et al., Opt. & Quantum Electron., 11, 276 (1979)
18. V. Hasson et al., Rev. Sci. Instrum., 50, 59 (1979)
19. H.M. Von Bergmann, J. Phys., E, 10, 1210 (1977)

20. A. Rotham and S. Rosenwaks, Opt. Commun., 30, 227 (1979)

21. R.W. Drefus and R.T. Hodgson, Appl. Phys. Lett., 20, 195 (1972)

22. L.Y. Nelson et al., Appl. Phys. Lett., 22, 79 (1973)

23. S.K. Searles and G.A. Hart, Appl. Phys. Lett., 25, 79 (1974)

24. S.K. Searles, Appl. Phys. Lett., 25, 735 (1974)

25. E.R. Ault et al., IEEE J. Quantum Electron., Q.E. - 10, 624 (1974)

26. J.H. Parks et al., Appl. Phys. Lett., 13, 142 (1968)

27. V.M. Kaslin and G.G. Petrash, JETP Lett., 3, 55 (1966)

28. M.Poyron et al., IEEE J. Quantum Electron., Q.E. - 6, 179 (1970)

29. A. Petit et al., Appl. Opt., 17, 3081 (1978)

30. B. Godard, IEEE J. Quantum Electron., Q.E. - 10, 147 (1974)

31. W.A. Fitzsimmons et al., IEEE J. Quantum Electron., Q.E.-10, 624 (1976)

32. J.G. Small, Laser Photo Chemistry, Tunable Lasers and other topics, Ed: S.F. Jacobs et al., Addison - Wesley (1976)

33. B.W. Woodward and M.W. Sasnett, Conf. on Laser and E-O systems, San Diego, California (1976)

CHAPTER III

PARAMETRIC STUDIES OF NITROGEN LASER.

3.1 INTRODUCTION.

A thorough knowledge of the optical as well as electrical characteristics of a laser is essential if one is to build a system with maximum possible efficiency and good long term stability. It has been found that the shape of the transmission line affects the lasing characteristics of transversely excited Nitrogen lasers.[1-4] Many researchers have reported[1-3] that a travelling wave excitation of the gas is the ideal method for attaining maximum efficiency.

In a travelling wave excited laser, the discharge starts at one end of the laser and propagates towards the other end with the velocity of light. So spontaneously emitted photons in the direction of laser axis sees maximum inversion and gets amplified to sufficient power levels in a single pass - which is the main principle behind the super-radiant mode of operation of the Nitrogen laser. High power build up is possible by this method because the gain for $C^3\Pi_u$ to $B^3\Pi_g$ transition is quite high owing to the short life time (about 20 ns, in effect) of the upper laser level. It has been shown later by Schwab and Hollinger[4] and Fitzsimmons et al[5] that travelling wave excitation is no more applicable to Nitrogen lasers using transmission lines having low characteristic impedances (less than 1 Ω) and which utilise a single spark gap. Only when using lines having high characteristic impedances (eg. 20 Ω), along with multiple spark gaps, the travelling wave theory is justifiable.

Hence, with a view to understand the nature and characteristics of the N_2 lasers using a Blumlein circuit, three different transmission lines were built and their performance studied. It has been predicted by Schwab and Hollinger[4] that given a fixed spark gap and cavity inductance and a particular thickness of dielectric the rate of current variation depends on the length of the line. In the present investigation, it was found that transmission lines with more length on the open-ended side of the channel gave longer duration pulses and higher output powers.

3.2 BLUMLEIN CIRCUIT AND E/P REQUIREMENTS.

Blumlein circuit is simply a high voltage pulse generator (Fig. 2.2) where the energy storage capacitors are of the same value (i.e. $C_1 = C_2$). Just before the spark gap is fired the full charging voltage V_o appears across the spark gap, while the voltage across the laser tube remains zero. When the spark gap fires, the LC circuit consisting of the capacitance C_2 and spark gap inductance L_s (plus stray inductances) begins to oscillate at $W = (L_s\ C_2)^{-\frac{1}{2}}$. At this instant the voltage across the laser tube also starts oscillating at the same frequency and the voltage rises to a maximum value of $2\ V_o$ due to the reflection of the voltage wave at the laser channel. In actual operating conditions this voltage will not reach $2\ V_o$ because the N_2 gas will breakdown at a lower voltage, near V_o. For practical purposes the peak value of V_o can be taken as the breakdown voltage and can be used for the calculation of the instantaneous electric field E using the relation,

$$E = \sqrt{2}\ V_o/d \qquad \text{(Volt/cm)} \qquad .. 3.1$$

where d is the electrode separation in cm.

Once the discharge is struck between the electrodes, the voltage falls off rapidly due to the development of a highly conducting plasma. The electrons in the nitrogen discharge may be assumed to be in a steady state with the instantaneous electric field. Since the maximum output power of Nitrogen lasers occur with E/P ratios in the range 70 - 120 Volts/cm. torr (Table 3.2), the laser plasma can be described in terms of an electron temparature given by[5]

$$L\, v_d = N_{gas} \int_0^{\infty} g\,(T_e, v)\, \sigma_i(v)\, 4\Pi\, v^3\, dv \quad -- \quad 3.2$$

where L - Townsend ionization co-efficient

v_d - the drift velocity

N_{gas} - ground state gas density

$g\,(T_e, v)$ - Normalised Maxwell - Boltzmann distribution

$\sigma_i(v)$ - velocity dependent ionization cross section for N_2 molecule.

For Nitrogen lasers with E/P in the range 20 to 150 V/cm.torr, Fitzsimmons et al.[5] has shown that,

$$v_d = 2.9 \times 10^5\ (E/P) \quad (cm/sec) \quad -- \quad 3.3$$

$$L/P = 1.4 \times 10^{-8}\ (E/P)^{3.7} \quad (torr.\ cm^{-1}) \quad -- \quad 3.4$$

and $$kT_e = 0.11\ (E/P)^{0.8} \quad (eV) \quad -- \quad 3.5$$

The effective electron temperature calculated using 3.5 enables one to predict the observed rates of ionization in nitrogen, which would be very much nearer to the excitation rates of the $C^3\Pi_u$ and $8^3\Pi g$ states, as these states lie very close to the ionization limit.

3.3 FABRICATION DETAILS OF PULSE FORMING NETWORKS.

Three typical transmission lines were made that can be used with the same laser cavity and spark gap. The first two designs have the conventional Blumlien circuit configuration ($C_1 = C_2$) and the only difference between them is that in the latter design two double side copper clad sheets are used, one above and the other below the cavity, so as to double the storage capacity. The length of the line is 57 cm in both the cases. In the third design, the length of the transmission line on the open ended side is increased so as to study the output power variation due to the change in the current variation rate. Because of the limitation in the size of available copper clad sheets, the maximum length utilised in the present study was 77 cm for the open ended stripline and 34 cm for the spark gap ended line. The width of the line was 44 cm in all the three cases.

The transmission lines were made as described in section 2.44. The capacitance, characteristic impedance and propagation delay calculated using 2.5, 2.6, and 2.7 for the three circuits are given in Table 3.1. The propagation delay of the double sided copper clad sheets used for the transmission lines was 14.4 ns/m. These lines were soldered to the laser tube and spark gap one after the other and the various parameters were studied.

3.4 MEASUREMENT OF PULSE WIDTH.

Nitrogen laser beam is directed on to a Hewlett Packard hp_2-4207, Silicon Pin Photodiode by an aluminium coated mirror strip. A scatterer is placed between the mirror and the detector to reduce the

TABLE 3.1

NITROGEN LASER CHARACTERISTICS

Laser Characteristics		Single Blumlein	Doble Blumlein	Double non-Blumlein
C_1 (nF)		6.51	13.02	8.00
C_2 (nF)		6.51	13.02	17.59
Characteristic impedance Z (Ohm)		0.632	0.316	0.316
Propagation del delay time T(ns)		8.24	8.24	11.10
Pulse width (ns)	FWHM	4	4	5
	Base	17	18	20
Stored energy at 10 kV(mJ)		325.5	651.0	879.5
Output energy/ pulse at 10 kV (mJ)		0.207 at 24.2 pps	0.246 at 10 pps	0.615 at 7.4 pps
Peak power output at 10 kV (kW)		51.8	62.5	123
Efficiency $=E_{out}/E_{stored}$ (%)		0.0636	0.0378	0.0699

incident power level. This photodiode has a junction capacitance of 5.5 pF and gives a rise time of 0.27 ns with a 50Ω load. The photodiode circuit is shown in Fig. 3.1. The whole circuitary including the photodiode and the load resistor were soldered on to a printed board and enclosed in an aluminium housing with a window for the laser emission to fall. A reverse bias of about 25 VDC was given to the photodiode from a dry cell enclosed in a shielded box. This bias was selected because at much lower voltages the rise time was found to increase. The voltage was fed into the diode housing using shielded cables. The housing was also earthed to avoid noise pick up. The output signal was taken out using a shielded cable from the BNC termination on the rear side of the housing and fed to a 100 MHz Tektronix Model 466 DM44 Storage Oscilloscope.

The pulse shapes for the three different configurations, viz. the single Blumlien, double Blumlien and the double non-Blumlien ($C_1 \neq C_2$), are recorded. Typical output traces are shown in Fig. 3.2. It is found that the pulse width at FWHM is 4 ns and at base is 17-18 ns for the single and double Blumlien Circuits. For the double non-Blumlien circuit, pulse width at FWHM is 5 ns and at base is 20 ns. The pulse width was also found to vary slightly with pressure (Fig. 3.3). The width at base was about 50 % larger than the propagation delay time of the line, as against the results of Mehendale and Bhawalker[6] who obtained a value about the same as that of the line. The reason for this anomaly is due to multiple reflections of the voltage wave at the discharge channel because of impedance mismatching. The additional increase in pulse

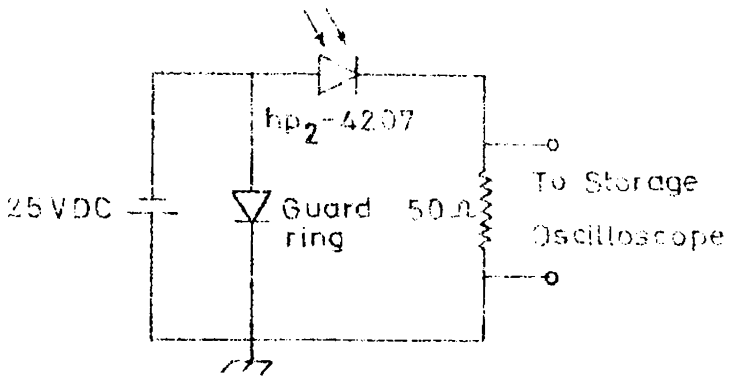

FIG. 3.1 [illegible]

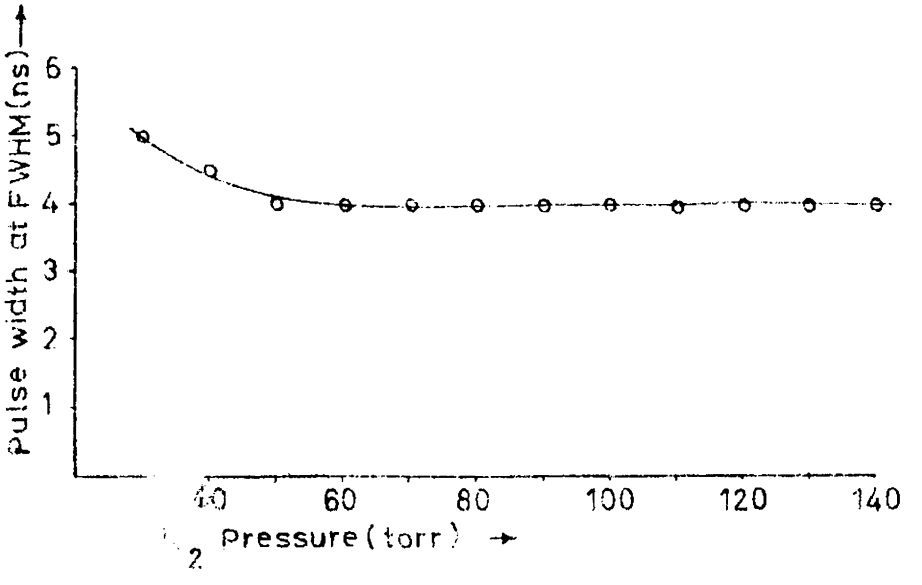

FIG. 3.2 VARIATION OF PULSE WIDTH WITH PRESSURE IN [illegible] LASER

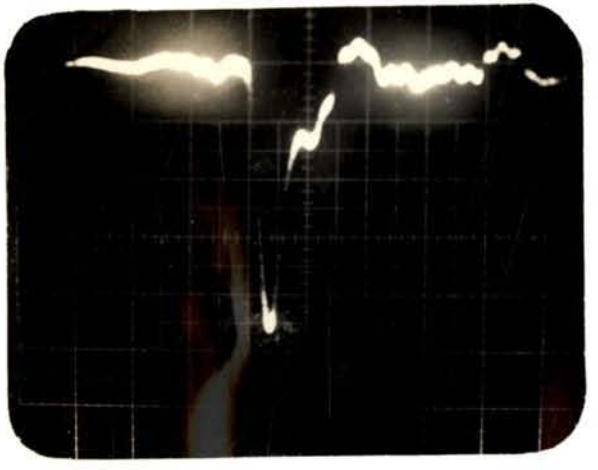

(A)

(B)

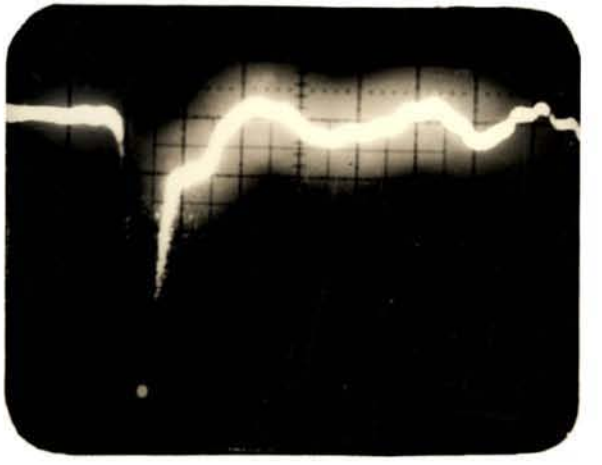

(C)

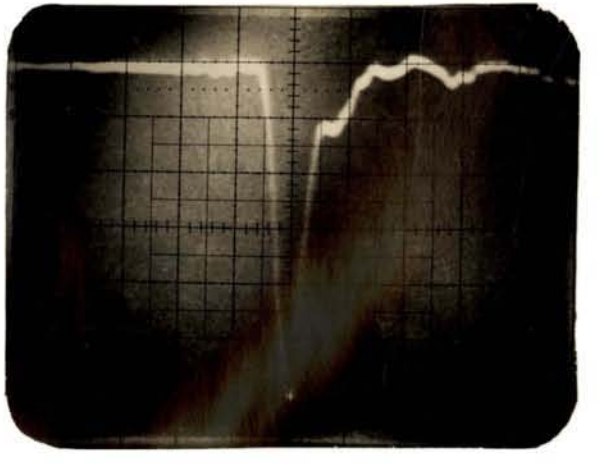

FIG. 3.2 NITROGEN LASER PULSE SHAPES AT 70 TORR N_2

SWEEP SPEED : 10 ns/DIV.

GAIN : 0.1 V/DIV.

A : SINGLE BLUMLEIN CIRCUIT

B : DOUBLE BLUMLEIN CIRCUIT

C : DOUBLE NON-BLUMLEIN CIRCUIT

width observed in the case of double non-Blumlien circuit is due to the increase in the propagation delay time (discharge time). Increasing the propagation delay beyond a certain extent will not contribute to increase in the pulse width because a higher rate of current variation and a better pumping efficiency is obtained if shorter is the length of the line.[4]

3.5 MEASUREMENT OF PULSE ENERGY AND PEAK POWER OUTPUT.

The average output power of the laser was measured using Scientech Model 38-0101 Volume absorbing 1 inch disc calorimeter (thermopile). The energy per pulse was obtained by dividing the average power by the repetition rate while the peak power was obtained by dividing the energy/pulse by the pulse width at FWHM. As the pulse width variation with pressure was not appreciable, we have used the pulse width at 70 torr for the calculation of peak power output.

The efficiencies of the three typical configurations are listed in Table 3.1. The double non-Blumlien circuit was found to give the maximum efficiency of 0.07 %. These overall efficiencies were calculated by dividing the optical output energy per pulse by the stored electrical energy ($CV^2/2$).

3.6 VARIATION OF OUTPUT ENERGY WITH PRESSURE.

The dependence of the output energy per pulse with nitrogen pressure for different charging voltages is shown in Fig. 3.4A for single Blumlien circuit, in Fig. 3.4B for double Blumlien circuit and in Fig. 3.4C for double non-Blumlien circuit. The readings

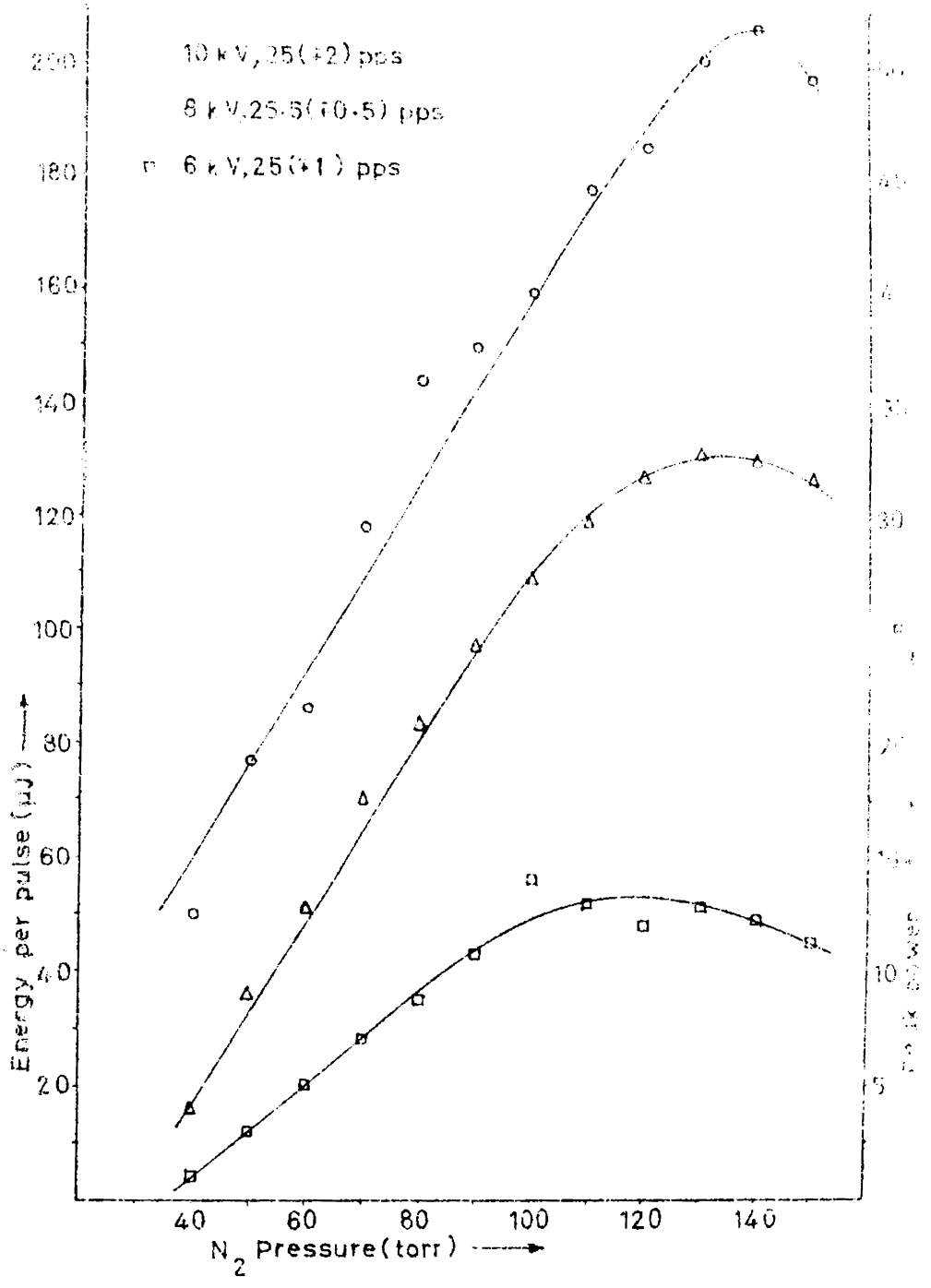

FIG. 7.4A OUTPUT ENERGY/PULSE AND PEAK POWER VARIATION WITH PRESSURE
IN LC ASSEMBLED CIRCUIT

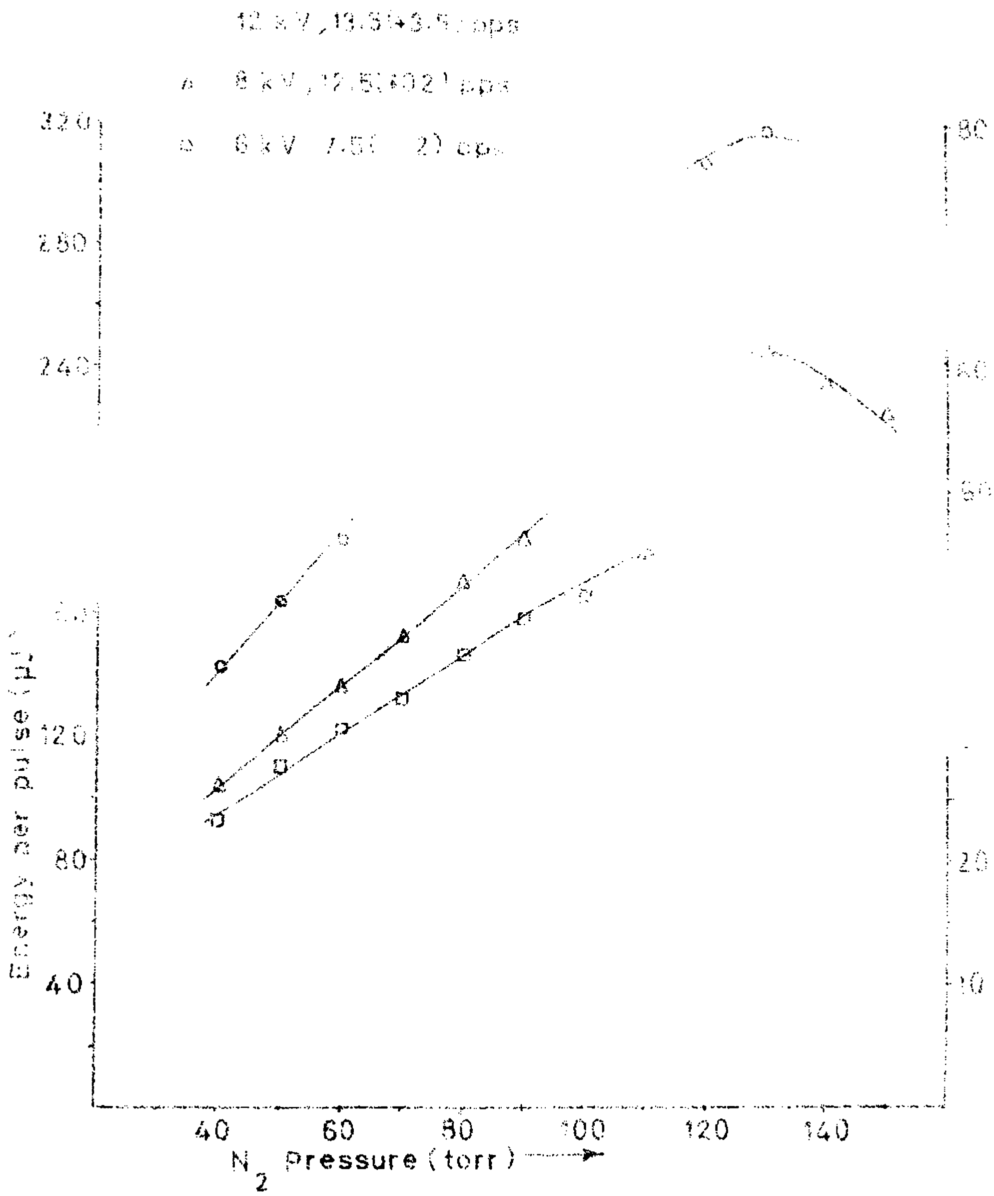

[illegible] OUTPUT ENERGY/PULSE AND PEAK POWER VARIATION WITH PRESSURE FOR DOUBLE BLUMLEIN CIRCUIT

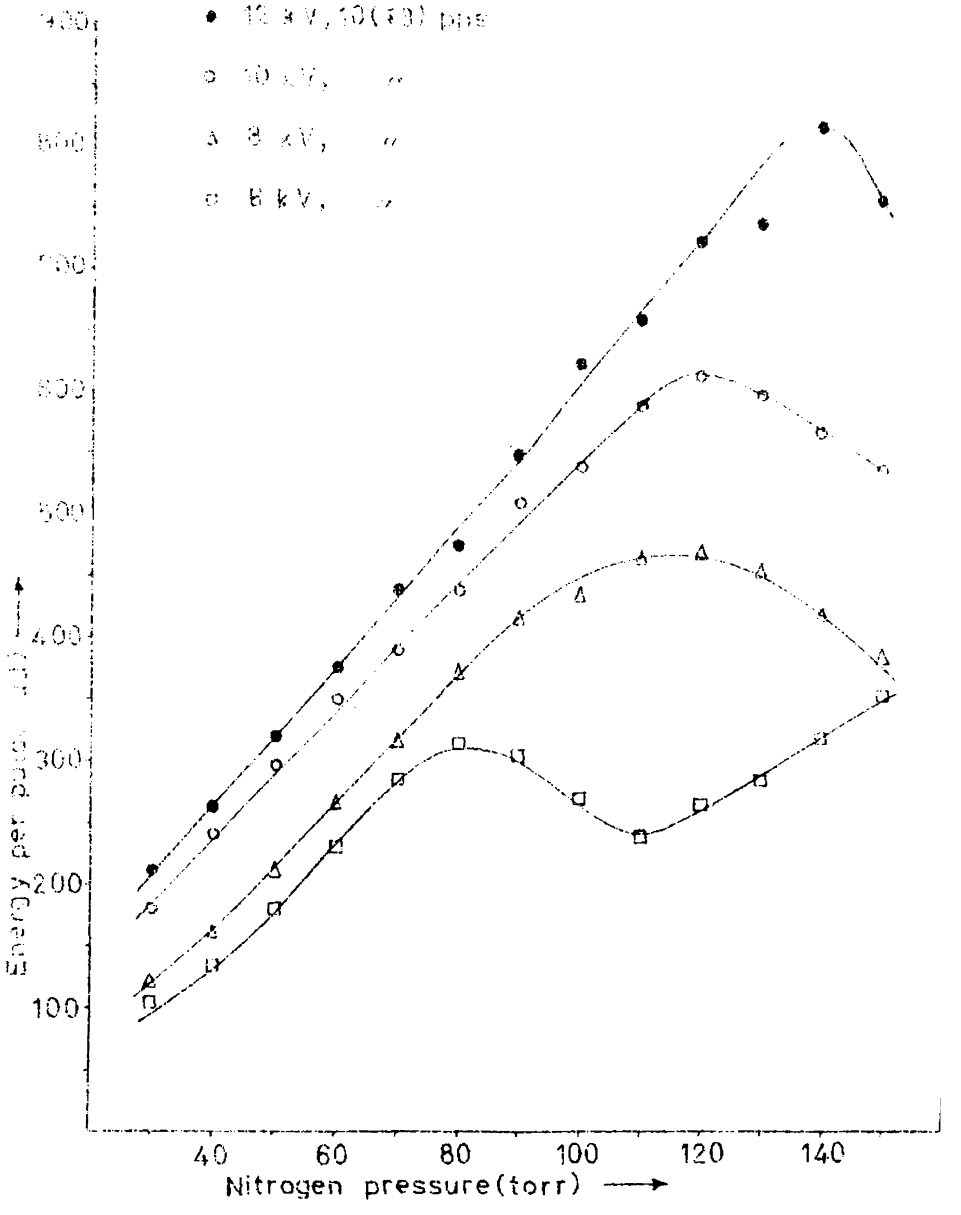

[illegible] ENERGY/PULSE AND PEAK POWER VARIATION WITH PRESSURE IN [illegible]

were taken in the pressure range 30 to 150 torr when the transmission lines were charged to 6 kV, 8 kV, 10 kV and 12 kV.

As is seen from these graphs, for a fixed voltage, the energy per pulse and hence the output peak power increases with pressure, reaches a maximum and then decreases with further increase in pressure. With increase in voltage, the pressure at which the power becomes maximum also increases. From the pressure at which the output peaks for different voltages, their E/P values and electron temparature (kTe) were calculated for the three different circuits and are tabulated in Table 3.2. The electric field was calculated using 3.1 taking d, the mean separation between the electrodes at the front and rear side as 1.1 cm.

The electrical power input to the laser tube is maximum when the impedance of the discharge is nearly equal to the impedance of the driving circuit. Fitzsimmons et al.[5] has shown that for Blumlien circuits the impedance matching and the optimum discharge conditions occur when the E/P value is about 80 Volt/cm.torr. When E/P is greater than 100 Volt/cm. torr the electron density increases rapidly with time. Now, as the discharge begins to load the electrical circuit, E/P falls off to a very low value and the output occurs when E/P passes through about 80 Volt/cm.torr (kTe $\simeq$ 4eV). At high E/P values the ions are the main discharge product while at lower E/P values the main products are excited electronic states. E/P values in the range of 70 - 120 Volt/cm. torr and electron temperature in the range of 3.3 - 5 eV obtained

TABLE 3.2

NITROGEN LASER DISCHARGE PARAMETERS

Transmission line	Applied voltage V_o(kV)	Electric field E (Volt/cm)	Optimum pressure P(torr)	Optimum E/P(Volt/ cm.torr)	Electron temperature kTe (eV)
Single Blumlein Circuit	6	7714	110	70.1	3.30
	8	10285	130	79.1	3.63
	10	12856	140	91.8	4.09
Double Blumlein Circuit	6	7714	110	70.1	3.30
	8	10285	130	79.1	3.63
	12	15428	130	118.7	5.02
Double Non-Blumlein Circuit	6	7714	80	96.4	4.25
	8	10285	110	93.5	4.15
	10	12856	120	107.1	4.63
	12	15428	140	110.2	4.73

in the present study are in agreement with the above observations of Fitzsimmons et al.[5]

When the gas pressure is larger than the optimum value for a particular voltage, there is a corresponding reduction in the electron temperature (3.5). Hence, the probability of excitation of the upper level is reduced and most of the discharge electrons waste their energy exciting lower lying levels. At low pressures, the available number of molecules for laser action is less. So, eventhough the electron temperature is high, the output power is less. A maximum peak power of 165 kW in 5 ns pulses was obtained for double non-Blumlien Circuit at an E/P value of 110 Volt/cm. torr.

3.7 VARIATION OF MAXIMUM OUTPUT PEAK POWER WITH SQUARE OF VOLTAGE.

The dependence of the peak power on the square of the charging voltage at the optimum E/P value is shown in Fig. 3.5 for the single, double and double non-Blumlien circuits. It is seen that the power varies linearly with the square of the charging voltage (i.e. with the stored energy). The rate of increase in peak power with the square of voltage is maximum for double non-Blumlien circuit. The increase in output power is due to the increase in electric field (E/P value) at higher voltages. Increase in E/P ratios suggest increase in electron drift (3.3), electron density and electron temperature (3.5).

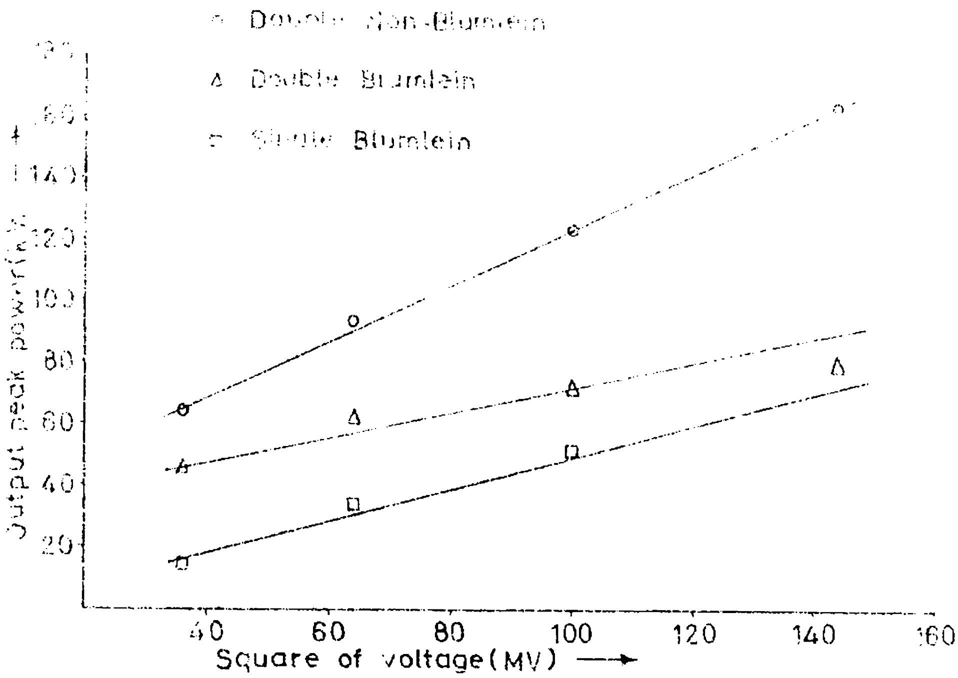

[illegible] OUTPUT PEAK POWER VARIATION WITH SQUARE OF CHARGING VOLTAGE AT
[illegible] PRESSURE (E/P VALUE)

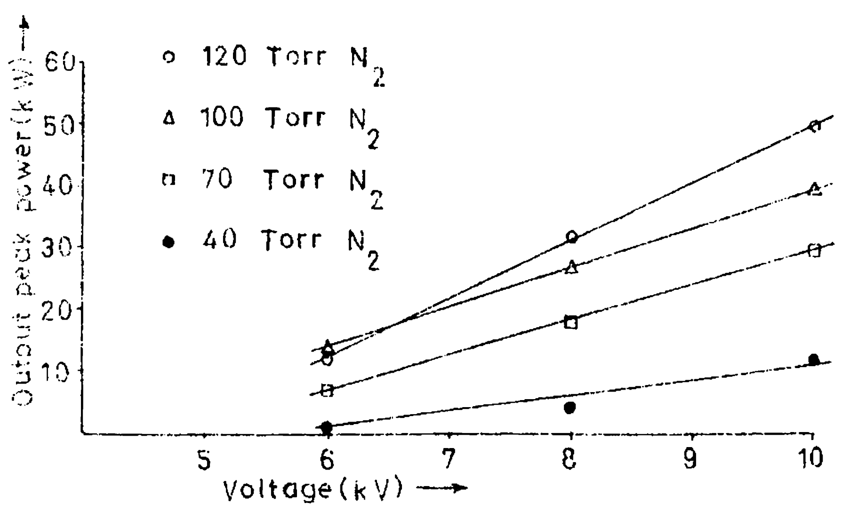

FIG. 3.[illegible]A OUTPUT PEAK POWER DEPENDENCE ON CHARGING VOLTAGE FOR SINGLE
BLUMLEIN CIRCUIT

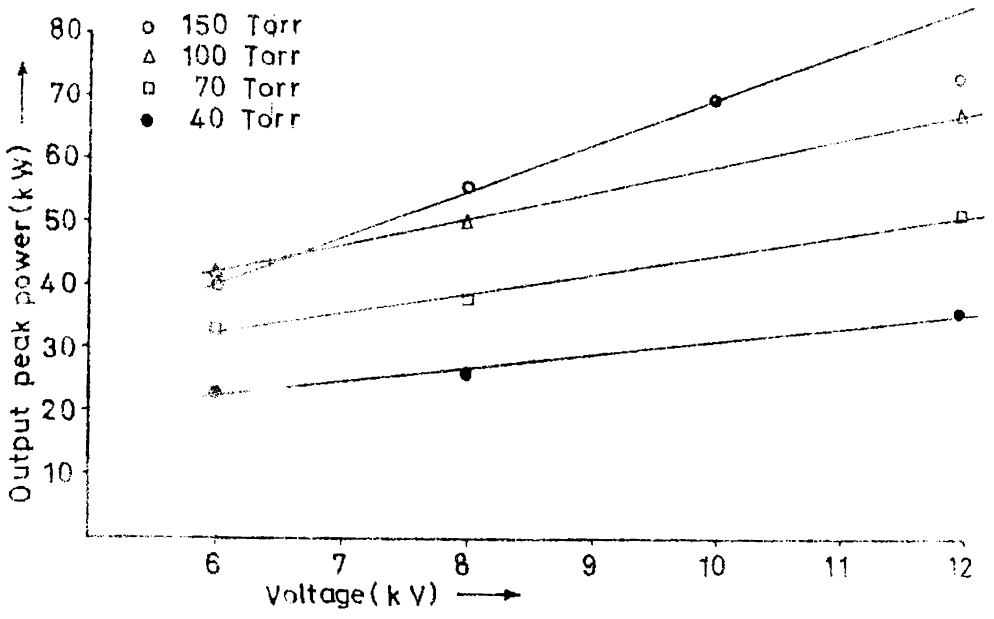

FIG. 3.6B OUTPUT PEAK POWER DEPENDENCE ON CHARGING VOLTAGE FOR
[illegible] GAS FILLING

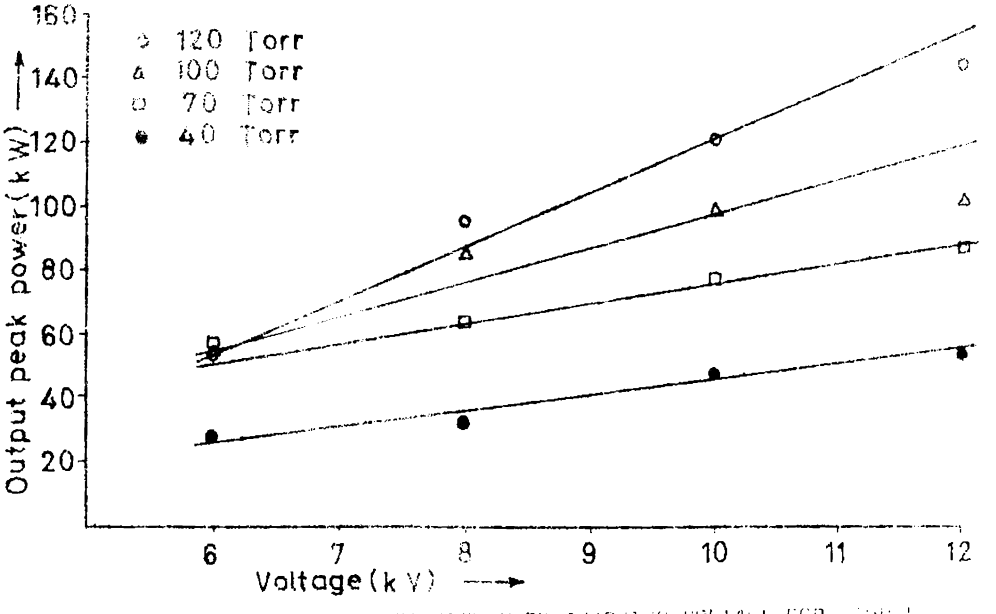

FIG. 3.6C OUTPUT PEAK POWER DEPENDENCE ON CHARGING VOLTAGE FOR [illegible]
NON-DUMPLEIN CIRCUIT

3.8 VARIATION OF OUTPUT PEAK POWER WITH VOLTAGE.

Fig. 3.6A, 3.6B and 3.6C show the change in output peak power with voltage at different N_2 pressures for the single, double and double non-Blumlien circuits respectively. It is seen that the variation in output power is linear with voltage for any pressure. The rate of increase of peak power with charging voltage is rapid higher the pressure.

3.9 VARIATION OF LASER POWER WITH REPETITION RATE.

The dependence of relative output intensity with the pulse repetition frequency of double Blumlein and double non-Blumlein circuit operated lasers are shown in Figs. 3.7A and 3.7B respectively. The average power readings were taken at 8 kV, 100 torr for both the systems. The gradual reduction in output power can be attributed to the lower number of ground state molecules available per laser shot as the repetition rate becomes higher and higher. Using rotary pump with a larger pumping speed (greater than 200 litres per minute) one can significantly increase the output power obtainable at high repetition rates. In Fig. 3.8, the change in output energy per pulse with repetition rate at 8 kV and 10 kV charging voltages, at 100 torr N_2, are shown for the double Blumlien laser.

3.10 LASER BEAM SIZE AND DIVERGENCE.

The laser spot size is rectangular with dimensions of (2 x 0.7) cm outside the exit window. Due to the particular configuration of Nitrogen lasers (without resonators) two values of

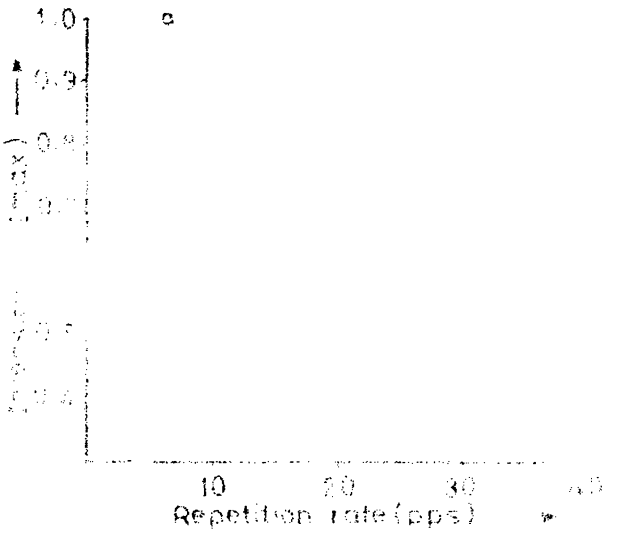
1.0
0.9
10
20
30
Repetition rate (pps)

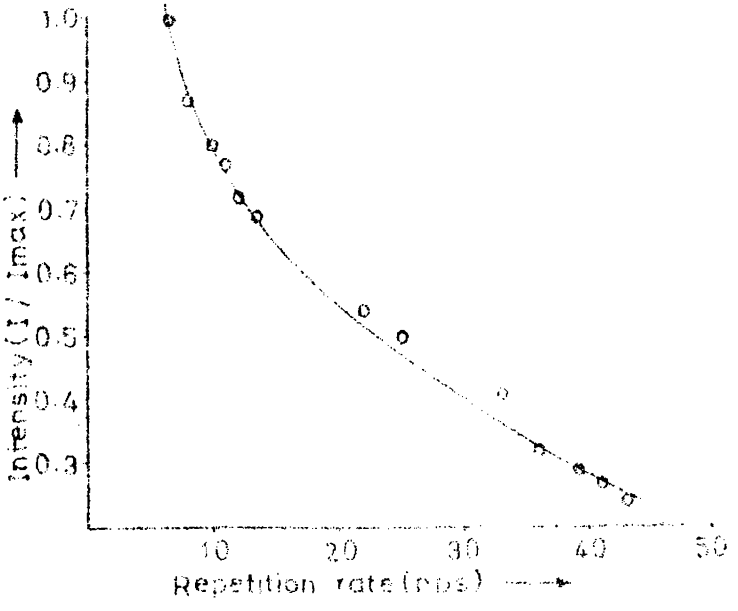
1.0
0.9
0.8
0.7
0.6
0.5
0.4
0.3
Intensity (I / Imax)
10
20
30
40
50
Repetition rate (pps)

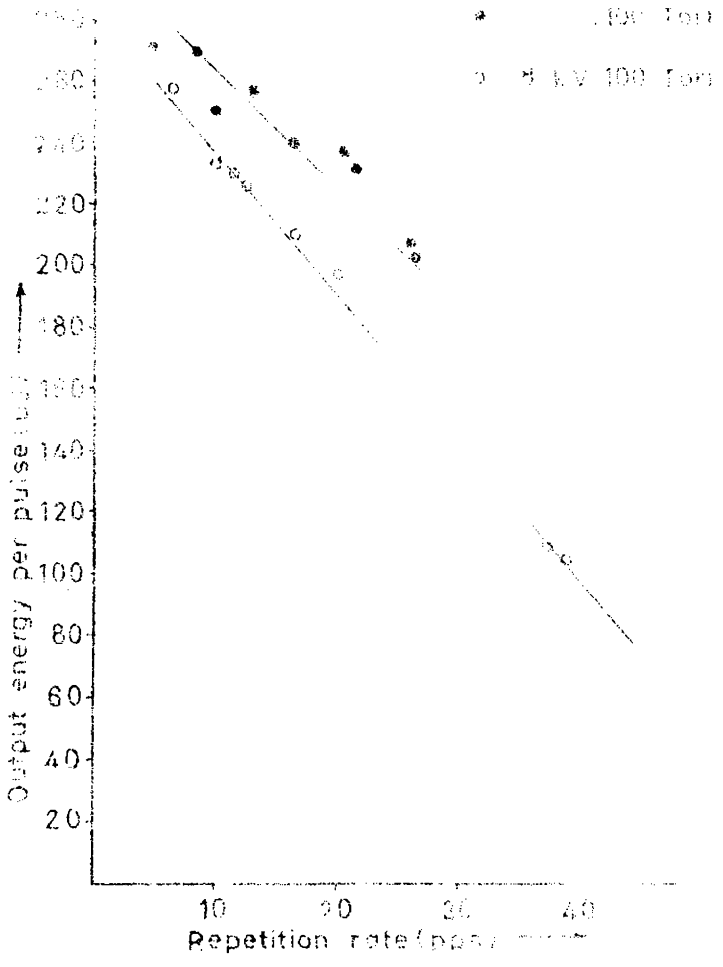

FIG. 3.8 OUTPUT PULSE ENERGY DECAY

divergence appear respectively in the plane containing the electrodes and in a perpendicular plane. We obtained for the present system, a full angle divergence of 0.279 mrad in the plane containing electrodes and 0.049 mrad in the perpendicular plane. Every effort was made to perfectly align the rear mirror perpendicular to the lasing axis before these readings were taken.

3.11 RESULTS AND DISCUSSION.

In the present investigation it has been found that the double non-Blumlein circuit gives higher output peak power and better efficiency than the conventional designs using the same transmission line dimensions (sheet size). Moreover, due to the propagation delay time being longer than that is possible with the conventional design, this laser gave slightly longer duration pulses. The increase in output power is due to the extra amount of energy that is stored in the transmission line because of $C_2 > C_1$ and also due to the attainment of a better impedance match with the laser cavity and the spark gap. With this particular configuration of discharge circuit, a maximum conversion efficiency of 0.07 % was obtained. Typical values reported are 0.05 % by Mehendale and Bhawalkar[6] and 0.085 % by Fitzsimmons et al.[5]

It may also be noted that in the initial experiments using the double non-Blumlein circuit laser still higher output powers were obtained, for example 255 kW in 5 ns pulses at 11 kV charging voltage with 120 torr N_2, at an efficiency of 0.12 %. At that time, the nitrogen gas used for the pressurisation of the spark

gap was flown through the cavity. But at higher N_2 pressures inside the cavity, it became very difficult to precisely control the spark gap pressure in order to maintain a fixed repetition rate for a particular operating voltage. So the gas flow system was modified to the present one in which the gas from the cylinder is separately flown into the spark gap and the cavity. It may be noted that the highest efficiency reported for laser action in nitrogen by Schwab and Hollinger[4] is (0.3 - 0.4) %.

So, if a pre-ionization technique, as has been used by Levatter and Lin[7], is incorporated into the present double non-Blumlien circuit so as to provide enough seeds for the main discharge to strike, it will be possible to compensate for the loss of ions or electrons due to the present gas flow system and achieve better system efficiency and higher output peak powers.

REFERENCES.

1. J.D. Shipman, Jr., Appl. Phys. Lett., 10, 3 (1967)
2. B. Godard, IEEE J. Quantum Electron. Q.E. - 10, 147 (1974)
3. D. Basting et al., Opto Electronics, 4, 43 (1972)
4. A.J. Schwab and F.W.Hollinger, IEEE J. Quantum Electron., Q.E. - 12, 183 (1976).
5. W.A. Fitzsimmons et al., IEEE J. Quantum Electron., Q.E. - 10, 624 (1976).
6. S.C. Mehendale and D.D. Bhawalkar, B.A.R.C., Laser Division Technical Report (1976).
7. J.I. Levatter and Shao Chin Lin, Appl. Phys. Lett., 25, 703 (1974)

CHAPTER IV

IDENTIFICATION OF NEW VIBRATIONAL BANDS IN THE NITROGEN LASER EMISSION SPECTRA.

4.1 INTRODUCTION.

Several laser emission bands have been observed in the second positive system of nitrogen molecule when excited either by electron beams[1,2] or longitudinal discharges[3]. But in transversely excited (TE) Nitrogen lasers, only the 337.1 nm radiation has been commonly observed. In 1966 Kaslin and Petrash[4,5] observed for the first time an amplification effect in the (0,1) 357.7nm and (1,0) 315.9 nm bands of the second positive system. The (1,0) band was obtained only by cooling the laser tube to liquid nitrogen temperature. Recently, Fitzsimmons et al.[6] has also found the laser emission to consist of a weak band at 357.7 nm. In 1975, Itani et al.[7] showed the laser spectra to contain a band at 357.7 nm when SF_6 was used as an additive to the nitrogen gas. In the same year, Suchard et al.[8] also reported bands due to (0,1), (0,2), (1,2) and (1,3) transitions in the N_2 - SF_6 laser emission.

Till now the Nitrogen laser spectral study was solely directed towards the analysis of the rotational structure of the (0,0) 337.1 nm band. Many researchers[9-13] have thoroughly analysed this band and have identified a large number of rotational lines belonging to the P and R branch transitions and all these transitions observed till 1976 have been listed by Beck et al.[14]

An understanding of the various vibrational bands and their intensity variation with voltage and pressure is essential for

optimisation of laser action at any of these wavelengths. In the present study, a large number of vibrational bands belonging to the $C^3\Pi_u - B^3\Pi_g$ second positive system of N_2 have been observed. In addition, bands due to $B^2\Pi - X^2\Pi$ system of NO molecule have also been observed and identified. Intensity variation of these bands with respect to changes in the operating parameters were also studied and the optimum conditions for stimulated emission at these wavelengths deduced.

4.2 IDENTIFICATION OF VIBRATIONAL BANDS.

The experimental set-up used in the present study is shown in Fig. 4.1. The output of the Nitrogen laser is deflected on to the entrance slit of a 0.5 meter Jarell - Ash Ebert Scanning Monochromator (Model 82-000) fitted with a 1180 grooves/mm, 500 nm blazed grating. For 1180 grooves/mm in the first order, the reciprocal linear dispersion is 1.6 nm/mm. Hence with an exit width of 5 microns the resolution obtainable is 0.008 nm. The photomultiplier tube (PMT) used was EMI Model. 9683 KQB which has S20 photo-cathode. This tube was operated at 1350 Volt DC taken from a high voltage power supply, EMI Model PM 288. The output of the PMT was amplified and fed to an X-t recorder, Omniscribe Model, B 127-11. In order to have sufficient resolution, the laser emission was scanned at a speed of 50 A°/min. with the X-t recorder operated at 5 cm/min. This combination gave 10 A°/cm on the chart paper. The emission spectra was found to consist of

FIG. 4.1 EXPERIMENTAL SETUP FOR RECORDING N_2 LASER EMISSION SPECTRA

various bands (Fig. 4.2) arising due to Nitrogen and NO molecules. The various vibrational bands observed are listed below in order of their intensities relative to the 337.13 nm (0,0) band of nitrogen molecule.

1. 331.83 nm Band

This band was observed in the emission spectrum with the maximum relative intensity (29 %) and was seen degraded to the red region unlike the $C^3\Pi_u - B^3\Pi_g$ bands degraded to the violet. The band head was observed at 331.68 nm, peaked at 331.84 nm and extended upto 332.5 nm. As this band could not be identified[15] with any in the second positive system (in fact, it lies between the (1,1) and (2,2) band positions) or any other N_2 systems or those belonging to NO, CO or CN systems, the spectra was rerun. The scanning speed now was set at 10 A°/min. and the chart speed at 10 cm/min. The spectrum obtained is shown in Fig. 4.3. The band head again appeared at 331.666 nm, peaked at 331.833 nm and extended upto 332.45 nm. The spectral width at FWHM was 0.42 nm. The two band systems reported to have frequencies in the vicinity of this band are the CN (6,4) band degraded to red, extending from 332.23 nm to 334.71 nm, belonging to the violet system $B^2\Sigma - X^2\Sigma$ and the N_2 (0,5) Goldstein Kaplan band of the $C'^3\Pi_u - B^3\Pi_g$ system with the band head at 332.52 nm and observed degraded to red.

Considering the accuracy of the measurements made, the positional mismatch of the observed band with the above two band

(4.2)

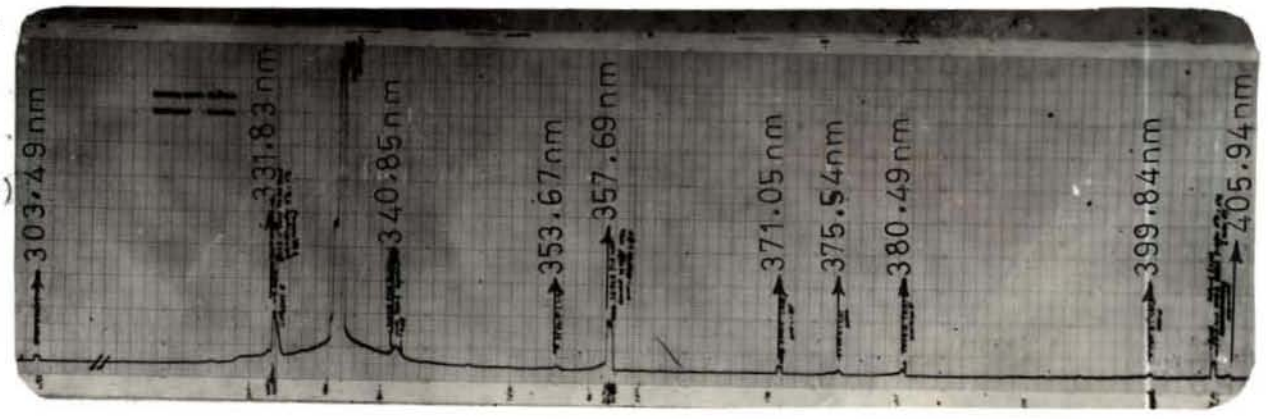

(4.3)

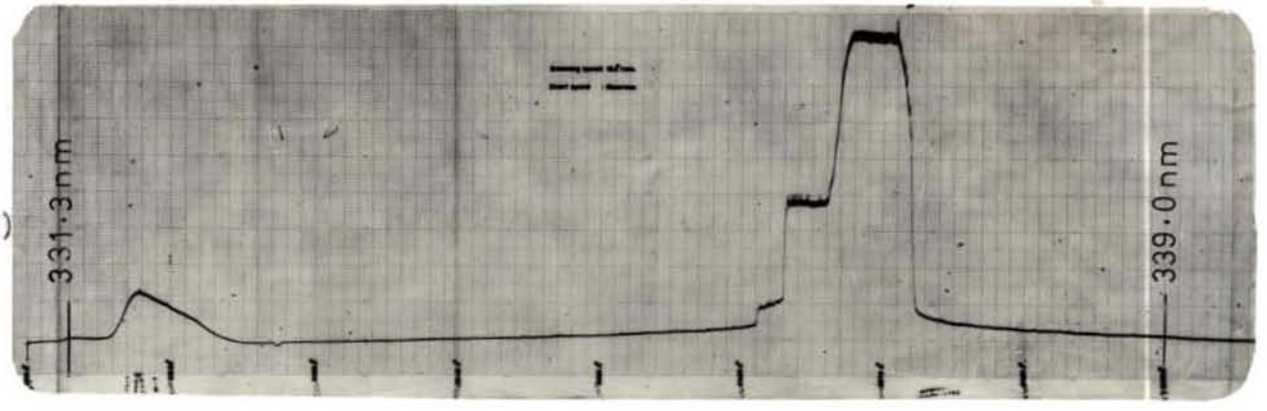

(4.4)

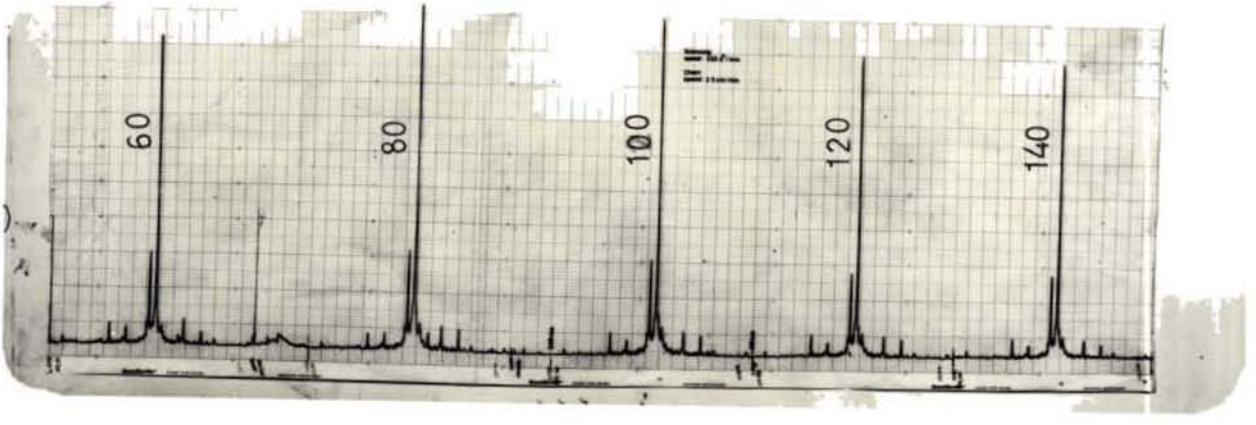

FIG. 4.2 RECORD OF THE LASER EMISSION SPECTRA
SCANNING SPEED: 50 A°/MIN., CHART SPEED: 5 cm/MIN.

FIG. 4.3 SLOW SPEED SCAN OF THE 331.03 nm BAND
SCANNING SPEED: 10 A°/MIN., CHART SPEED: 10 cm/MIN.

FIG. 4.4 RECORD OF THE VARIATION IN INTENSITY OF THE LASER SPECTRA WITH PRESSURE (60, 80, 100, 120 AND 140 TORR N_2) AT 12 kV
SCANNING SPEED: 250 A°/MIN., CHART SPEED: 25 cm/MIN.

systems are serious as to permit one to assign this band to any one of the CN or N_2 systems suggested. Thus, this can only be a new transition arising out of rotational vibrational levels between which normal transitions with large intensities are not reported.

2. 340.85 nm band.

This band with a relative intensity of about 8.2 % was observed degraded to red with its head at 340.85 nm peak at 341.16 nm. This band extended upto 341.6 nm with a spectral width at FWHM of approx. 0.6 nm. This is the (3,11) band which appears in the $B^2\Pi - X^2\Pi$ β system of NO molecule.[15] These NO bands appear in nitrogen spectrum due to small amounts of oxygen present as impurities in the discharge volume.

3. 357.69 nm band.

This is the (0,1) band of the second positive system of nitrogen molecule and has been previously reported by Kaslin and Petrash[4], Massone et al.[16] and Fitzsimmons et al.[6] Massone et al.[16] has also done the rotational analysis of this band. In the present spectra this band was observed degraded to violet with a mean relative intensity of 7.4 %. This band extends from 357.79 nm and has a spectral width of 0.5 nm at FWHM.

4. 303.49 nm band.

This band arises due to the (0,7) $B^2\Pi - X^2\Pi$ transition in the β system of NO molecule and is seen degraded to red. The relative intensity of this band is 7 % approx. and has a spectral

width of 0.34 nm at FWHM.

5. 371.05 nm band

This is the (2,4) band of the second positive system of nitrogen and is observed degraded to violet, as usual. The relative intensity is 5.9 % and the spectral width at FWHM is 0.36 nm. The band extends from 337.15 nm to 370.66 nm.

6. 315.93 nm band

This is the (1,0) band of the second positive system of nitrogen and appears degraded to violet with a mean relative intensity of about 5 %. This band was earlier reported by Kaslin and Petrash[5] in nitrogen laser spectra at liquid nitrogen temperature.

7. Other bands.

Many other weak bands with relative intensities below 2 % were also observed in the laser emission spectra. They are (0,2) 380.49 nm, (0,3) 405.94 nm, (1,3) 375.54 nm, (1,4) 399.84 nm and (1,2) 353.67 nm bands belonging to the $C^3\Pi_u - B^3\Pi_g$ second positive system of nitrogen.

4.3 INTENSITY VARIATION OF EMISSION BANDS WITH PRESSURE AND VOLTAGE.

The variation in intensity of the prominent bands observed in the emission spectra of the laser was studied with regard to change in the gas pressure and operation at different voltages. A grating with 1180 grooves/mm, blazed at 190 nm was used in the 0.5 meter Jarell-Ash Monochromator and the emission spectra was scanned from 260 nm to 410 nm. The entrance slit width was 70 microns while the exit slit width was 140 mircrons. This

gave a resolution of 0.224 nm in the first order. The scanning speed was 250 A°/min. and the recorder chart speed was 2.5 cm/min. The spectrum was recorded at 40 torr, 60 torr, 80 torr, 100 torr, 120 torr and 140 torr of nitrogen at 6 kV, 8 kV, 10 kV and 12 kV charging voltage.

The whole experiment lasted about six hours and was carried out at a stretch so as to maintain the same operating conditions throughout. Moreover, the electrical input to the laser system was stabilised before feeding in. Even with all these precautions the repetition rate was found to vary slightly (less than 5 %) during scanning. But the main difficulty was in adjusting the spark gap pressure to maintain the same repetition rate at all these voltages and pressures. This of course, was a constraint with the particular laser system, developed and used herein. Typical spectra obtained with 60 torr, 80 torr, 100 torr, 120 torr and 140 torr N_2 at 12 kV charging voltage are shown in fig. 4.4.

4.4 RESULTS AND DISCUSSION.

The intensity of the various emission bands were measured at different pressures and voltages and plotted. Figs. 4.5A, 4.5B, 4.5C, 4.5D, 4.5E, 4.5F and 4.5G represent the plots for 337.13 nm, 331.83 nm, 340.85 nm, 357.69 nm, 303.49 nm, 371.05 nm and 315.93 nm respectively. It may be noted that for most of the bands the intensity does not peak at lower charging voltages while for 315.93 nm band the intensity does not show any peak whatever be the charging voltage. In all these cases, the intensity was

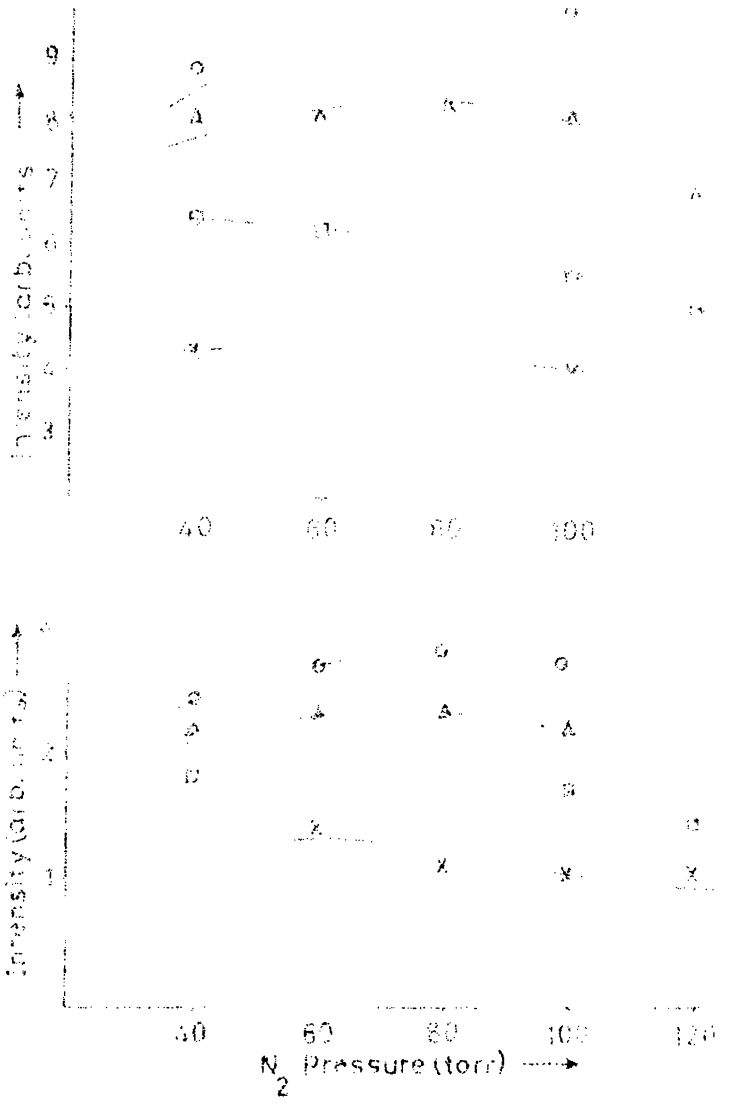
Intensity (arb. units)
9
8
7
6
5
4
3
40
60
80
100
Intensity (arb. units)
2
1
40
60
80
100
120
N_2 Pressure (torr)

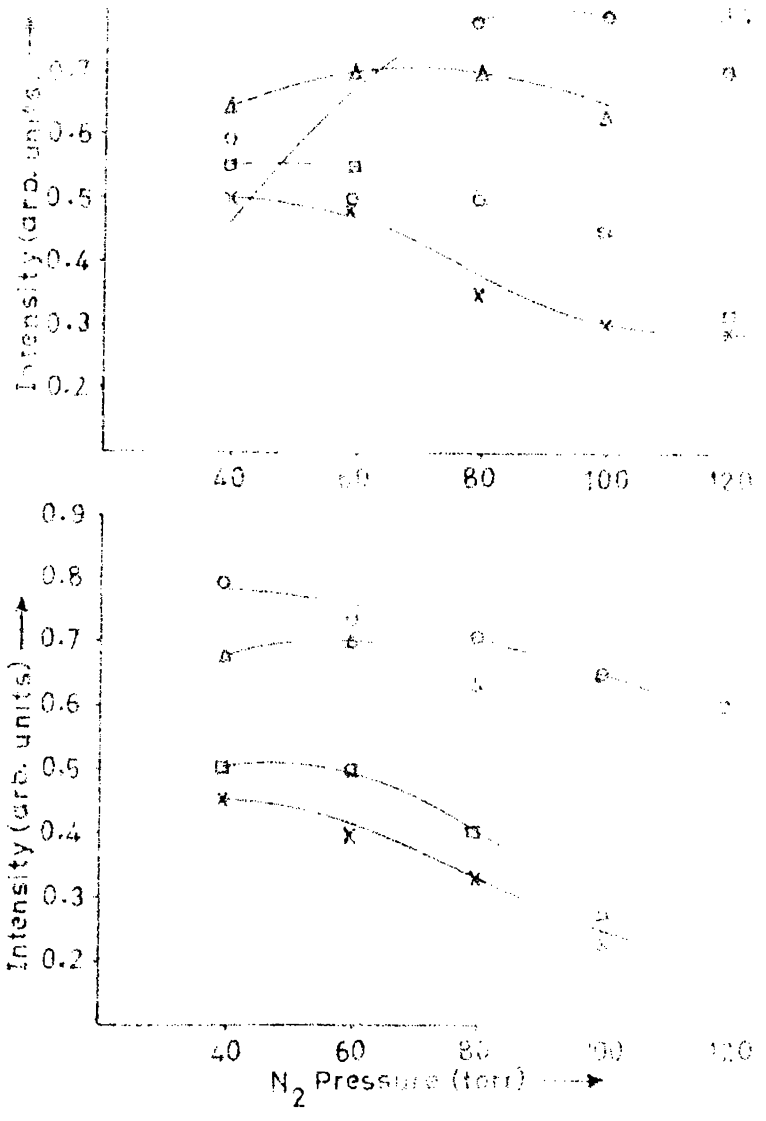
Intensity (arb. units)
0.9
0.8
0.7
0.6
0.5
0.4
0.3
0.2
40
60
80
100
120
N2 Pressure (torr)

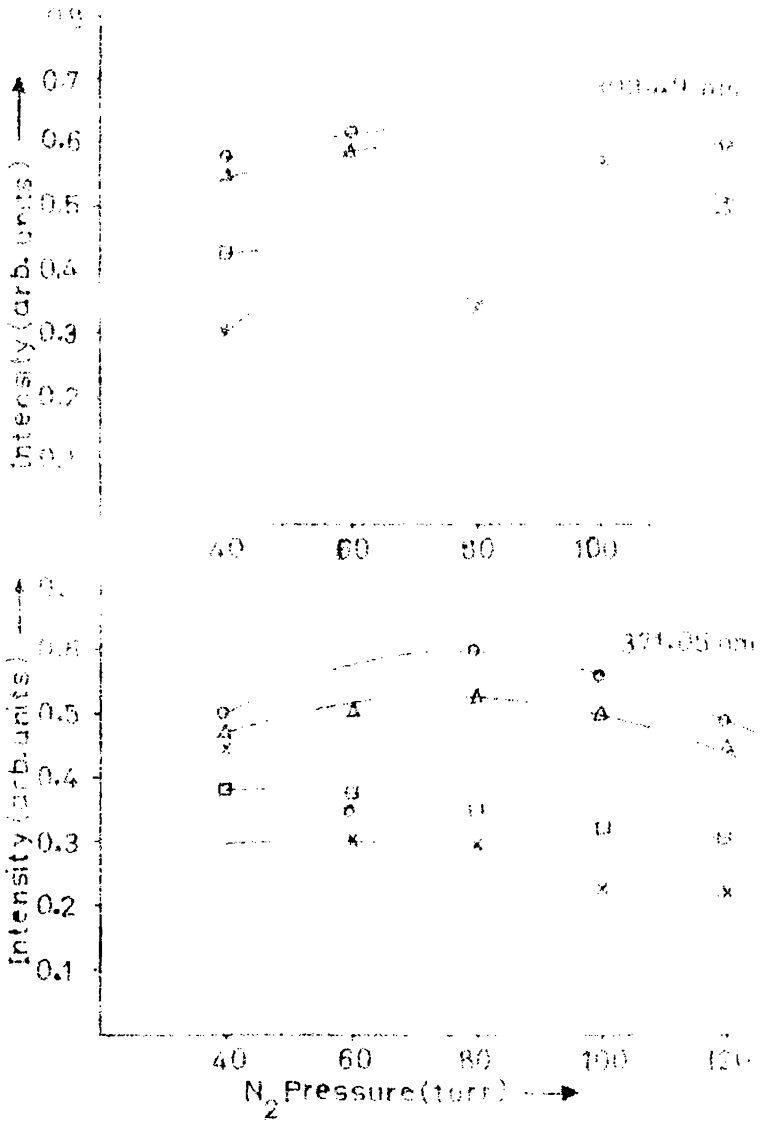
Intensity (arb. units)
0.7
0.6
0.5
0.4
0.3
0.2
0.1
40
60
80
100
Intensity (arb. units)
0.5
0.4
0.3
0.2
0.1
40
60
80
100
120
N2 Pressure (torr)

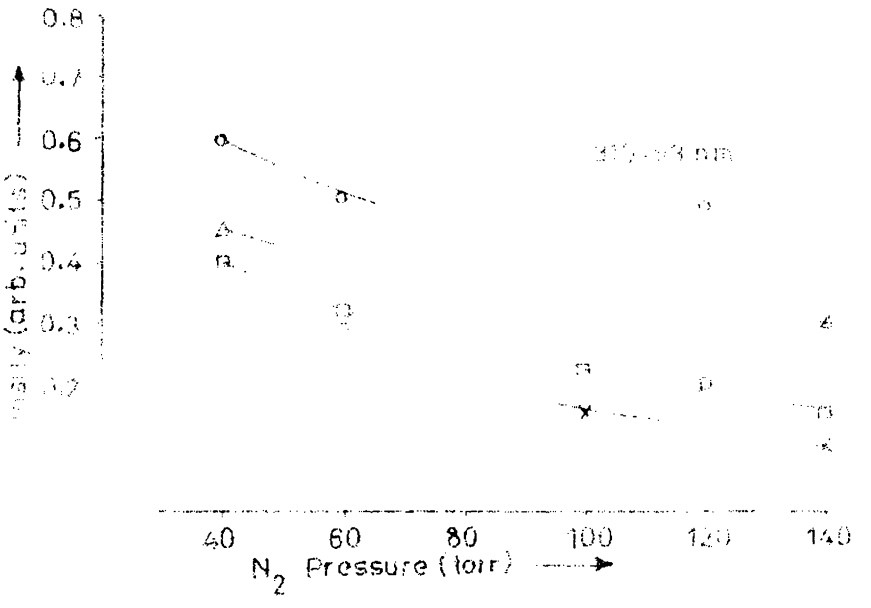

FIG. 4.59 [illegible]

maximum at lower pressures and it kept on decreasing as the pressure was increased. The reason for this behaviour is that the intensity peak for these bands may probably be at still lower pressures. For any specific pressure, the intensity of all observed bands was found to increase with increase in voltage. However, for a chosen voltage, the increase of pressure gives maximum intensity at different pressures for the various bands. By energy transfer mechanism if the intensity of a particular band is to be altered in relation to another, the most suitable approach is to vary the pressure.

Optimum E/P and electron temperature values calculated using the pressure corresponding to the maximum intensity is shown in Table 4.1. The electron temperature was determined using 3.1. It was suggested by Fitzsimmons et al. that these calculations will give the effective electron temperature only if the E/P values are in the range 20 - 150 volts/cm. torr. But, in the present case, the E/P values are more often outside this range and hence, are not used to predict the rates of ionization observed in nitrogen systems or to confirm the assignments of the various electronic states involved in the observed laser transitions.

From the intensity values obtained from the chart, the intensity of the various emission bands relative to the 337.13 nm main band were calculated. Fig. 4.6A and Fig. 4.6B show the variation in relative intensity with nitrogen pressure at 10 kV and 12 kV charging voltages respectively. The relative intensity

TABLE 4.1A

NITROGEN LASER SPECTRA ASSIGNMENTS

Laser emission Wavelength (nm)	Charging Voltage V(kV)	Optimum Pressure P (torr)	Optimum E/P (Volts/cm.torr)	Electron Temperature kTe(eV)	Upper lasing level energy (eV)	Mean Relative Intensity (%)	Assignment
337.13	12	80	192.85	7.41	11.18	100	Second Positive System $C^3\Pi_u - B^3\Pi_g$ (0,0) band of Nitrogen
	10	80	160.70	6.40			
	8	40*	257.00	9.32			
	6	60	128.57	5.35			
331.83	12	80	192.85	7.41	..	28.34	A possible new band.
	10	70	183.66	7.12			
	8	50*	205.70	7.80			
	6	60	128.57	5.35			
340.85	12	90	171.42	6.74	6.1	8.16	β System $B^2\Pi - X^2\Pi$ (3,11) band of NO species.
	10	70	183.66	7.12			
	8	50	205.70	7.80			
	6	40	192.85	7.41			
357.69	10	60	214.30	8.06	11.18	7.36	Second Positive System $C^3\Pi_u - B^3\Pi_g$ (0,1) Band of Nitrogen
	8	50	205.70	7.80			
	6	40	192.85	7.41			

* Denote cases where the emission intensity did not peak.

TABLE 4.1B

NITROGEN LASER SPECTRA ASSIGNMENTS

Laser emission Wavelength (nm)	Charging voltage V(kV)	Optimum Pressure P (torr)	Optimum E/P (Volts/cm.torr)	Electron Temperature kTe(eV)	Upper lasing level energy (eV)	Mean Relative Intensity (%)	Assignment
303.49	12	100	154.28	6.19	5.7	7.04	β System $B^2\Pi - X^2\Pi$ (0,7) band of NO species.
	10	70	183.66	7.12			
	8	60*	171.42	6.74			
	6	60	128.57	5.35			
371.05	12	80	192.85	7.41	11.67	5.91	Second Positive System $C^3\Pi_u - B^3\Pi_g$ (2,4) band of Nitrogen
	10	80	160.70	6.40			
	8	50*	205.70	7.80			
	6	40*	192.85	7.41			
315.93	12	40*	385.70	12.89	11.42	5.03	Second Positive System $C^3\Pi_u - B^3\Pi_g$ (1,0) band of Nitrogen.
	10	40*	321.40	11.14			
	8	40*	257.00	9.32			
	6	40*	192.85	7.41			

* Denote cases where the emission intensity did not peak.

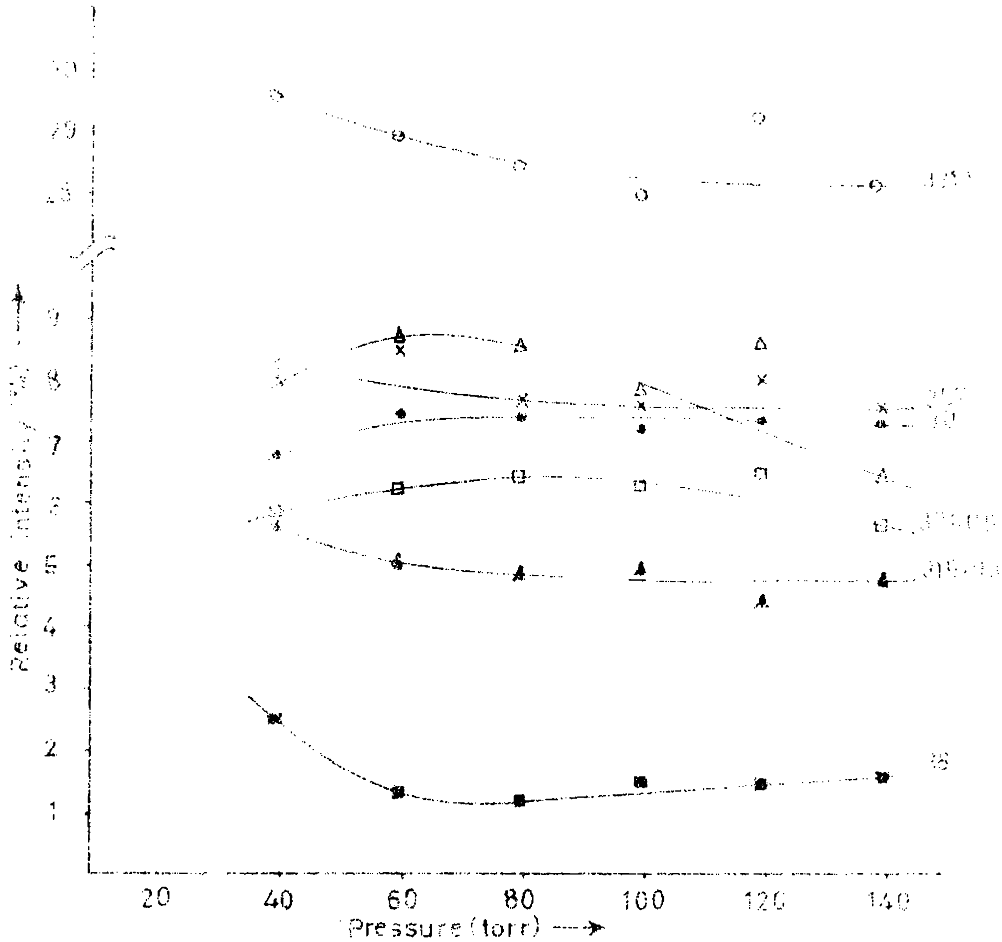

[illegible]NSITY VAR[illegible] N_2 [illegible]
[illegible] AT 10 kV

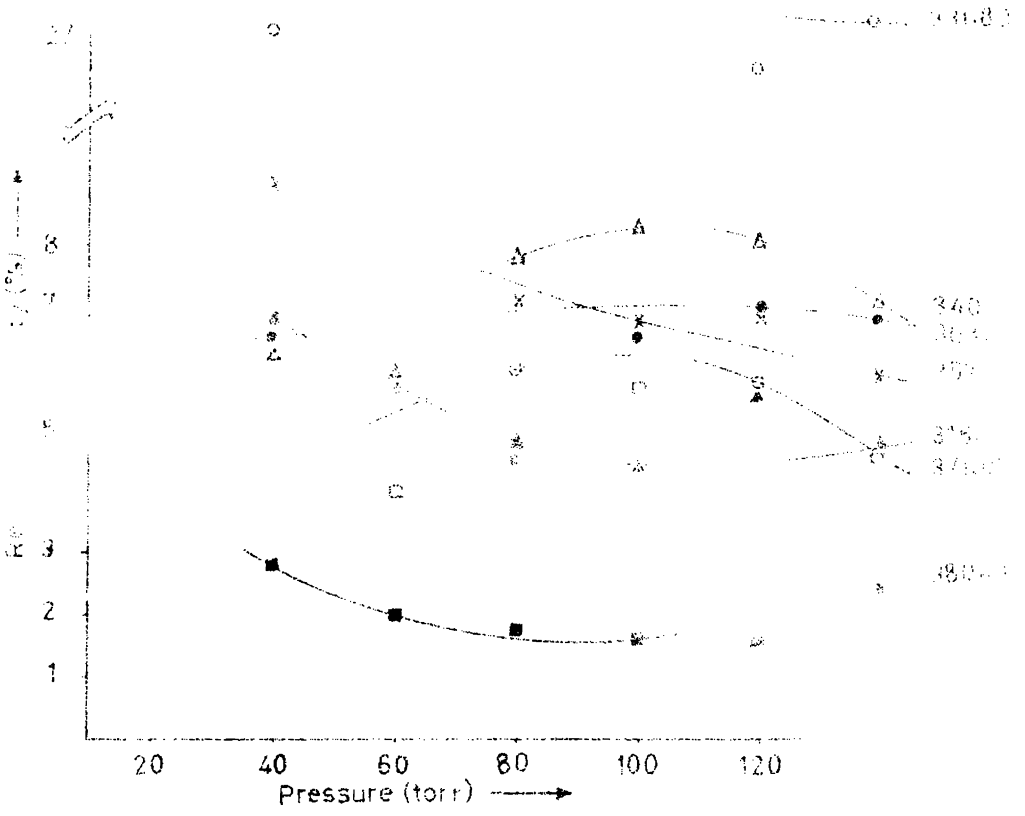

FIG. 4.[illegible] RELATIVE INTENSITY VARIATION OF [illegible] AT 12 kV

of 331.83 nm, 357.69 nm, 315.93 nm and 380.49 nm bands is maximum at low pressures and it keeps on decreasing as the pressure is increased. All the other lines peak in intensity at a particular pressure. The relative intensity of these bands averaged over different voltages and pressures are given in Table 4.1.

The most important observation worth mentioning is that 331.83 nm line which has a relative intensity of about 29 % has never been observed before even though the 357.69 nm band with a relative intensity of 8 % was reported earlier.[4,6,16] The (3,11) 340.85 nm band and the (0,7) 303.49 nm band of the β system of NO molecule have not been reported earlier from Nitrogen laser emission. In addition the (2,4) 371.05 nm, (0,2) 380.49 nm, (0,3) 405.94 nm, (1,3) 375.54 nm, (1,4) 399.84 nm and (1,2) 353.67 nm bands belonging to the second positive system have also been observed for the first time.

As most of the bands observed in this study are quite intense, there is every possibility that stimulated emission has taken place at these wavelengths in nitrogen. If one replaces the aluminium coated mirror at the rear end of the laser tube by dielectric mirrors narrow band coated for any of these wavelengths, and also provide suitable discharge conditions for the selected band, it is possible to enhance the stimulated emission intensity of that band.

REFERENCES.

1. S.K. Searles and G.A. Hart, Appl. Phys. Lett., 25, 79 (1974)

2. N.G. Basov et al. JETP Lett., 20, 53 (1974)

3. I.I. Magda et al., Sov. J.Quantum Electron, 3, 260 (1973)

4. V.M. Kaslin and G.G. Petrash, JETP Lett., 3, 55 (1966)

5. V.M. Kaslin and G.G. Petrash, Sov. Phys. JETP, 27, 561 (1968)

6. W.A. Fitzsimmons et al., IEEE J. Quantum Electron, Q.E. - 10 624 (1976)

7. J. Itani et al., Appl. Phys. Lett., 27, 509 (1975)

8. S.N. Suchard et al., Appl. Phys. Lett., 26, 521 (1975)

9. T. Kasuya and D.R. Lide Jr., Appl. Opt., 6, 69 (1967)

10. J.H. Parks et al., Appl. Phys. Lett., 13, 142 (1968)

11. M. Gallardo et al., Appl. Opt., 7, 2418 (1968)

12. A. Petit et al., Appl. Opt., 17, 3081 (1978)

13. J.P. Singh and S.N. Thakur, Appl. Opt., 19, 1697 (1980)

14. R. Beck et al., Table of Laser Lines in Gases and Vapors, Springer Verlag, p. 36 (1976)

15. P.W.B. Pearse and A.G. Gaydon, The Identification of Molecular Spectra, Chapman and Hall, 4th. Ed., (1976)

16. C.A. Massone et al., Appl. Opt., 11, 1317 (1972)

CHAPTER V.

FABRICATION AND PARAMETRIC STUDIES OF PULSED, ELECTRO-OPTICALLY Q-SWITCHED AND DYE Q-SWITCHED Nd: GLASS LASERS

5.1 INTRODUCTION.

Laser action at 1.06 μm in Neodymium doped barium crown glass was demonstrated for the first time in 1961 by Snitzer.[1] Later, Mauer[2] used dichroic reflectors for operation at 1.37 μm. But for laser action at 0.92 μm, operation at a reduced temperature was needed in addition to dichroic reflectors.[3] For operation at different wavelengths many new glass laser systems were developed using various dopant-host combinations. A detailed review of the various ions that have been made to lase in glass and their characteristics is given by Snitzer.[4]

The next major step in the development of solid-state lasers was the production of high intensity, short duration pulses by Q-Switching.[5-8] The population is inverted to a very high value when the cavity Q is low. When the population reaches its peak value, the Q of the cavity is restored back to its normal (high) value. Now, oscillations are built up and a high intensity, short duration pulse is emitted. The pulse width depends on the type of Q-switching employed. Commonly adopted techniques are rotating prism, bleachable absorbers, and electro-optic (E-O) devices. The shortest pulse duration so far obtained using Q-switching techniques was by the E-O method.

The first mechanical Q-switch was reported by Collins and Kisluk[9] who used a rotating disc with an aperture, inside the

cavity. Later, many new devices[10-12] with faster switching speeds, using mirrors and prisms, were put into use. Pulses upto 15 ns were obtained by Davydov et al.[12] using this technique.

A passive Q-switch[13,14] using a bleachable absorber (dye) was first put into operation in 1964. The dye Q-switch consists of a dye cell, kept between the laser rod and the rear mirror, whose absorption varies with the intensity of light incident on it. The laser will start oscillating only when the incident light intensity is sufficient to bleach the dye. For Q-switching Ruby lasers cryptocyanine or pthalocyanine dye in methanol is used while for Nd: glass lasers Eastman Kodak 9860, 9740 or 14015 in 1,2 - Dichloroethane is used. The pulse width obtained depends on the particular dye, solvent and its concentration and is usually in the range 50-250 ns.

The electro-optic Q-switch consists of an E-O element, either a crystal or a liquid, which becomes birefringent[15] under the influence of an external field. In the former case it is called a Pockels cell and in the latter case a Kerr cell. Pockels cells are ideal for Q-switching because of its lower operating voltages. There are two types of Pockels cells - one in which the electric field is applied in the direction of optical beam and the other in which it is perpendicular to the beam. The voltage applied on the crystal is determined by the crystal used, the wavelength of operation and the operating mode.[16-17] Crystals of potassium dihydrogen phosphate (KDP, KH_2PO_4) and its isomorphs belonging to the point

group symmetry $\bar{4}2m$ are commonly used for Q-switching purposes.[18-20] As these crystals are hygroscopic, they are usually operated in index-matching fluid-filled cells with AR-coated windows.[18] When using transverse fields $LiNbO_3$ crystals are preferred because they are not hygroscopic and can be operated with light propagation along the optic axis. The only drawback is their lower power handling capability (10-50 MW/cm^2) compared to those of the KDP family ($>$200 MW/cm^2). Typical Glass or Ruby lasers can deliver in the Q-switched mode 0.1 to 10 J of energy in 10 to 30 ns., depending on energy input and the size of the rod. Pulse widths variable upto 600 ns have been obtained from E-O Q-switched lasers using feedback loops to control the switching process.[21]

For producing ultrashort duration pulses, i.e., pulses in the picosecond regime, the technique usually employed is mode-locking.[22,23] By this technique the longitudinal modes emitted by a laser are phase-locked and the output pulse width becomes inversely proportional to the bandwidth of laser emission. By mode-locking an Nd-glass laser using thin (a few mm thick) dye cells pulse trains about 50-200 ns wide containing 5-20 ps pulses were produced. Weichel[24] and Everett[25] have given the engineering aspects of modelocked Nd-glass lasers. Typical modelocked Nd-YAG lasers have given 20-40 psec pulses with a dye cell of 1 mm thickness.[26]

Using optical gates external to the oscillator, a single pulse from the modelocked train can be selected out for further

amplification in laser amplifier chains to very high power levels, typically, a few hundred Tera Watts. Similar systems are used at the Lawrence Livermore Laboratory, California and other places for fusion experiments and other laser interaction studies.[27]

In the present chapter, the emphasis has been given to the designing and engineering aspects of Glass lasers. A laser designed for general research work has to be operated in several different modes, like, conventional, E-O Q-switched, dye Q-switched, etc. and hence, system flexibility and possibility for expansion and modification are generally more important than any other factor. It is with this purpose that the present Nd-glass laser system was designed and fabricated. It has been operated in the conventional pulsed, Pockels cell Q-switched and dye Q-switched modes and the operating parameters have been studied thoroughly and optimised.

5.2 LASING CONSIDERATIONS AND SELECTION OF LASER ROD.

Energy levels involved in laser action in a typical Nd-glass rod are shown in Fig. 5.1. The Nd^{3+} ion in glass represents a four-level system with laser action taking place at 1.06 μm between the lower lying levels of $^4F_{3/2}$ and $^4I_{11/2}$. The lifetime of the upper level varies in the range 220-900 μs depending upon the dopant, the percentage of doping and the host material.[4] The lower level empties its energy to the $^4I_{9/2}$ ground level by radiationless phonon transitions in 10-100ns.

Assuming a Lorentzian shape for the atomic line, with a width of $\Delta\nu$ at FWHM, the threshold condition for laser oscillation can be written as[28]

FIG.

$$n_2 - n_1 g_2/g_1 \geq 4\Pi^2 \nu_0^2 \Delta\nu T_{21}/T_c c^3 \qquad -- 5.1$$

where n_1, n_2 are the population of the lower and upper laser levels and g_1, g_2 are their degeneracies, ν_0 is the frequency corresponding to the centre of the atomic transition line, T_{21} is the life time of the upper laser level, T_c is the decay time constant of photons inside the resonator, and c is the speed of the light in the medium.

This equation enables one to calculate the threshold population inversion (n_t) for laser oscillation to begin. If n_i is the initial inversion (atoms/cm^3) attained by pumping and V is the rod volume (cm^3), then the total energy of the emitted pulse is $n_i h\nu V$, since for an ideal four-level laser system, $n_1 \simeq 0$. Using this equation one can approximately determine the rod volume required for any output energy. It may be noted that in Q-switched lasers, the initial inversion goes upto approximately $5n_t$ and hence, this value has to be taken for calculation purposes. Thermal conductivity considerations, which favour small diameters and larger lengths, dictate the size of the laser rod. Considering all these factors, a 152.4 mm long, 6 mm diameter silicate glass laser rod (LSG - 91H) manufactured by Hoya Electronics Ltd., Japan was chosen for the present laser system. The physical as well as the optical properties of this laser glass are given in Table 5.1. The threshold population inversion without Q-switch was calculated and was found to be 3×10^{17} atoms/cm^3 approximately. With Q-switch, a total energy/pulse value of 0.112 Joules was obtained. Assuming a pulse width of 10 ns in the E-O Q-switched mode, equivalent peak power is 11.2 MW.

TABLE - 5.1

LASING PROPERTIES : SILICATE LASER GLASS LSG-91H

Nd_2O_3 (Wt. %)	: 3.1
Nd^{3+} concentration (10^{20} ions/cm^3)	: 3.04
Cross Section for stimulated emission (10^{-20} cm^2)	: 2.7
Life time (μ sec)	: 300
Specific gain ($cm^{-1}/J/cm^3$)	: 0.133
Flourescence half-line width at 290° K (A°)	: 252
Center lasing wavelength (μ)	: 1.062
Loss coefficient at 1.055 μ (m^{-1})	: 0.1 (1.062 μ)
Relative Scattering intensity (6328 A°)	: 1
Slope efficiency (%) (Rod:10 dia. 160 mm) (R = 80 %)	: 1.15
Lasing threshold input energy (J) (Rod:10 dia. 160 mm) (R=80%)	: 52
Relative figure of merrit σ/n_2	: 1
Laser damage threshold at 30 nsec pulse (J/cm^2)	: 400 Internal : 25 Surface

OTHER PROPERTIES :

Non linear refractive index coefficient n_2 at peak λ(x 10^{-3} esu)	: 1.43
Refractive index at 1.062 μ	: 1.5498
Yield point	: 505°C
Thermal expansion coefficient (100-300°C) (10^{-7}/ °C)	: 105
Thermal conductivity (25°C) (K cal/m.h. °C)	: 0.89
Sp. heat (Cal/g. °C)	: 0.15 at 50°C
Density (g/cm^3)	: 2.81
Stress optical coefficient (nm/cm/kg cm^2)	: 2.16

The end faces of the laser rod were plane (surface accuracy - $\lambda/20$ at 1.06 μm) and parallel (parallelism between faces $\leq$ 5 arc sec.) These faces were anti-reflection (A.R) coated for 1.06 μm to facilitate the use of the same rod in different configurations.

5.3 CONVENTIONAL MODE GLASS LASER OSCILLATOR.

The laser system is shown in Fig. 5.2A. The laser rod placed between a 100 % reflecting and a partially reflecting dielectric coated mirror is optically pumped in a pumping chamber by flashlamps filled with noble gasses. For pumping Nd-glass rods Xenon filled flashlamps are always used because its emission has a better match with the absorption spectrum of Nd ions in glass. The mirrors (99.95 % or 50 % reflecting) used in the present system were of 1 inch dia. and were supplied by M/s. Laser Optics, U.S.A. These mirrors had a surface accuracy of $\lambda/20$ at 1.06 μm and were narrow band dielectric coated for 1.06 μm. For the partially reflecting mirrors the other face was A.R. coated for 1.06 μm. The mirrors were fitted on mirror mounts specially designed and built for the purpose. Even though the system developed (Figs. 5.2B and 5.2C) had provision for operation upto 10 ppm the laser was usually operated in single shot or at low repetition rates (1-2 ppm). Hence, no cooling jackets were provided for the flashlamps. In this mode of operation the output pulse width of the laser depends linearly on the flashlamp pulse duration.

5.31 PUMPING CHAMBER.

The overall efficiency of a laser system depends mainly

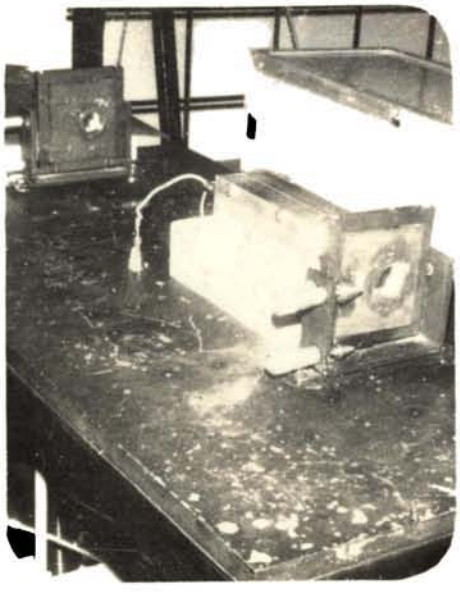

FIG. 5.2B CONVENTIONAL MODE GLASS LASER WITH DOUBLE CIRCULAR PUMPING CHAMBER

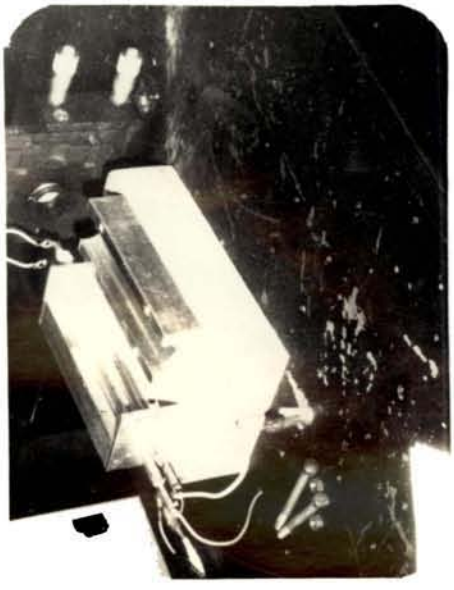

FIG. 5.4B DOUBLE CIRCULAR CHAMBER WITH FLASHLAMPS AND LASER ROD MOUNTED

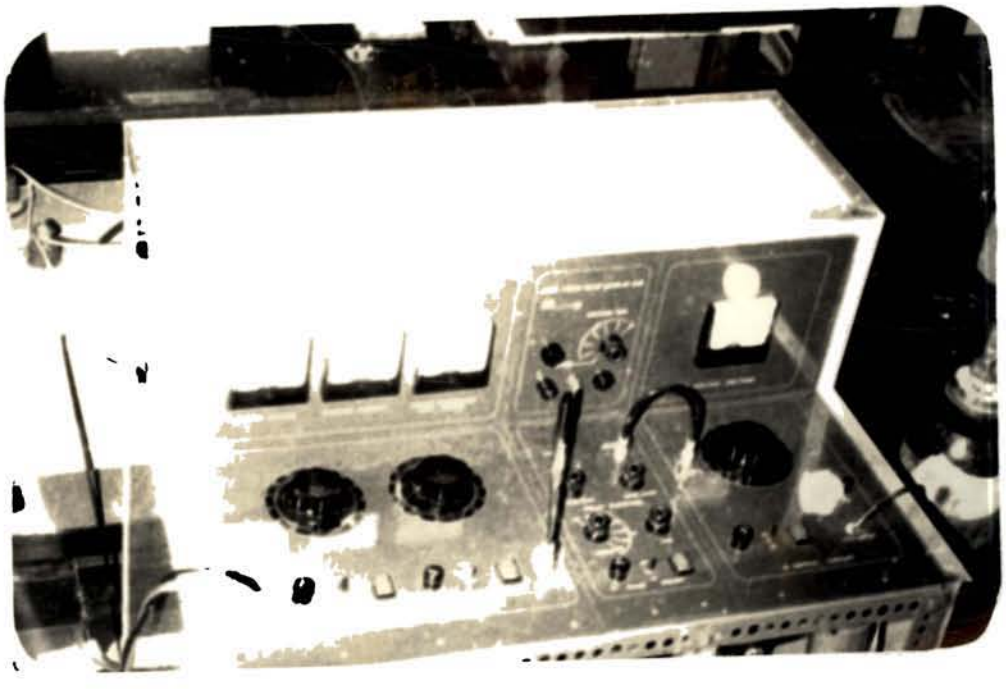

FIG. 5.2C GLASS LASER SYSTEM CONTROL PANEL

on the efficiency of transfer of radiation from the lamp to the laser rod. Not only does the pump cavity provide good coupling between the lamp and the rod but also it determines the pump density distribution in the rod which in turn affects the output beam uniformity, divergence and optical distorsions. Moreover, when high output energies are required more flashlamps are to be used so that one can safely increase the input energy into the system. Considering all these factors, two pumping chambers were built - one incorporated a single flashlamp in an elliptical cylindrical geometry while the other had two flashlamps in a double circular cavity.

In the elliptical cylindrical pumping geometry the flashlamp and the laser rod are arranged along its two focal lines, as shown in Fig. 5.3A. The rays emanating from the lamp falls on the rod directly or after reflections at the chamber surfaces. Nonuniform illumination of the rod cross section is reduced by immersion of the rod in a liquid of refractive index $(n_{im}) \gtrsim$ that of rod. The present system was designed for use with 10 % Sodium nitrate aqueous solution[29] which had the additional property of a uv filter. The depth of immersion liquid for maximum concentration of radiant flux within the laser rod of radius R_r is given by

$$d = R_r (n_{im} - 1) \qquad \text{— 5.2}$$

The efficiency of the pumping arrangement can be improved by making the eccentricity of the ellipse small. But the limit is

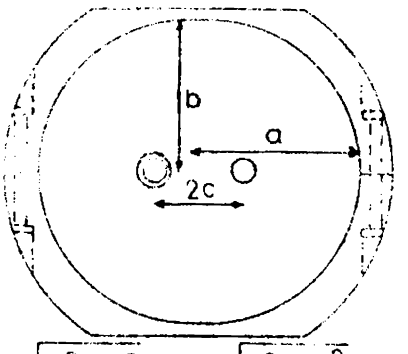

$b = \sqrt{a^2 - c^2}$, $c = \sqrt{a^2 - b^2}$ $e = c/a$

$2c = 28\,mm$, $2a = 102\,mm$, $2b = 98mm$

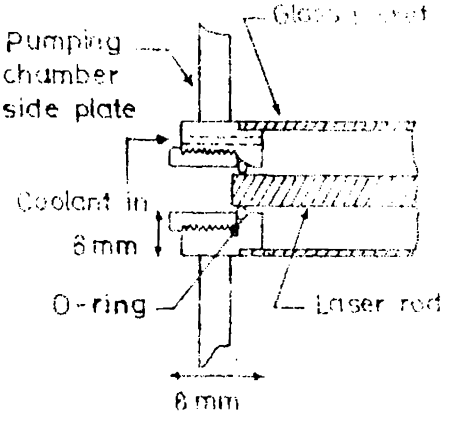

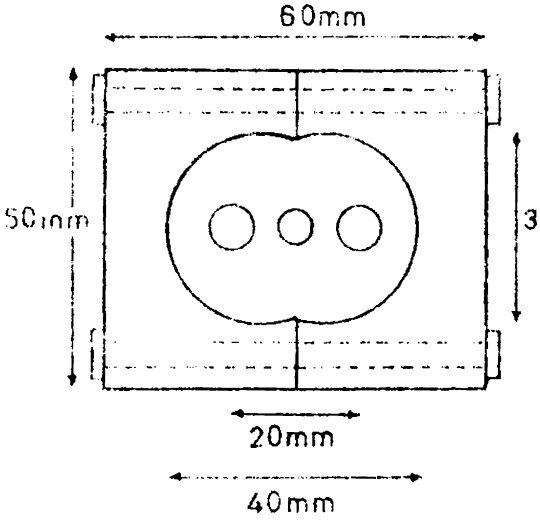

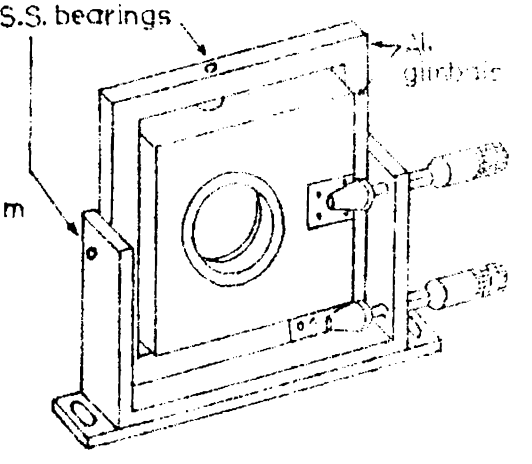

set by the size of the outer jackets of the rod and the lamp. Taking these factors into consideration an elliptical cylindrical chamber of the following dimensions was built.

Major axis of the ellipse	: 102 mm
Minor axis of the ellipse	: 98 mm
Distance between the focal lines	: 29 mm
Length of the elliptical cylinder	: 150 mm

For optimum matching with the laser rod a xenon flashlamp with an arc length of 152.4 mm and inner diameter of 6 mm (Model 6F6 - G, ILC Technology, U.S.A.) was chosen. This flashlamp had a quartz-envelope for absorbing the unwanted uv radiations.

The pumping chamber was machined out of extruded aluminium rod. Initially the rod was sliced longitudinally through the centre, then levelled and bolted together. As the eccentricity was small, the ellipse was formed by cutting two circles through the rod and then machining out the in-between portions. The elliptical surfaces were then polished and buffed. This method is much simpler than the one suggested by Hornik et al.[30] and is suited, especially for large cylinder lengths. The inside of the side plates were also machined flat, polished and buffed. These side plates had holes exactly at the foci of the ellipse for the insertion of the laser rod and the flashlamp. The laser rod was mounted on a rod holder (Fig. 5.38) made of brass. The O-ring seal prevents leaking of sodium nitrate solution. Care was taken to maximise the rod volume exposed to flashlamp radiation when the rod

holder assembly was designed. The size of the holder was determined by the depth of immersion fluid calculated using 5.2.

When the laser has to be operated in the Q-switched mode, the cavity losses are more and hence, more energy has to be delivered into the system for achieving threshold. For use in the present E-O Q-switched laser, a close-coupled double circular cavity of a very simple design was built. (Figs. 5.4A and 5.4B) whose dimensions are given below.

Length of the cavity	:	148 mm
Diameter of the circular reflector	:	30 mm
Separation between lamps	:	20 mm
Distance between the centres of the circular reflector	:	10 mm

The extruded aluminium rod was cut and machined to size and bolted together. The circular surfaces were made by drilling two 30 mm diameter holes through the 148 mm length block. The inside portions were then finely polished and buffed. The side plates were 4 mm thick and had holes, for mounting the flashlamps and the rod. In this design the rod was mounted without any cooling jacket, as the system was meant for operation only in single shots or at 1-2 ppm. It may be noted that, for maximum pumping efficiency, the centres of the lamp and rod should be equally separated from the centre of the circular reflector throughout its length.

5.32 LASER SUPPORT STRUCTURE AND MIRROR MOUNTS.

Laser systems for general research are either of the optical bench type with sliding carriages or of the type in which the mounts and positioners are screwed on to a rigid platform. Usually such platforms are either of granite or mild steel, mounted on shock absorbing support structures.

A mild steel table (100 cm x 50 cm) with a 1 inch thick top was built with an 'H' type support structure. The table top was machined flat and $\frac{1}{4}$ inch holes were drilled at a separation of 2 inches on the entire surface and were then tapped. This enabled rigid mounting of the optical components and other devices of the system. The support structure was fitted on 4 inch dia. anti-vibration mounts. The stability of the present design could be taken from the fact that once aligned the laser system could be operated usually for a period of one month without the need for any further adjustments, though routine checkups were made everyday before operating the system.

The mirror mounts (Fig. 5.5.) were similar in design to the one described by Pace and Atkinson.[31] This gimbal type mount was designed for 1" laser mirrors and it provided independant orthogonal rotation about the vertical and horizontal axes. High angular resolution was achieved by using a conical adapter attached to the end of micrometer screws. The linear motion of the conical section was converted into rotational motion by allowing the cones to pressure contact (using spring leaves) a rubbing

block on the gimbals. The cones were made of brass while the gimbals were made of aluminium. The angle of the conical section determines the angular resolution. For a 15° cone, a resolution of 0.02" was obtained.

5.33 FLASHLAMP DRIVE CIRCUITS.

The flashlamp drive circuit consists of a charging unit, a pulse-forming network (PFN) and a trigger circuit. The charging unit charges the PFN, which is basically a LC network, within a specified time and the trigger circuit initiates the discharge of the stored energy into the flashlamps.[32] There are two methods of triggering, viz. series triggering and external triggering.[33] As 100 % trigger reliability[34] is essential in Q-switched laser systems, the present design utilized series triggering scheme as shown in Figs. 5.6 and 5.7.

For current densities exceeding 500 Amperes/cm^2 the V-I characteristic of flashlamps can be represented as[35,36]

$$V = \pm K_o l i l^{\frac{1}{2}} \qquad \text{--- 5.3}$$

where K_o is a parameter usually specified by the manufacturer[37] and is a function of the lamp type and dimensions.

Since the flashlamp does not follow the linear relationship of a constant resistance, Markiewicz and Emmett[38] developed a design procedure for determining the inductance, capacitance and operating voltage for a given type of lamp, energy input, pulse duration and pulse shape factor. The following equations represent the results of their analysis.

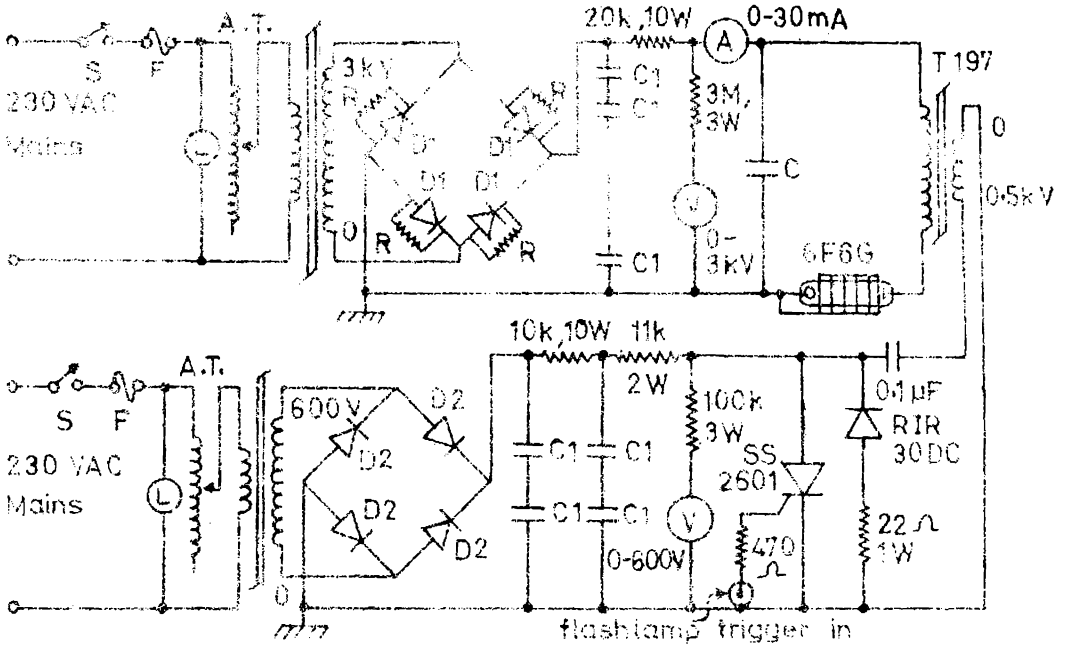

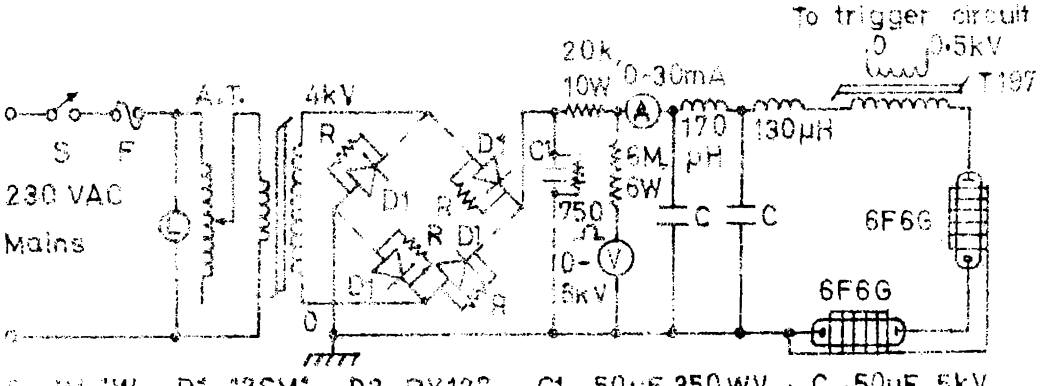

R - 1M, 1W ; D1 - 12SM1 ; D2 - BY127 ; C1 - 50μF, 350 WV ; C - 50μF, 5kV
A - auto transformer

[illegible] FLASHLAMP DRIVE CIRCUIT

$$C^3 = 2E_o \alpha^4 T^2/K_o^4 \quad .. 5.4$$

$$L = T^2/C \quad .. 5.5$$

$$V_o = (2E_o/C)^{\frac{1}{2}} \quad .. 5.6$$

where C - Capacity in farads

E_o - Stored energy in Joules

T - One-third of the desired pulse width in seconds

K_o - the impedance parameter in ohms . $(\text{amperes})^{\frac{1}{2}}$

L - inductance of the discharge circuit in henries

V_o - initial voltage on capacitor bank

α - the damping parameter of the discharge circuit (for a critically damped discharge $\alpha = 0.8$).

In a given situation the desired energy input and pulse width are chosen. Using 5.4, 5.5 and 5.6, C, L and V_o are found. The equations for the determination of other important parameters like peak current, peak power density, one shot explosion energy, inside wall load and expected life are given in Tables 5.2A and 5.2B along with the optimised circuit parameters calculated for the 6F6G single flashlamp and two flashlamps in series circuits. Usually, in order to achieve a lifetime of 10^6 pulses,[37] α has to be around 0.8 and $E_o/E_x = 0.197$. As the pulse width determines the single shot explosion energy (E_x), E_o and other parameters can be found for any desired pulse duration so as to obtain a life in excess of 10^6 shots. But if the system requires more input energy either two flashlamps are to be used in series or those with higher power handling capability selected.

TABLE - 5.2A.

OPTIMISATION OF FLASHLAMP DISCHARGE CIRCUIT PARAMETERS.

	Formula	Single Flash - lamp	Two lamps in series	Unit
Lamp designation	6F6G			
Bore diameter (d)	6			mm
Arc length (l)	6			inches
Gas	Xenon			
Pressure	450			Torr
Inside wall area(s)	Π dl	28.7	57.4	Sq.cm.
Cross section area(A)	$\Pi d^2/4$	0.28	0.28	Sq.cm.
Volume (V)	$\Pi d^2 l/4$	4.31	8.62	c.c.
Lamp impedance (K_o)	1.472 l/d	32.5	65	Ohm $Amp^{\frac{1}{2}}$
Input energy (E_o)	$K_o^4 C^3/2\alpha^4 T^2$	100	648.3	Joules
Pulse width (t=3T)	$3 (LC)^{\frac{1}{2}}$	134	550	micro.sec
Pulse Rep.rate(R)		2	0.1667 (10 ppm)	pulses/sec
Capacitance (C)	$C^3=\frac{2E_o\alpha^4 T^2}{K_o^4}$	50	100	MFD
Inductance (L)	T^2/C	40	336.1	µH
Voltage (V_o)	$(2E_o/C)^{\frac{1}{2}}$	2000	3600	Volts

TABLE - 5.2B

OPTIMISATION OF FLASHLAMP DISCHARGE CIRCUIT PARAMETERS.

	Formula	Single Flash - lamp	Two lamps in series	Unit
Circuit impedance(Z_o)	$(L/C)^{\frac{1}{2}}$	0.9	1.833	Ohms
Peak current(I_{peak})	$0.497V_o/Z_o$	1138.7	976.15	Amps.
Peak current density	I_{peak}/A	4029	3486.25	Amps/cm.^{2}
RMS current (I_{rms})	$0.707\ I_{peak}.$ $(3R\sqrt{LC})^{\frac{1}{2}}$	13	6.6	Amps.
Init. Rate current rise	V_o/L	50	10.7	Amps./μs
Peak power (P_{peak})	$E_o/3T$	1249	1178.7	kW
Average power (P_{av})	E_oR	200	108.04	Watts
Peak power density	P_{peak}/V	290	136.74	kW/cc
Ave. power density	P_{av}/V	46.4	12.54	Watts/cc
1 shot explosion energy (Ex)	$K_eT^{\frac{1}{2}}$	1504	2978.8	Joules
Fraction of explosion energy (F)	E_o/Ex	0.07	0.217	
Expected life	$F^{-8.5}$	$>10^6$	0.42×10^6	
Inside wall load	P_{av}/s	7	1.88	Watts/cm.^{2}
Alpha (α)		0.77	0.8	
Pulse width at 70 %	$2\ (LC)^{\frac{1}{2}}$	89.3	366.7	μs

When α is less than the optimum value, current reversal occurs, resulting in increased bombardment of the cathode and hence, the reduction in lamp life. It is also important not to exceed the peak and r.m.s. current ratings of the series trigger transformer. When the peak current exceeds the rated value, lifetime is reduced due to acceleration beyond acceptable limits of the ablation wall material inside the lamp and from the sputtering of the electrode material on to the envelope walls.

The output of the 3 kV, 20 mA step up transformer is rectified by a full wave bridge (Fig. 5.6). The arms of the bridge comprise of three 12 SM1 diodes with 1M, 1W resistors across each. The output is filtered by a capacitor formed by connecting eighteen 50 MFD, 350 WV, capacitors in series. The charging time of the PFN is decided by the RC value. The energy storage capacitor (50 MFD, 5 kV) was supplied by M/s. Madhav Capacitors, Pune. The saturated inductance (40 μH) of the secondary of the series trigger transformer (T 197 ILC Model) provides the needed current limitation. When the SCR connected to the primary of T 197 fires, 1 MFD, 600 V capacitor discharges and a trigger pulse of magnitude determined by the SCR voltage is generated. T 197 steps up 500 V pulse to 18 kV. It should also be noted that for reliable triggering of flashlamps a ground reference, usually in the form of a 20-30 SWG copper wire wound over the lamp envelope, is needed.[33]

In the circuit with two flashlamps, because of the capacity being larger, the PFN consisted of two meshes as shown in Fig. 5.7.

The number of meshes (n) needed for the network, was determined by the limitations on the risetime of the current pulse[28] and is governed by the relation,

$$t_r = (LC)^{\frac{1}{2}}/n \qquad .. 5.7$$

The total inductance and capacitance value divided by n gives the L and C values per section. Inductance per mesh in this circuit was 168 μH and capacitance per mesh was 50 μF. As the trigger transformer secondary winding (40 μH) was coming in the discharge circuit, an inductance of 128 μH was only needed there. These inductances were made by winding 18 SWG Super Enamelled Copper wire. The number of turns (N) required for an aircore inductor (L μH) is given by

$$N^2 = L(9a + 10b)/a^2 \qquad .. 5.8$$

where a and b are respectively the diameter and length of the tube in inches. A PVC tube with a = 1.87" was used for making the inductance. The number of turns needed for 170 μH and 130 μH were 110 and 86 respectively and were wound over a length of 9" and 7" respectively.

The output pulse shapes were recorded for the single flashlamp circuit and the two flashlamps in series circuit and are shown in Figs. 5.8 and 5.9 respectively. Fig. 5.8 was recorded using a PMT (EMI Model 9684 QB) with all dynodes connected to anode and grounded through a 10 k resistor. Anode to cathode voltage was 100 V and the output was stored on a 100 MHz Tektronix Oscilloscope (Model 466 DM44) and photographed using C-30P

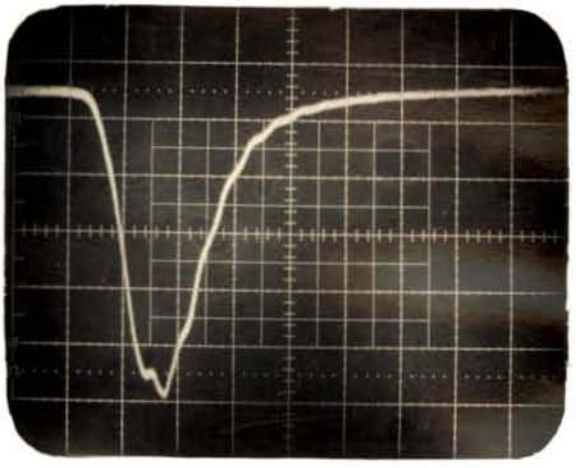

FIG. 5.8 SINGLE FLASHLAMP CIRCUIT OUTPUT PULSE SHAPE

WITH E_{in} = 126 J

SWEEP SPEED : 50 us/DIV.

GAIN : 2 V/DIV.

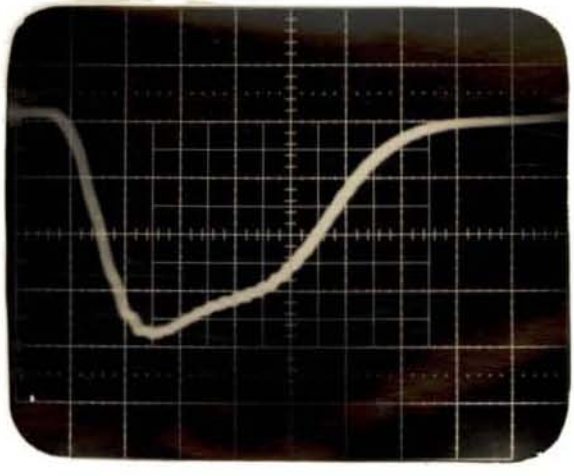

FIG. 5.9 DOUBLE FLASHLAMP CIRCUIT OUTPUT PULSE SHAPE

WITH E_{in} = 200 J

SWEEP SPEED : 0.1 ms/DIV.

GAIN : 10 mV/DIV.

Polaroid camera. Fig. 5.9 was recorded using a Hewlett Packard hp 2 - 4207 photodiode with a 50 ohm load. The pulse widths taken respectively from Fig. 5.8 and Fig. 5.9 are 250 μs and 650 μs at the base and 55 μs and 300 μs at the 70 % point. The rise-time of the current pulse from 10 % to 80 % level for the single mesh network is about 60 μs at 200 Joules and for the double mesh network it is about 100 μs at 450 Joules. These values are relatively tolerable [28] and has not caused any appreciable electrode sputtering or quartz envelope crazing in the present system.

5.4 ALIGNMENT OF THE LASER CAVITY.

The procedure[39-41] chosen for aligning the optical components of the laser cavity depends basically on the type of mirrors chosen. As plane mirrors were used in the present system a high degree of accuracy in alignment was needed. Fig. 5.10 shows the alignment technique utilised. The E-O modulator and the Glan Thomson Polariser used in the Q-switched mode are also shown in the same figure. The He-Ne laser beam reflected by the rear and front mirrors are made to fall one over the other on the pinhole by slowly adjusting the micrometer screws on the mirror mounts. When the mirrors get exactly aligned the two spots coincide and a circular fringe pattern is observed with the pinhole at the centre. All the other optical components are kept slightly tilted away from the lasing axis to avoid reflections back into the cavity.

5.5 PERFORMANCE EVALUATION.

The set up for the measurement of the output energy and pulse

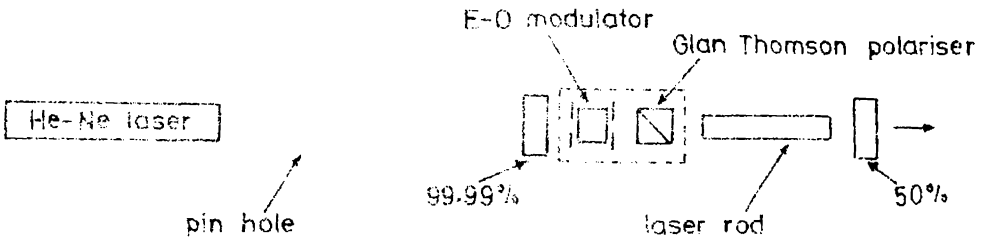

. 5.10 LASER

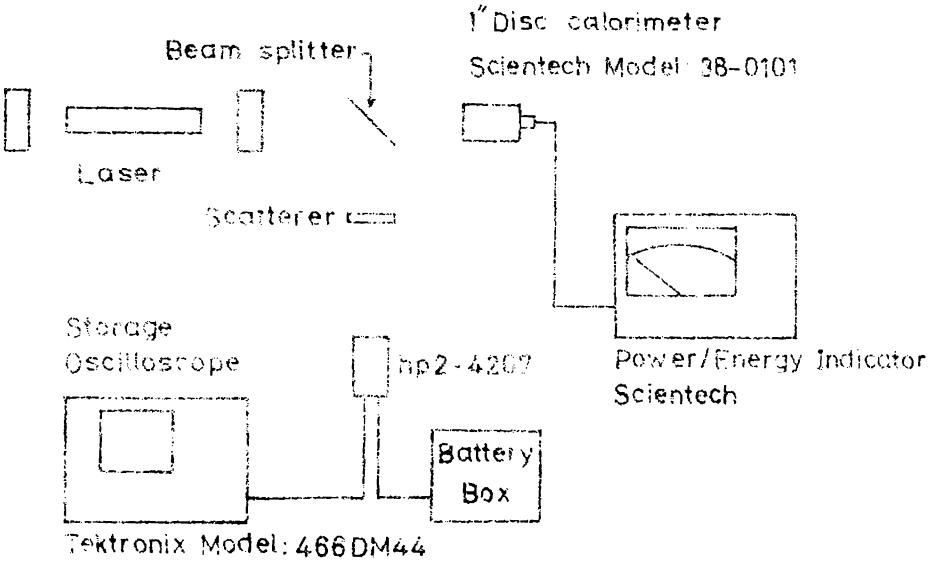

FIG. 5.11 OUTPUT ENERGY AND

width of the laser emission is shown in Fig. 5.11. The detector used was either a PMT (EMI Model 9684 QB) modified to work as a photo tube with V_{k-d_1} = 100 V and R_L = 10 k or a photodiode (Hewlett Packard Model hp2 - 4207) with a bias voltage of 20 V and R_L = 50 Ω . Typical traces recorded with the laser operated in the pulsed (conventional) mode for one and two flashlamp discharge circuits are shown in Figs. 5.12A and 5.12B respectively. The spiking behaviour exhibited is due to the relaxation oscillations taking place inside the cavity. The variation in output energy and pulse width measured at the base with input energy are shown in Figs. 5.13 and 5.14 for the single flashlamp circuit and in Figs. 5.15 and 5.16 for the double flashlamp circuit.

5.51 ESTIMATION OF THE OPTICAL LOSSES AND PUMPING COEFFICIENT.

From Fig. 5.13 and Fig. 5.15 it is seen that the threshold energy is smaller for the 50 % reflecting mirror. Measuring the threshold values for two different mirror reflectivities, the total optical losses in the resonator (L) and the pumping coefficient (K) can be determined using the relation,[28]

$$L = \frac{P_{th}'' (\ln R_1') - P_{th}' (\ln R_1'')}{P_{th}'' - P_{th}'} \quad .. 5.9$$

and

$$K = \frac{\ln (R_1' / R_1'')}{2(P_{th}'' - P_{th}')} \quad .. 5.10$$

where P_{th}' and P_{th}'' are the threshold input powers or the threshold input energies for mirrors of reflectivities R_1' and R_1'' respectively

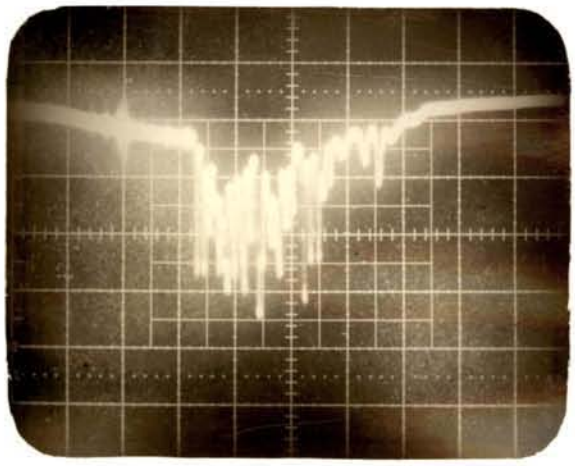

FIG. 5.12A CONVENTIONAL MODE LASER OUTPUT STRUCTURE WHEN PUMPED USING A SINGLE FLASHLAMP (R_1 = 0.4 AND E_{in} = 225 J)

SWEEP SPEED : 20 us/DIV.

GAIN : 0.2 V/DIV.

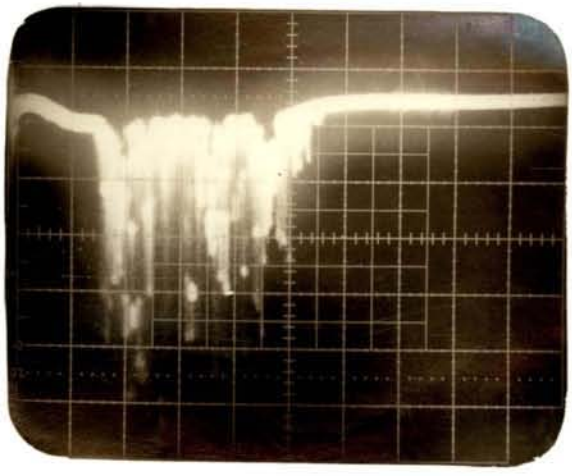

FIG. 5.12B CONVENTIONAL MODE LASER OUTPUT STRUCTURE WHEN PUMPED USING TWO FLASHLAMPS (R_1 = 0.4 AND E_{in} = 450 J)

SWEEP SPEED : 0.1 ms/DIV.

GAIN : 10 mV/DIV.

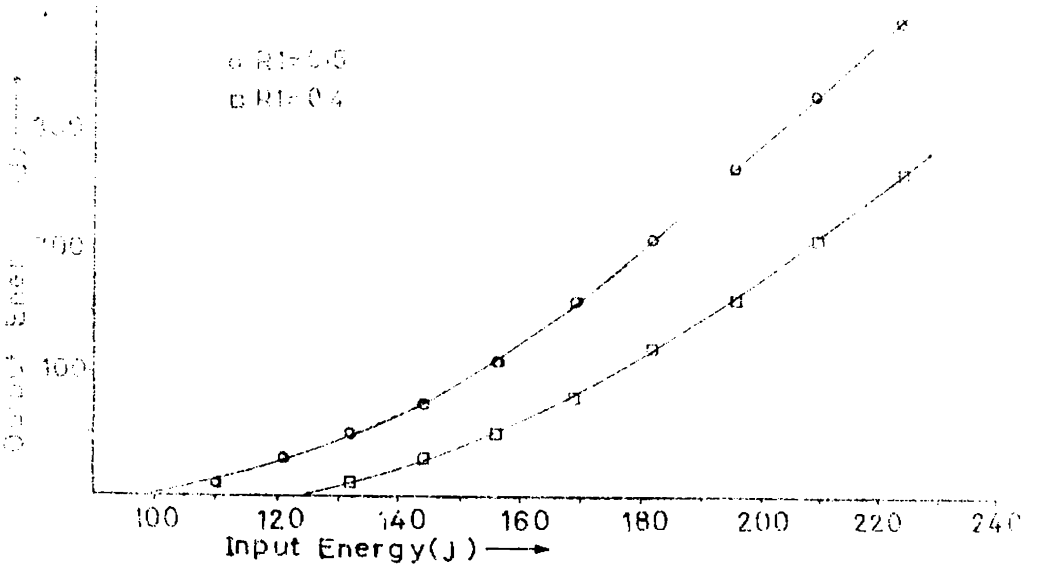

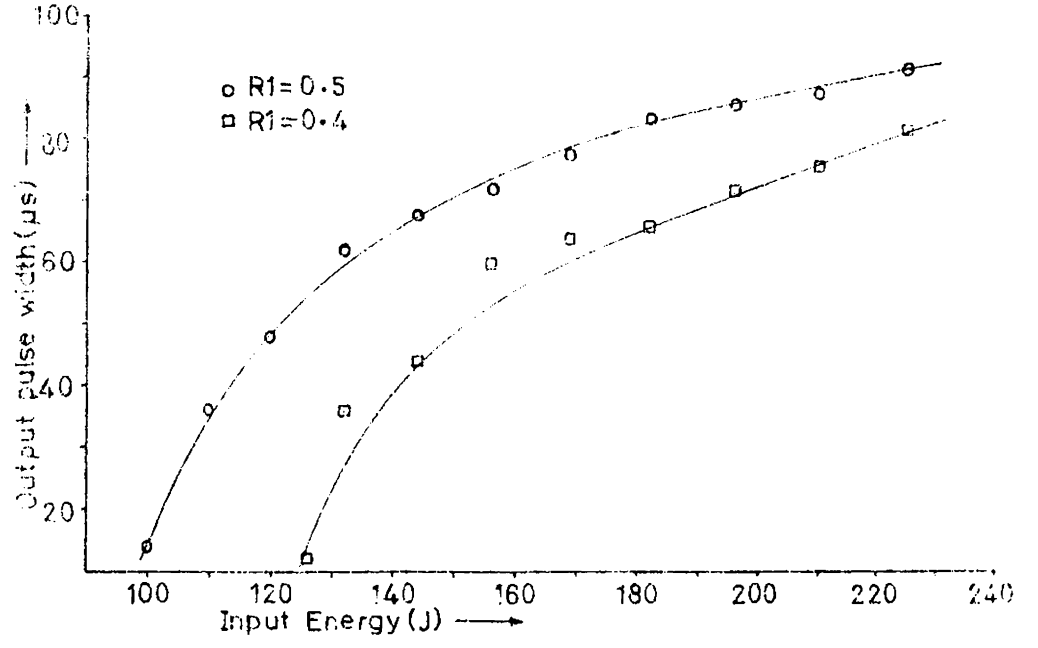

5.14 LASER PULSE WIDTH (AT BASE) VARIATION WITH INPUT ENERGY FOR THE ELLIPTICAL CYLINDRICAL PUMP SYSTEM

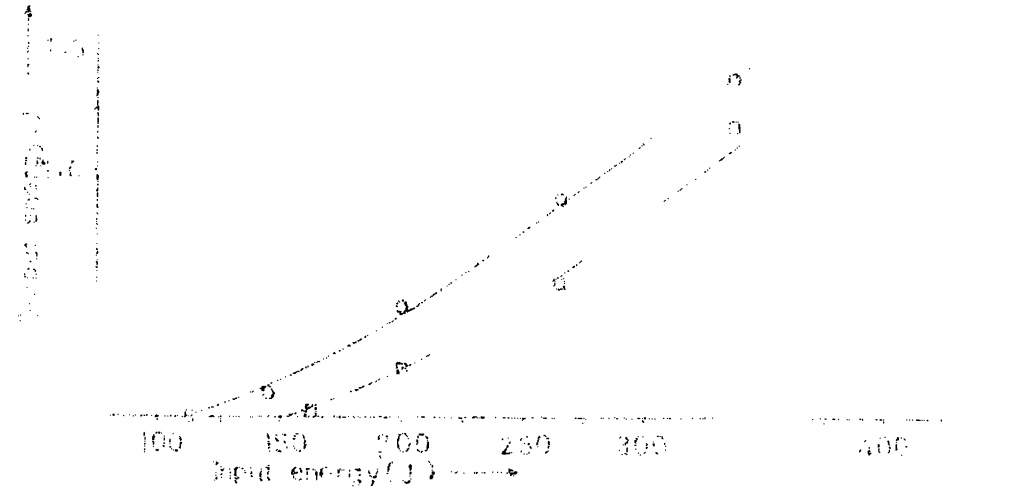
100
150
200
250
300
400
Input energy(J) ——→

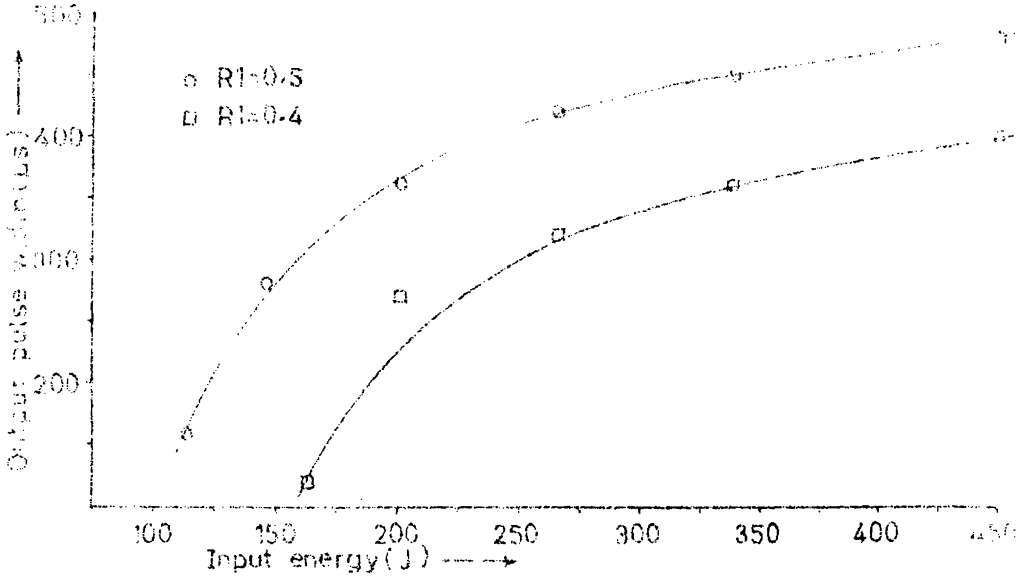
R1=0·5
R1=0·4
200
400
100
150
200
250
300
350
400
Input energy(J) ——→

The threshold input energies, pumping coefficients, slope efficiencies, etc., obtained in the present study are listed in Table 5.3 along with the results obtained by Koechner.[28] With the pumping coefficient (K) known, the small signal single pass gain of the laser rod (G_o) and the gain coefficient (g_o) are determined using[28]

$$\ln G_o = g_o l = K P_{th} = K E_{th} \qquad .. 5.11$$

where l is the length of the laser rod in cm.

The values of G_o and g_o determined using 5.11 are plotted as a function of input energy in Fig. 5.17. For a lamp input of 1000 Joules, Koechner obtained a value of 0.07 cm^{-1} for g_o and 2.9 for G_o. From Fig. 5.17, knowing the threshold input energy the percentage of inversion of the total ground state population and the total fluorescence output at threshold can also be determined.[28]

5.52 MEASUREMENT OF DIVERGENCE.

The divergence of the laser beam was measured by recording the burn patterns on a photographic film at the exit mirror and at a distance of 370 cm. With the 100 μF capacitor bank charged to 2.8 kV and fired, the beam had a diameter of 6 mm and 8 mm at the two points of observation. This gives a full angle divergence of 0.0094 mrad.

5.6 ELECTRO-OPTICALLY (E-O) Q-SWITCHED LASER.

In the E-O Q-Switched laser designed to operate in the Quarter-wave mode, the optical components are arranged as shown in Fig. 5.10. The fabricated system is shown in Fig. 5.18.

TABLE 5.3

PUMPING COEFFICIENTS AND RESONATOR LOSSES.

Laser rod	Pumping chamber	Mirror reflectivity	Input energy at threshold $E_{th}(J)$	Slope efficiency	Pumping coefficient $K(J^{-1})$	Optical losses in the resonator (L)
152.4 mm x 6mm dia. Hoya LSG 91H (Present work)	elliptical cylindrical	0.50	100	3.17×10^{-3}	4.29×10^{-3}	0.165
		0.40	126	2.7×10^{-3}		
	double circular (close cou coupled)	0.50	110	6.47×10^{-3}	2.23×10^{-3}	0.202
		0.40	160	6.72×10^{-3}		
150 mm x 10 mm dia. Owens Illinois ED-2 Glass(Koechner's data [28])	double elliptical	0.60	340	17×10^{-3} (typical)	1.11×10^{-3} (graphical)	0.21 (graphical)
		0.45	460			

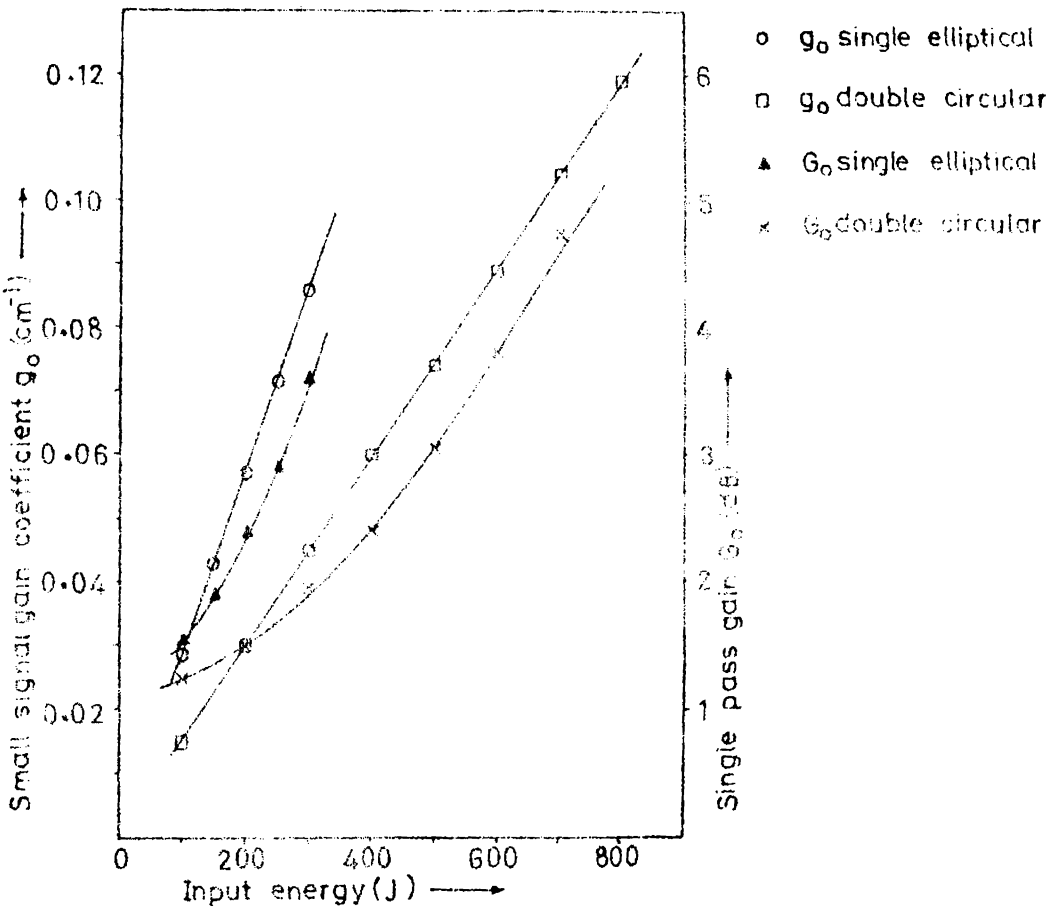

FIG. 5.[illegible] SMALL SIGNAL GAIN COEFFICIENT AS A FUNCTION OF INPUT ENERGY

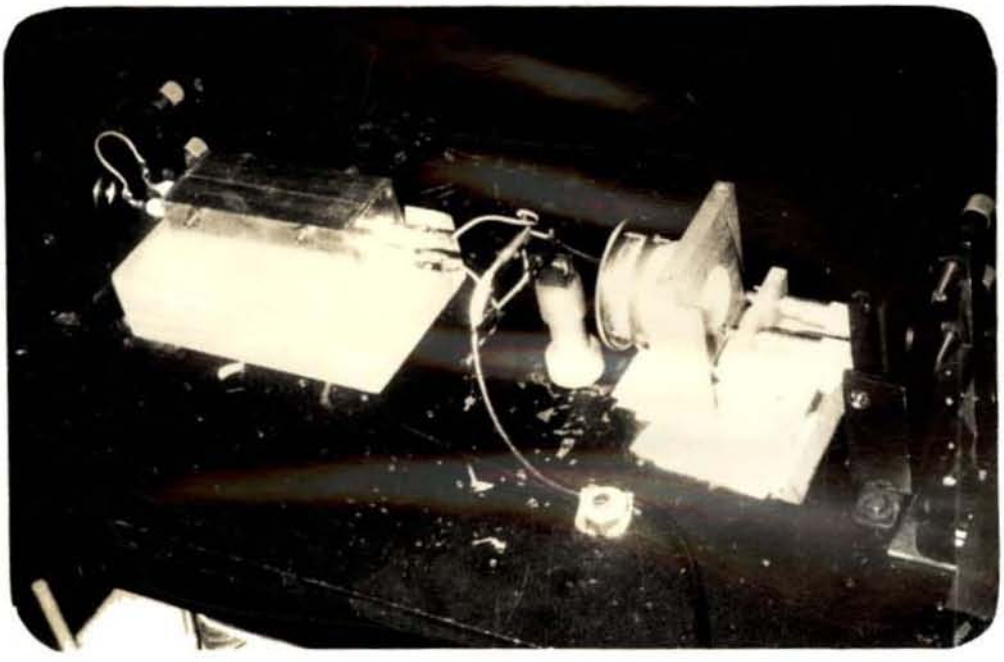

FIG. 5.18 E-O Q-SWITCHED GLASS LASER

FIG. 5.32 DYE Q-SWITCHED GLASS LASER

The pockels cell - Glan Thomson polariser (Karl Lambrecht, [redacted] combination[42] does the Q-Switching process. The Pockels cell[43] consists of an electro-optic crystal[44] kept between two electrodes. These crystals lack a centre of point symmetry and becomes birefringent when an electric field is applied. The longitudinal mode of operation is utilised here. The crystal is oriented with its optic axis along the direction of the beam and the electric field. In this mode, the voltage required to obtain a phase shift of $\Pi/2$ is given by

$$V\ \lambda/4 = \frac{\lambda}{4\ n_o^3\ \gamma_{63}} \qquad .. 5.12$$

where λ is the wavelength of operation, n_o is the ordinary index of refraction and γ_{63} is the only independent electro-optic coefficient which describes the changes in ellipsoid when a longitudinal field is applied to the crystal.

Hence, when a voltage of magnitude $V\ \lambda/4$ is applied on the Q-Switch during the flashlamp pulse, the linearly polarised light incident on it emerges out circularly polarised. The direction of rotation of this beam is reversed on reflection at the mirror and as it passes once again through the crystal becomes linearly polarised but at 90° to the incident direction of polarisation. So this radiation is ejected out of the cavity by the polariser. When the voltage applied on the crystal is switched off, the linearly polarised beam traverses the E-O element without any birefringence or phase shift and a Q-switched pulse is emitted.

5.61 DESIGN OF THE E-O Q-SWITCH.

A schematic diagram of the Q-switch assembly is shown in Fig. 5.19. A 1" x 1" x $\frac{1}{2}$" KDP crystal, supplied by BARC Technical Physics Division, Bombay, cut with faces (1" x 1") perpendicular to the optic axis (Z-axis) and with a length of $\frac{1}{2}$" in the Z direction was used. The two faces perpendicular to the Z-axis (X-Y planes) were polished on a bees-wax lap and etched using ethylene glycol.[45] The crystal was kept pressed between two flat circular copper electrodes which had an aperture of 6 mm dia. and the whole assembly was kept immersed in silicone fluid. The leads connected to the electrodes were taken out using a co-axial cable. The nylon casing which was fabricated in two pieces, was bolted together with a teflon rope seal to prevent the oil from leaking out. In case of minor leaks, there was provision for refilling it. The quartz windows were sealed on to the nylon casings using Araldite. This Q-switch was found to have a capacitance of 15 pF.

5.62. MEASUREMENT OF HALF WAVE VOLTAGE AND EXTINCTION RATIO.

The extinction ratio is defined as the ratio of maximum to minimum transmitted intensity obtained between crossed polarizers as the applied voltage is varied through a half-wave voltage. The set up for the measurement of extinction ratio is shown in Fig.5.20. The He-Ne laser beam was made to propogate along the optic axis of the crystal. The alignment of the optic axis was accomplished by inserting a scatterer between Polariser 1 and the Q-switch and rotating Polariser 2 to visualize the Maltese-cross pattern on a

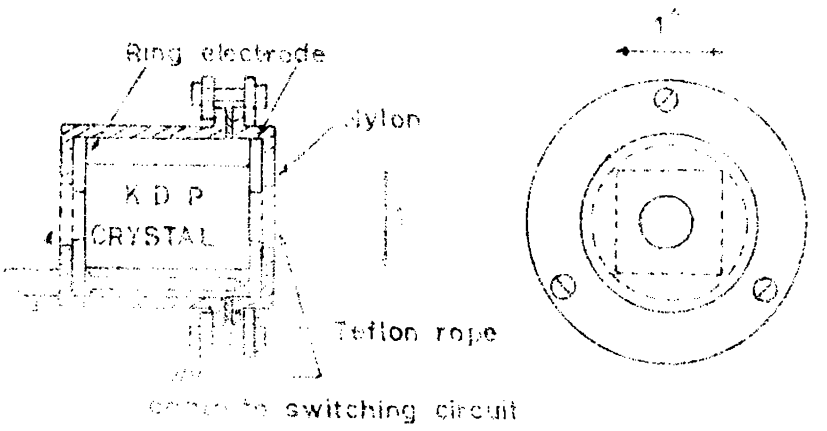

E-O Q-SWITCH ASSEMBLY

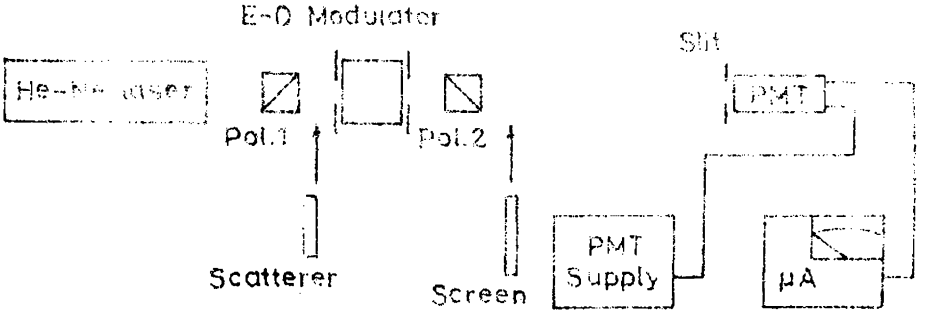

SETUP FOR THE MEASUREMENT OF EXTINCTION RATIO AND HALF WAVE VOLTAGE

screen kept between the PMT and the Polariser 2. Now, the He-Ne spot was made to coincide with the centre of the cross pattern. The modulator bias was increased to 9 kV in steps of 1 kV and then decreased and the PMT output current was noted. Net current at any voltage was determined by substracting the ambient value from the mean value of current for that voltage. Dividing the current value at any particular voltage by the value without bias on the modulator, the extinction ratio was obtained. Fig. 5.21 is a plot of the modulator extinction ratio with voltage. The polarisers were now made parallel without the Q-switch and the maximum output current was noted. Using this maximum current reading, the percentage of transmission for various bias voltages were calculated and plotted in Fig. 5.22 along with the output current values obtained in the crossed position.

The transmission curve was found to peak around 9 kV. This value of voltage can be taken as the half-wave voltage for 632.8 nm. From this value, assuming a linear variation of half-wave voltage with wavelength, the quarter-wave voltage at 1.06 μm was found to be 7.5 kV. At this voltage, the Q-switch has an extinction ratio of 130 (Fig. 5.21). Usually, a turn off ratio better than 100 : 1 is needed for efficient Q-switching.[18]

5.63 Q-SWITCHING CIRCUIT.

The commonly used switching circuits utilise vacuum tubes, cold cathode tubes, thyratrons, SCR's or avalanche transistors, as the switching element. Usually the voltage to be switched ranges

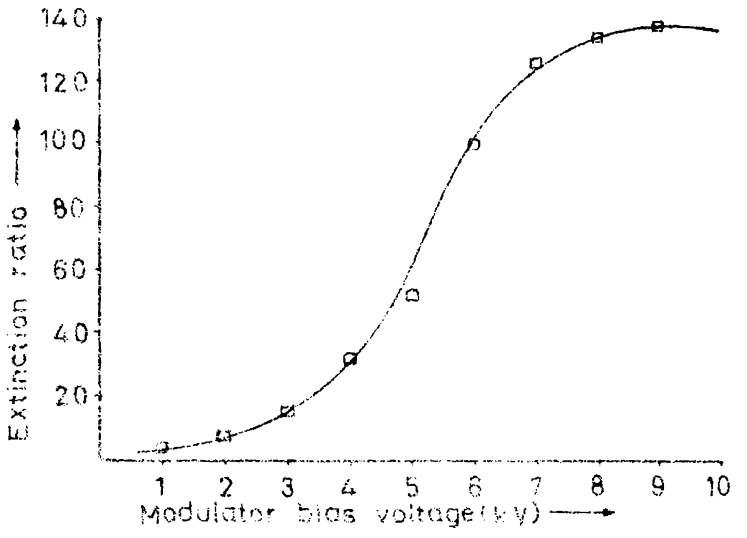
140
120
100
80
60
40
20
Extinction ratio
1 2 3 4 5 6 7 8 9 10
Modulator bias voltage (kV)

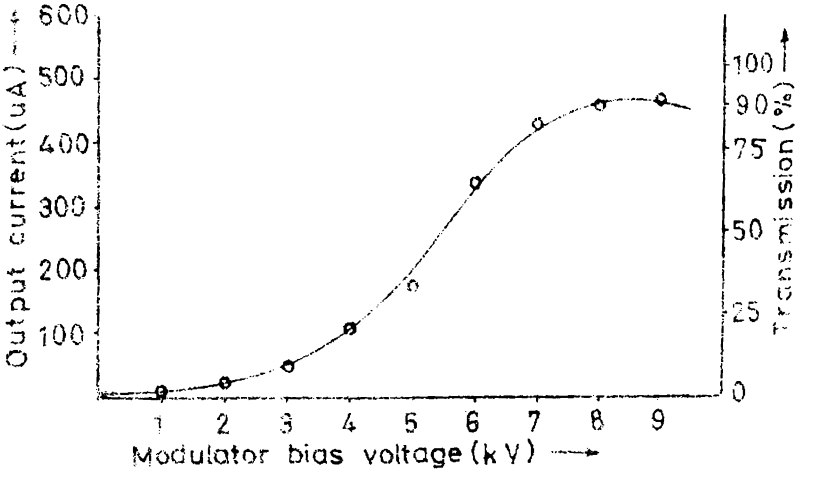
600
500
400
300
200
100
Output current (uA)
100
90
75
50
25
0
Transmission (%)
1 2 3 4 5 6 7 8 9
Modulator bias voltage (kV)

between 3 kV and 10 kV depending on the crystal and the wavelength. The switching time is dertermined by the type of switching. Krytrons circuits have very fast switching time but the lifetime of the tube is limited. If switching speed is not critical SCR circuits can be used to obtain switching times upto 250 ns.[46] But, higher switching speed (a few ns) and longer life can be achieved by using simple spark gaps as the switching element.[47,48] The initiation of these shutters can either be electrical or optical. For reliable as well as precise timing of the output pulse, electrical rather than optical triggering schemes are more suited.

Fig. 5.23 shows the circuit designed and built into the present system. The spark gap was pressurised (upto 4 atmospheres) by feeding N_2 gas from the gas cylinder through a needle valve. The fabrication details of the spark gap are given in Fig. 5.24. The electrodes were made of aluminium and were hemispherical. The trigger pin used was a Kanthal wire inserted through a glass capillary which in turn was inserted through the hole at the centre of the grounded electrode. The other electrode was connected to the 10 kV supply through a high voltage cable and to the Pockels cell through a RG 58 coaxial cable. The Pockels cell was charged to the required voltage through the 20 k resistor. When the spark gap fires, the energy stored in this capacitor (Pockels cell) is discharged through the RG 58 transmission line in about 1 ns. The line impedance was matched to the load by putting a 50 ohm resistor at the load end. Because of this, the discharge current

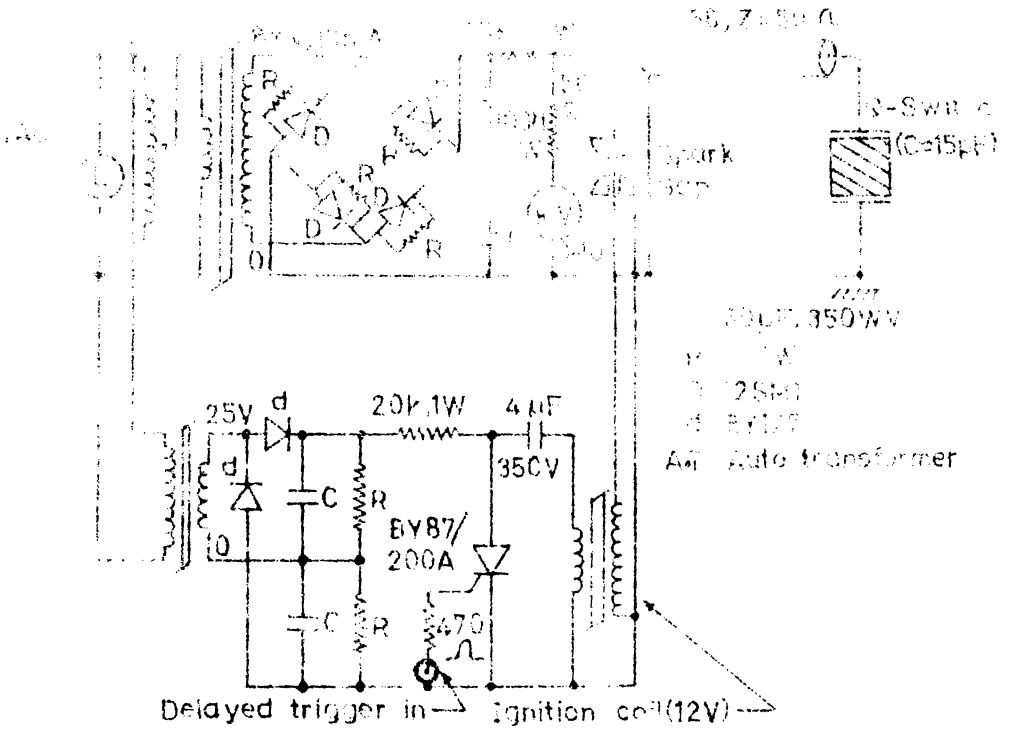
25V
d
20k 1W
4 μF
350V
C
R
BY87/
200A
470
Delayed trigger in
Ignition coil (12V)
Auto transformer

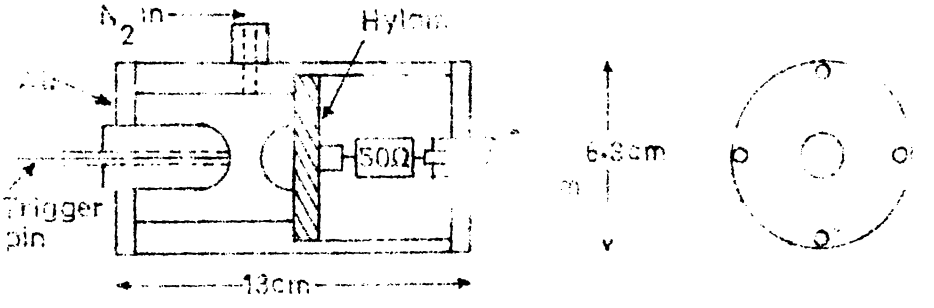
N_2 in
Hylon
500Ω
Trigger
pin
13cm
6·3cm

will be a single rectangular pulse of amplitude $I_1 = V_o/2\ Z_o$ and duration $T = 2d$ (V_o is the initial voltage on the transmission line and d is the one way transmission time of the line). Mismatching of the load introduces a series of steps into the transient discharge due to reflections.

The high voltage pulse for triggering the spark gap was generated by the SCR (16 Amp., 200 Volts PIV) connected to the primary of the 12 V ignition coil. The 4 uF capacitor charged to about 70 Volts by the output of the full wave voltage-doubler gets discharged when the SCR is triggered by the delayed output of the rate generator.

5.64 RATE GENERATOR AND DELAY CIRCUIT.

The repetition rate of the laser was controlled by a rate generator. In E-O switched lasers two trigger pulses, one for firing the flashlamp and the other for driving the Q-switch, are required. The delay between these two pulses should be adjustable to facilitate optimisation of the output power.

Fig. 5.25 shows the circuit diagram of the rate generator and the delay circuit. The first NE 555 IC connected for astable operation functions as the rate generator with pulse repetition rates of 1,2,3,4,5 and 10 ppm.

The 2 μF capacitor (C) is charged through the 50 ohm resistor (R_B) and the resistance (R_A) selected by the repetition rate selector switch, until the capacitor voltage exceeds 2/3 V_{cc} and is then discharged through R_B until the capacitor voltage is just less

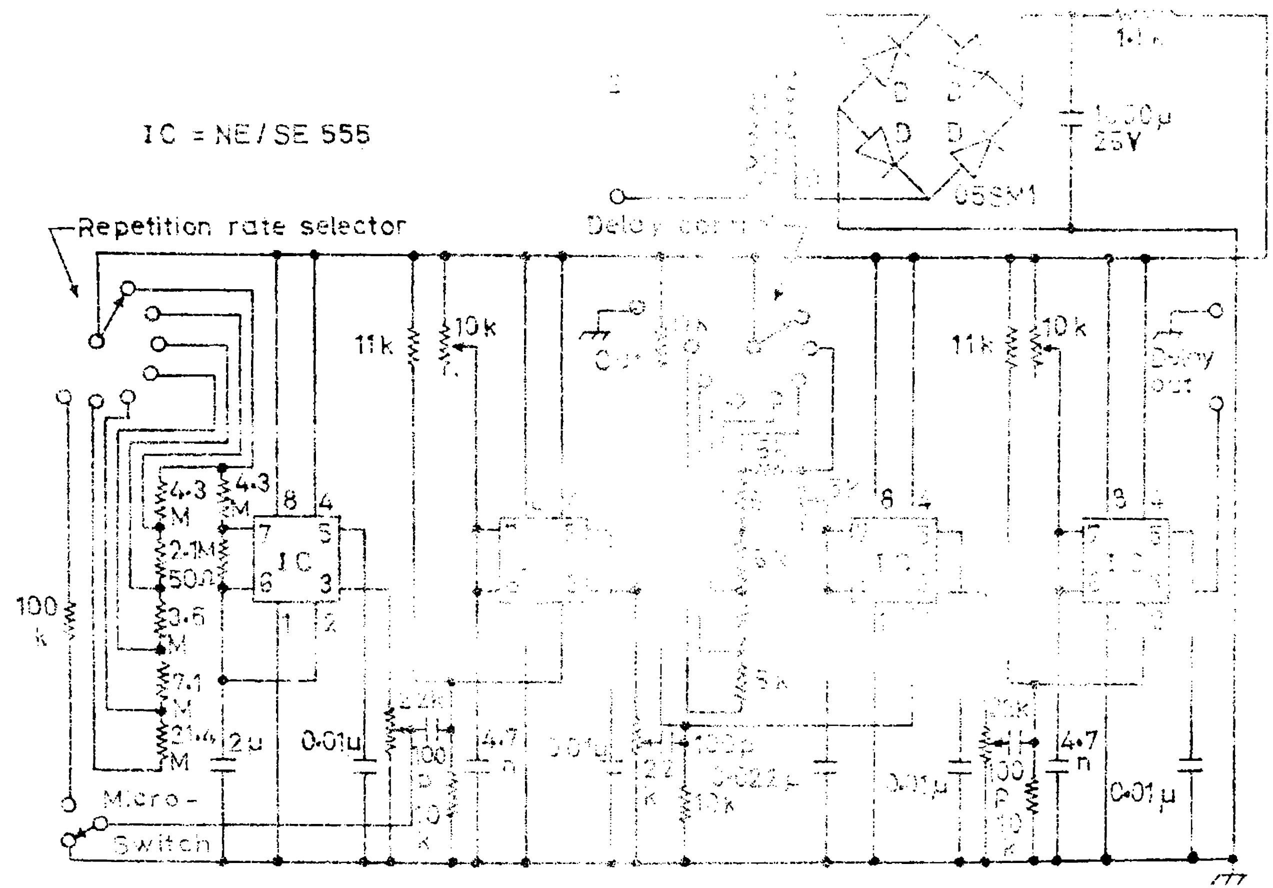
IC = NE/SE 555
Repetition rate selector
Micro-
Switch
100 k
4.3 M
4.3 M
2.1M
50Ω
3.6 M
7.1 M
21.4 M
2μ
0.01μ
IC
8
4
7
5
6
3
1
2
11 k
10 k
4.7 n
100 p
10 k
0.01μ
0.022μ
5 k
D
05SM1
1.1 k
25V
Delay out
Out

FIG. 3.25 RATE

than 1/3 V_{cc}. The charge (output high) and discharge (output low) times are given by $T_1 = 0.693\ (R_A + R_B)\ C$ and $T_2 = 0.693\ R_B\ C$ respectively. The total period and duty cycle are given by $T = 0.693\ (R_A + 2R_B)\ C$ and $D = (R_A + R_B)/(R_A + 2R_B)$ respectively. Since $R_B \ll R_A$ this timer has a duty cycle of nearly 100 %.

The second, third and fourth NE 555 timers operate in the monostable mode. Suitable resistances are connected from pin 2 to V_{cc} and ground to hold the trigger input comfortably above 1/3 V_{cc} in the absence of a trigger pulse applied through the 100 pF capacitor. The time for which the output is in the high state is given by $T = 1.1\ R_c C$, where R_c and C are the charging resistance and the capacitor connected to pins 6 and 7.

The first monostable multi is triggered by the output of the rate generator or the voltage pulse generated by the microswitch (for single shot operation). As these monostable multis are triggered by the trailing edge of the trigger pulses, the output of the fourth timer will be delayed with the output of the second timer by a time determined by the resistance chosen by the delay control and the capacitor connected to pins 6 and 7 of the third timer. The two 10 k pots facilitate independent pulse width control for the output pulses. With the present set up pulse delays continuously variable upto 700 μs were obtained. The output of the second timer was used for triggering the SCR in the flashlamp discharge circuit, while the delayed output was used to trigger the SCR in the Q-switching circuit.

5.65 ALIGNMENT OF THE Q-SWITCH INSIDE THE CAVITY.

It is necessary, for the proper functioning of the Pockels cell, that the optic axis (Z-axis) of the crystal be parallel to the laser beam direction to within $\pm$ 60 arc sec. With the modulator and polariser kept inside the cavity (Fig. 5.10) a He-Ne laser beam is passed through the assembly and the 100 % mirror is aligned. Now, a sheet polariser is inserted between the 100 % mirror and the modulator. Also, a lightly ground glass plate is inserted in the beam near the modulator to have a divergent beam passing through the crystal. The sheet polariser is rotated so that the Maltese cross interference pattern, i.e. a set of circular rings on a cross, is seen on the screen kept between the Glan Thomson polariser and the laser rod. The centre of the cross which corresponds to the direction of the optic axis is made to coincide with the He-Ne laser spot on the screen. If the voltage on the modulator is now raised to its half wave value, the Maltese cross pattern shifts into a hyperbola and the centre of the cross which was earlier dark becomes bright. The line joining the hyperbola foci is adjusted, by tilting the crystal, to make an angle of 45° with the X-Y axes of the crystal. This assures that the electric field of the incident light makes an angle of 45° with the electrically induced X' - Y' axes, or an angle of 0° or 90° with the crystallographic X-Y axes. The output mirror is also aligned by the technique described in 5.4 and lasing is tested.

5.66 OPTIMISATION OF Q-SWITCH DELAY AND BIAS VOLTAGE.

The delay between the firing of the flashlamp and the opening of the Pockels shutter was varied from 240 μs to 480 μs and the output energy was measured using a 1" scientech disc calorimeter (Model 38-0101). The capacitor (100 μF) charging voltage was fixed at 3 kV. The cavity length was 60 cm and the output mirror reflectivity was 50 %. The variation of output energy with delay is shown in Fig. 5.26. It is found that for an input energy of 450 Joules, the optimum Q-switching delay is 380 μs.

Now, the Q-switch delay was set at 380 μs and the input energy at 450 Joules. The modulator bias was varied from 6.8 kV to 8 kV and the output energy was measured. The variation in output energy with Q-switch voltage is plotted in Fig. 5.27. It is seen from the graph that the output energy is maximum around a Q-switch bias voltage of 7.35 kV. This is in good agreement with the values already evaluated (5.62).

5.67 MEASUREMENT OF OUTPUT ENERGY AND PULSE WIDTH.

The Q-switch was biased at its optimum value (7.35 kV) and the delay between the flashlamp firing and Q-switch opening was set at 380 μs. The output energy was measured for different input energies and plotted as shown in Fig. 5.28. At a pump energy of 575 J, a Q-switched pulse of 85 mJ output energy was obtained.

The output pulse width was recorded on a 100 MHz Tektronix Storage Oscilloscope 466 DM 44, keeping a beam splitter in the beam and directing it on to a hp_2-4207 photo diode (R_L = 50 Ω, Bias = 23 V) through a ground glass plate scatterer. The output

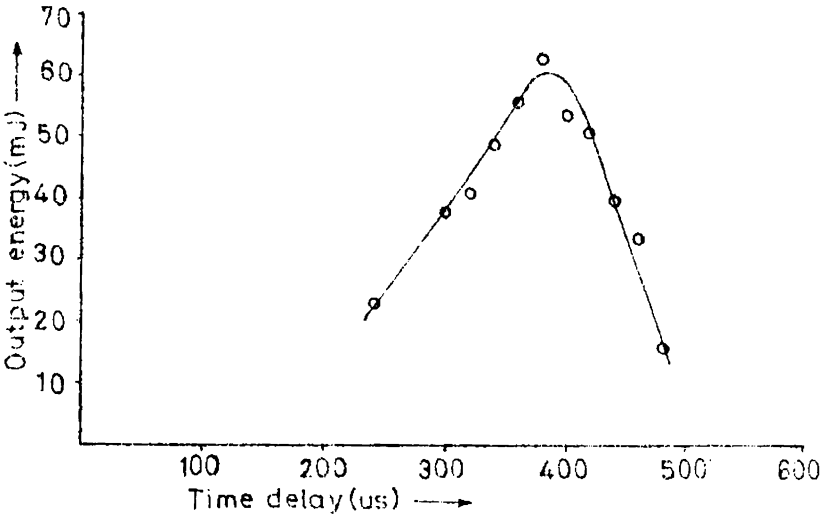

FIG. 5.26 OUTPUT ENERGY VARIATION WITH Q-SWITCHING DELAY

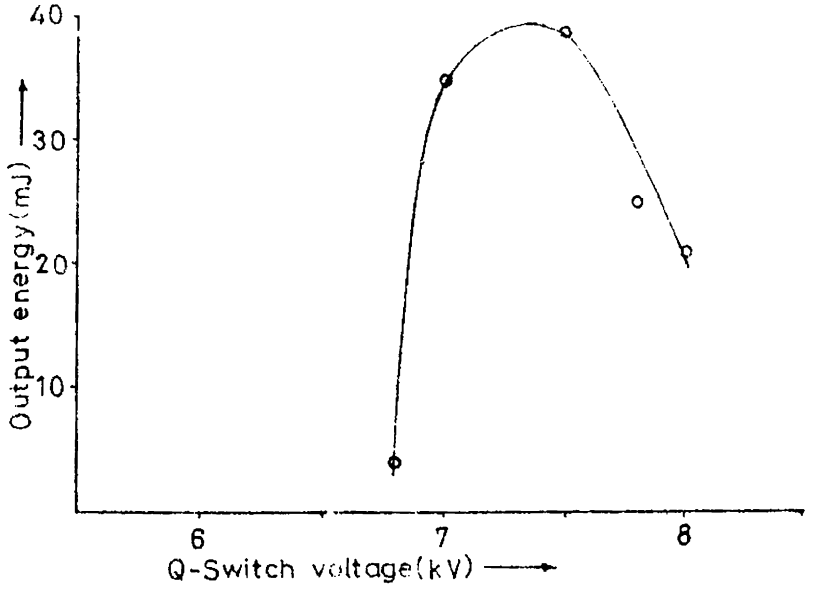

FIG. 5.27 OUTPUT ENERGY VARIATION WITH Q-SWITCHING VOLTAGE

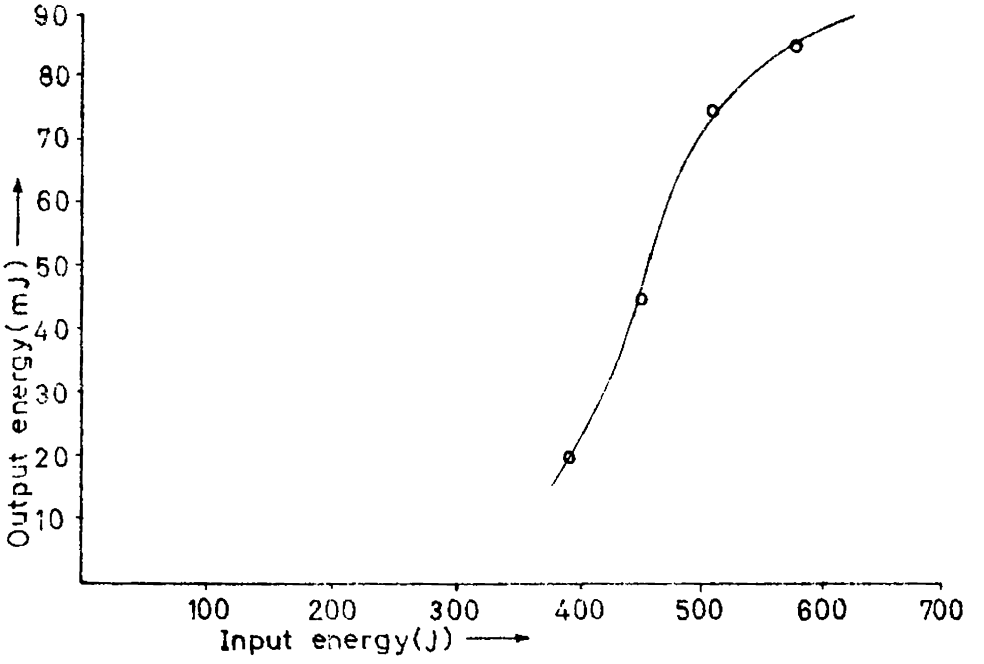

FIG. 5.28 [illegible]

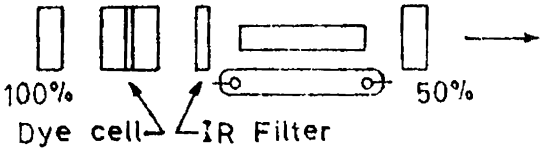

FIG. 5.31 DYE Q-SWITCHED LASER - [illegible]

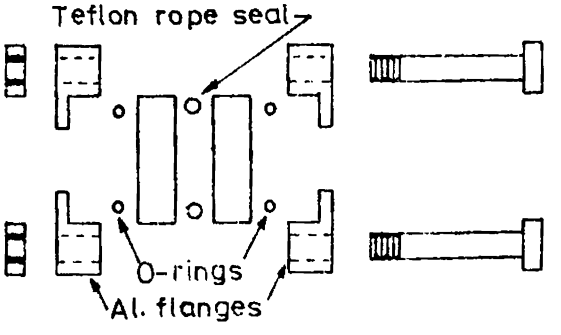

FIG. 5.33 DYE Q-SWITCH - [illegible]

pulse shape recorded at 3.2 kV charging voltage is shown in Fig. 5.29. The modulator bias voltage was 7.6 kV and the Q-switching delay was 380 μs. This delay was verified by looking at the pulse at a very low sweep speed (Fig. 5.30). The Q-switched pulse had a width of 15-18 ns at FWHM and about 40 ns at base. A maximum output energy of 110 mJ was recorded at 3.6 kV. This corresponds to a peak power of about 7.3 MW.

5.7 DYE Q-SWITCHED GLASS LASER.

Passive Q-switches using organic dyes are of great importance because of its simplicity in design and operation.[13,14,49,50] Another advantage is that the emission linewidth is very narrow (0.02 A°, typically). The dye Q-switched laser essentially consists of a dye cell inserted in the cavity as shown in Fig. 5.31. Fig. 5.32 is the experimental set up. The IR filter (1.06 μm transmitting) is to cut off the flashlamp emission from bleaching the dye solution. The bleaching process is essentially the saturation of a spectral transition by absorption of photons emitted from the laser rod.

Only very few dyes (Eastman Kodak 9860, 9740, 14015 and 14617) have been used with neodymium lasers for Q-switching. The solvents used for these dyes are 1,2 - dichloroethane, chlorobenzene, iodomethane, and methyl sulphoxide. The solvent chosen determines the relaxation time of the dye solution. Dyes with shorter relaxation times, of the order of a few ps, tend to mode-lock the output pulse instead of Q-switching and produce pulses in the

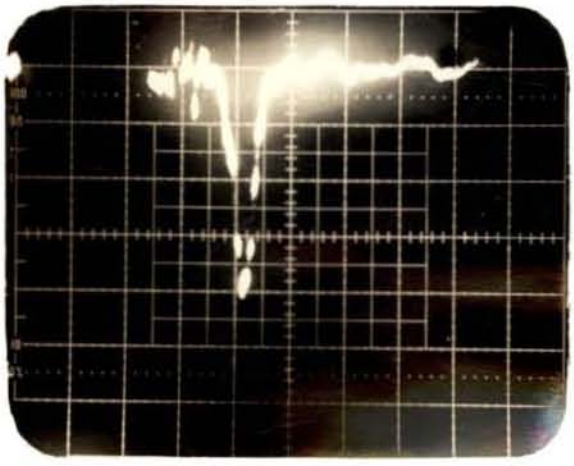

FIG. 5.29 E-O Q-SWITCHED GLASS LASER OUTPUT

SWEEP SPEED : 50 ns/DIV.

GAIN : 0.1 V/DIV.

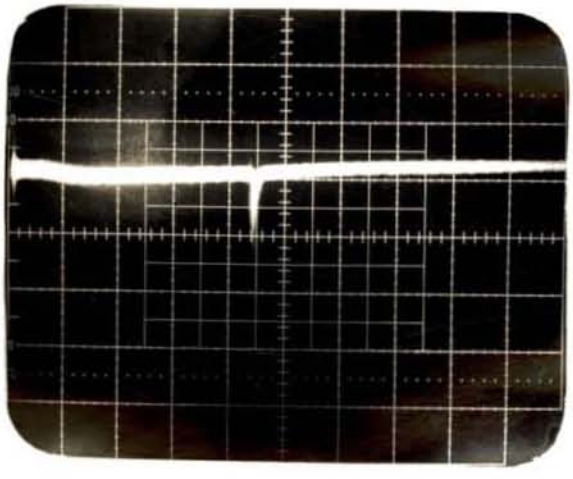

FIG. 5.30 E-O Q-SWITCHED LASER PULSE RECORDED AT REDUCED SWEEP SPEED

SWEEP SPEED : 0.1 ms/DIV.

GAIN : 0.2 V/DIV.

picosecond regime.[52] For efficient Q-switching to take place, the relaxation time has to be greater than or nearly equal to the cavity transit time. In this mode, the output energy and pulse width depends on the dye concentration and the path length of the Q-switch. The saturation power density of the dye solutions is of the order of 50 Mw/cm^2.

5.71 DESIGN OF A SIMPLE DYE Q-SWITCH.

Two fused silica blanks (CVI Laser Corporation, U.S.A.) of $\lambda/20$ surface accuracy (at 1.06 μm) and A.R coated for 1.06 um were held together with a circular teflon seal in between, as shown in Fig. 5.33. Teflon rope was made into a circular ring with edges bend outward and the small gap thus formed was used for filling the Q-switch. When assembled the dye cell had a separation of about 1 mm.

5.72 OPTIMISATION OF Q-SWITCH PERFORMANCE.

Eastman 9860 Q-switch solution diluted with 1-2, dichloro-ethane (Eastman Kodak) was transferred into the dye cell with a syringe. The dye cell and the IR filter were then inserted into the cavity and the laser system was aligned. The Nd-glass laser rod was pumped using a 6F6G Flashlamp in the elliptical cylindrical pumping chamber already described (See 5.31). The laser output pulse shape was monitored with hp_2 - 4207 photodiode (R_L - 50 ohm) coupled to a Model 466 DM 44 Tektronix Storage Oscilloscope. The output energy was simultaneously measured using the Scientech 1" Disc Calorimeter, Model 38-0101.

Dye solution of known transmission was taken in the Q-switch. The input energy into the flashlamp was slowly increased from a low value and lasing action was checked. At a particular input energy, known as the threshold energy, the system started oscillating and a Q-switched pulse was emitted. If, even with very low input energies, the output exhibit spiking behaviour, then it is to be assumed that the dye concentration is very low and bleaching action has occured at very low photon fluxes. In such cases, the % transmission of the dye solution has to be reduced for observing Q-switch action.

As the input energy was increased, the output also increased (Fig. 5.34) and at a certain input energy the output was found to consist of two pulses (Fig. 5.35B). This is due to a second bleaching action that has taken place after the dye molecule had relaxed to its ground level. The delay between the two pulses was about 20 μs. At still higher input energies, tripple pulses (Fig. 5.35C) were also observed. The delay between the second and third pulses was about 12 μs while the delay between the first and second pulses remained the same as in the previous case.

In Fig. 5.34 energy values related only to single pulse operation are plotted for different dye transmissions. The starting point of the curve for each dye transmission is the threshold input energy for Q-switching operation at that optical density. It is seen that as the dye transmission percentage is reduced

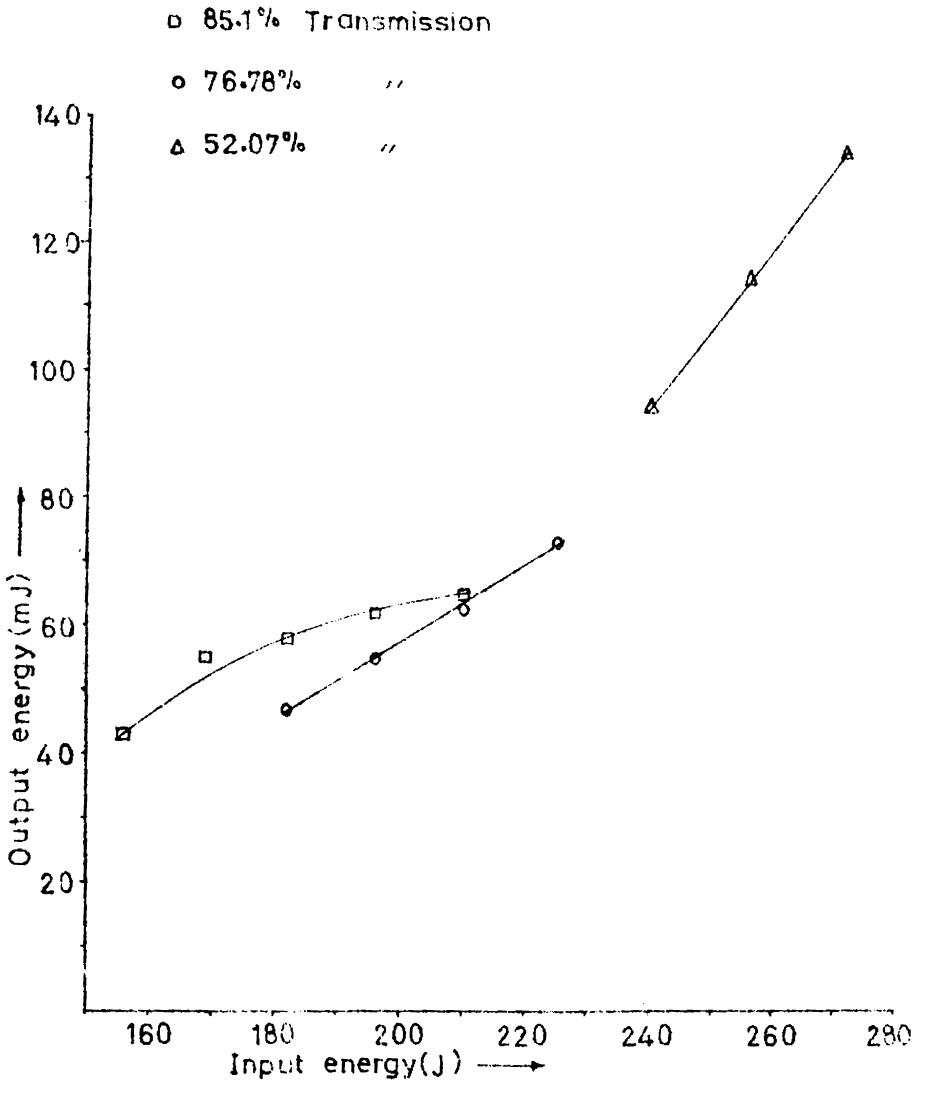
□ 85.1% Transmission
○ 76.78% ″
△ 52.07% ″
140
120
100
80
60
40
20
Output energy (mJ)
160
180
200
220
240
260
280
Input energy(J)

(A)

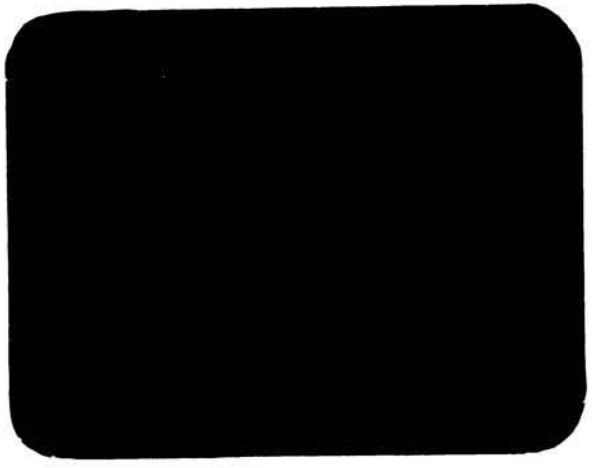

(B)

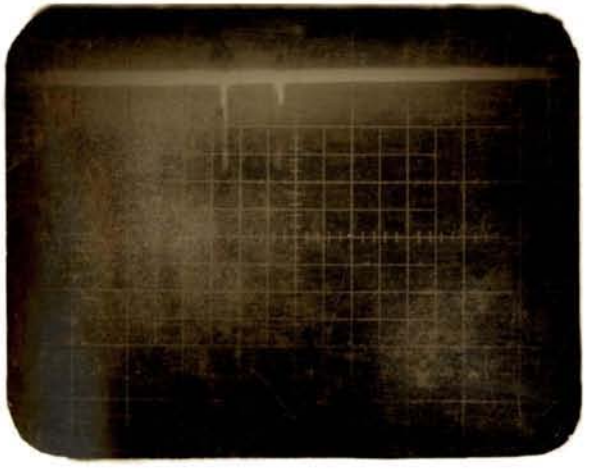

(C)

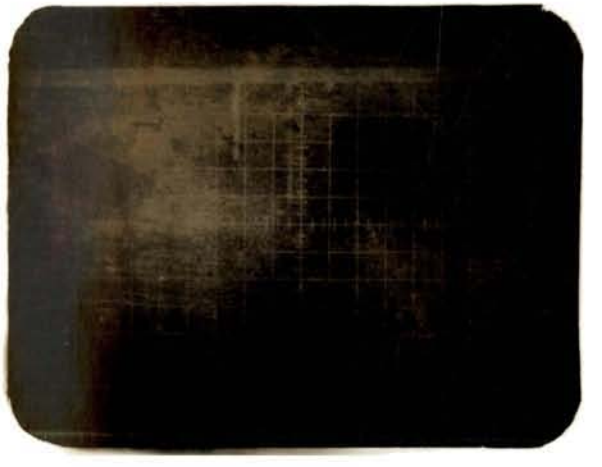

FIG. 5.35 DYE Q-SWITCHED OUTPUT PULSES

A - SWEEP SPEED: 2 us/DIV., GAIN: 0.2 V/DIV.

B - SWEEP SPEED: 20 us/DIV., GAIN: 1 V/DIV.

C - SWEEP SPEED: 20 us/DIV., GAIN: 1 V/DIV.

the threshold energy value also decreases. Transmissions lower than 52.07 % were not tried because the system could not be operated at charging voltages in excess of 3.3 kV. Percentage of dye transmission was determined by measuring the intensity of light at 1.06 μm incident and transmitted through the dye cell with and without dye solution.

Maximum output energy obtained with the present pumping configuration was 135 mJ and the output pulse was about 100 ns at FWHM (Fig. 5.35A).

5.8 RESULTS.

A versatile laser system, operating at 1062 nm was built around a 152.4 mm x 6 mm dia. Nd: Glass laser rod. The system was initially operated in the pulsed mode in an elliptical and a double circular pumping chamber. These pumping chambers as well as the related mechanical and electronic circuits, which include the flash lamp drive circuit and the rate generator circuit, were fully designed, built and tested successfully. The threshold input energy values for this laser rod when pumped in the elliptical and double circular pumping chambers were 100 and 110 Joules respectively for an output mirror reflectivity of 50 %. The gain coefficient and the small signal single pass gain of the laser rod in these two pump configurations were also determined. It was observed that the variation in output energy with input energy was larger for the double circular cavity. When the laser rod was pumped inside this double circular cavity, for an input of 450 Joules,

an output pulse of 2.2 Joulses in 400 μs was generated with a slope efficiency of 0.647 %. The laser when operated in this configuration had a full angle divergence of 0.0094 mrad.

An E-O Q-Switch was built using a KDP crystal as the birefringent material. The quarter wave voltage and the extinction ratio of the Q-switch that has a 1" x 1" x ½" crystal was found to be 7.5 kV and 130 respectively. A Q-switching circuit that can remove the voltage applied on the E-O Q-switch at the desired instant was designed and built. The timing was precisely controlled by a rate generator cum delay circuit developed using NE 555 timers. For an input energy of 450 Joules, the optimum delay was 380 μs. The important feature of the switching circuit was that it utilised a simple pressurised spark gap as the switching element and attained switching speeds of the order of a few ns. Output pulses as narrow as 15 ns at FWHM were obtained. The output energy was 110 mJ for an input of 648 Joules into the flashlamps. The output peak power was 7.3 MW and the slope efficiency was 0.034 %.

A simple dye cell with a thickness of about 1 mm suitable for Q-switching applications was designed and built using two A.R. coated windows. With Eastman 9860 Q-switch solution in 1-2, dichloroethane output energies as high as 135 mJ in about 100 ns was obtained with a slope efficiency of 0.125 % for an input of 272 Joules. It may be noted that in all these experiments no mode selection technique was utilised and hence, the output structure was multimode.

REFERENCES.

1. E. Snitzer, Phys. Rev. Lett., 7, 444 (1961)
2. P.B. Mauer, Appl. Opt., 3, 153 (1963)
3. R.D. Maurer, Appl. Opt., 2, 87 (1963)
4. E. Snitzer, Proc. IEEE, 54, 1249 (1966)
5. R.W. Hellwarth, Advances in Quantum Electronics, p.334, Columbia Univ. Press (1961)
6. F.J. Mc Clung and R.W. Hellwarth, J. Appl. Phys., 33, 828 (1962)
7. R.W. Hellwarth, Lasers Vol. 1, p.253, Marcel Dekker (1966)
8. W.G. Wagner and B.A. Lengyel, J. Appl. Phys., 34, 2040 (1962)
9. R.J. Collins and P. Kisliuk, J. Appl. Phys., 33, 2009 (1962)
10. W. Buchman et al., IEEE J. Quantum Electron., QE-6, 747 (1970)
11. I.W. Mackintosh, Appl. Opt., 8, 1991 (1969)
12. B.A. Davydov et al., Sov. J. Quantum Electron., 4, 1406 (1975)
13. P. Kafalas et al., Appl. Phys., 35, 2349 (1964)
14. B.H. Soffer, J. Appl. Phys., 35, 2551 (1964)
15. M. Born and E.Wolf, Principles of Optics, 2nd. Edn. Macmillan (1964)
16. B.H. Billings, J. Opt. Soc. Am., 39, 797 (1949)
17. B.H. Billings, J. Opt. Soc. Am., 39, 802 (1949)
18. W.R. Hook and R.P. Hilberg, Appl. Opt., 10, 1179 (1971)
19. D. Milam, Appl. Opt., 12, 602 (1973)
20. L.L. Steinmetz et al., Appl. Opt., 12, 1468 (1973)
21. R.V. Lovberg et al., IEEE J. Quantum Electron., QE-11, 17 (1975)

22. A.J. De Maria, Proc. IEEE, 57, 2 (1969)

23. D.D. Bhawalkar, Proc. Indian Nat. Sci. Acad. A, 37, 200 (1971)

24. H. Weichel, J. Appl. Phys., 44, 3635 (1973)

25. P.N. Everett, Rev. Sci. Instrum., 41, 1495 (1970)

26. A.R. Clobes and M.J. Brienza, IEEE J. Quantum Electron., QE-6, 651 (1970)

27. Lawrence Livermore Laboratory, Laser Program Annual Report UCRL - 50021 (1975 - 1979)

28. W. Koechner, Solid-state Laser Engineering, Springer-Verlag (1976)

29. W.F. Hagan, J. Appl. Phys., 40, 511 (1969)

30. R.H. Hornik et al., Rev. Sci. Instrum., 33, 776 (1962)

31. P.W. Pace and J.B. Atkinson, Rev. Sci. Instrum., 47, 1215 (1976)

32. D.H. Dishington et al., Appl. Opt., 13, 2300 (1974)

33. W.R. Hook et al., IEEE Trans. on Electron Devices, ED-19, 308 (1972)

34. W.F. Herg and R.C. Lee, IEEE Trans. on Electron Devices, ED-23, 1164 (1976)

35. J.H. Goncz, J. Appl. Phys., 36, 742 (1965)

36. ILC Technical Bulletin : An Introduction to Flashlamps.

37. ILC Data Sheet on Flashlamps.

38. J.P. Markiewcz and J.L. Emmett, IEEE J. Quantum Electron, QE-2, 707 (1966)

39. P.N. Everett, Rev. Sci. Instrum., 37, 375 (1966)

40. L.V. Koval' chuk, Sov. J. Quantum Electron., 2, 450 (1973)

41. J.N. Bradford and R.C. Ectar, Appl. Opt., 8, 480 (1969)

42. R.P. Hilberg and W.R. Hook, Appl. Opt., 2, 1939 (1970)

43. F. Pockels, Abb. Goettingen Ges. D. Wiss., 39, 169 (1894)

44. A. Kastler, Progress in Electro-Optics (Ed. Ezio Camatini) Nato Advanced Study Institutes Series, Plenum Press (1975)

45. B.A. Fuchs, Appl. Opt., 18, 1125 (1979)

46. W.R. Hook et al., Proc. IEEE, 59, 1126 (1971)

47. M. Michon et al., Rev. Sci. Instrum., 40, 263 (1969)

48. D. Von Der Linde et al., Opt. Commun., 2, 215 (1970)

49. W.R. Sooy, Appl. Phys. Lett., 7, 36 (1965)

50. B.B. Mc Farland et al., Nature, 207, 1180 (1965)

51. K.H. Drexhage and G.A. Reynolds, IEEE J. Quantum Electron., QE-10, 720 (1974)

52. D. Huppert and P.M. Rentzepis, Appl. Phys. Lett., 32, 241 (1978)

CHAPTER VI.

THERMAL EFFECTS IN HOYA LSG - 91H SILICATE LASER ROD PUMPED IN A DOUBLE CIRCULAR CLOSE-COUPLED CAVITY.

6.1 INTRODUCTION.

Various thermal effects occur in laser rods due to non-uniform temperature distribution produced while pumping these rods optically. This results in a distortion of the laser beam because of the temparature and stress dependent variation of the refractive index. The important thermal effects that usually occur are the thermal lens effect due to refractive index variation and the birefringence effect due to photoelastic effect of thermal strains.[1-6] The temperature profile developed in the laser rod depends on whether the laser system is operated in the single shot, cw or repetitively pulsed mode. Knowledge of the magnitude of even a small induced focussing may be an important consideration in the designing of the laser resonant cavity.

Theoretical as well as experimental investigations have shown that the governing mechanisms that distort the mode structure and polarised output power of solid-state lasers are these thermal effects.[7] Kogelnik[8] and Steffen et al.[9] have given a theoretical analysis of an optical resonator with a birefringent laser rod inside.

Different techniques have been developed to measure the thermal time constant and the associated lens effects. Many workers[10-15] have used interferometric methods to study these

thermal distortion effects. Though these measurements gave information about the spatial as well as temporal variation of the distortion, they were difficult to interpret. Another technique commonly adopted is to measure the thermal relaxation by passing a probe beam through the laser rod and to observe the changes in the beam intensity during and after the pump pulse.[2,4,16-18] Burnham[4] measured the thermal time constant of a 178 mm x 6.3 mm laser rod pumped in a close coupled configuration. The spatially filtered He-Ne beam coming out of the rod was focussed by a lens on to a pinhole (125 μm) and the intensity variation was measured with a photo diode kept beyond the pinhole.

Chun and Bischoff[16] also measured the thermal time constant from the lensing effect. They observed that when pumped with a 400 μs lamp pulse, the rod behaved as a negative lens initially for about 120 ms, then behaved as a positive lens that increased in strength and reached a maximum in 250 ms after the lamp pulse and then slowly decayed in about 1.8 sec. whereas their computed value was only 0.45 sec. Similarly the measurement of Hotz[17] from lensing effect for a Nd: YAG rod found this value to be five times more than the theoretically computed value.

Recently Marchetti et al.[18] studied the thermal effects in Nd: Glass laser rods in a pseudoelliptic close-coupled pumping chamber. In addition to the usual focussing effects, they observed a prismatic effect in these rods when pumped in single shots and at low repetition rates.

The purpose of the present investigation was to analyse the thermal effects in the Nd: Glass laser rod used in the high power E-O Q-switched laser described in Chapter V. The same double circular cavity was used without any cooling system for pumping the 152.4 mm x 6 mm laser rod.

6.2 THEORY.

In any high power laser system, about 5-7 percent of the input electrical energy is dissipated as heat by the laser rod.[19] Because of the low thermal conductivity of glass laser rods and the insufficient rate of heat removal, a temperature gradient is established during pumping. This temperature gradient generates mechanical stresses inside the laser rod, as the hotter inside region is not free to expand because of the cooler outer zone. These thermal stresses produce thermal strains in the rod which in turn give rise to variations in refractive index through the photoelastic effect.

6.21 THERMALLY INDUCED FOCAL LENGTH.

The thermally induced lens focal length measuring set up is shown in Fig. 6.1 and is somewhat similar to the one described by Marchetti et al.[18] Here the natural divergence of the He-Ne laser beam was utilised instead of beam expanders or other coupling optics that may introduce additional aberrations. For measuring the rod focal length the iris was usually moved along the optical axis to locate the focal spot of the lens. As there was considerable error involved in this technique, while measuring rod

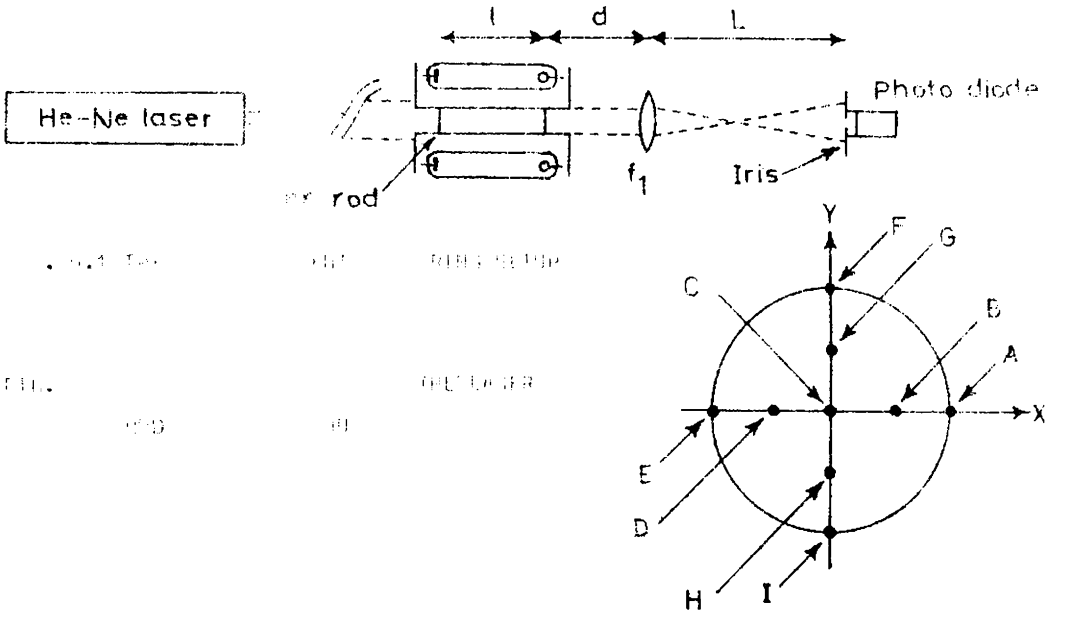

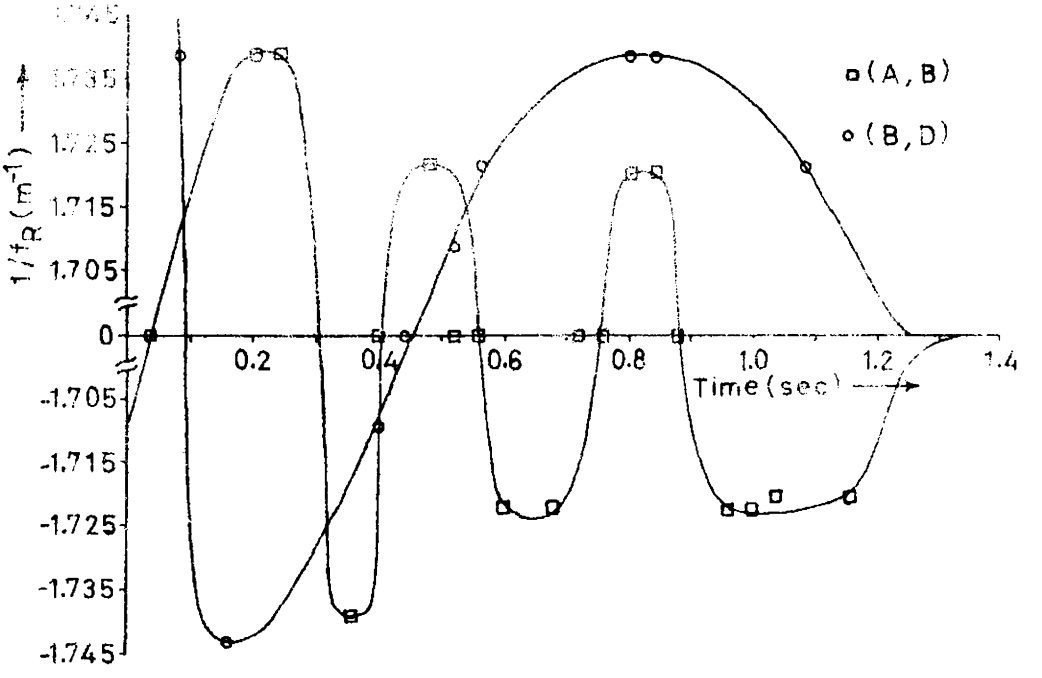

FIG. 5.4A INDUCED FOCAL LENGTH VARIATION WITH TIME

focal lengths, the intensity variations at chosen points in the beam profile were measured with an out-of-focus iris.

When the rod is pumped it behaves like a thick symmetric lens and the distance (h) between the thick lens principal plane and the rod ends is given by[2]

$$h = l/2n \qquad : 6.1$$

where l is the rod length and n, the refractive index.

Considering the rod as a thick lens located at the principal plane with a focal length f_R, the system equivalent focal length f_{eq} is given by[20]

$$1/f_{eq} = 1/f_R + 1/f_1 - d_1/f_1 f_R \qquad : 6.2$$

where d_1 (=d+h) is the testing lens to rod-lens principal plane separation and d is the testing lens to rod separation.

For a rod of diameter D, the system equivalent focal length can be computed from the value of the beam diameter (W_D) at the iris using the relation,[18]

$$a f_{eq}^4 + b f_{eq}^2 + c f_{eq} + d = 0 \qquad : 6.3$$

where $a = 4\lambda^2/\Pi^2 D^2$

$$b = D^2\left(1 - \frac{d_1}{f_1 - d_1}\right) - W_D^2$$

$$c = -2Db\left(L + \frac{d_1 f_1}{f_1 - d_1}\right)$$

and $$d = D^2\left(L + \frac{d_1 f_1}{f_1 - d_1}\right)$$

The computation of the rod focal length from the direct measurement of W_D is possible only in the repetitively pulsed mode. The computer program for the determination of f_R starting from 6.3

is given in Appendix A. In the single shot mode, W_D is calculated as given below, taking into account the intensity variation in the probe beam due to the prism like and the lens like effects.

The intensity distribution of a He-Ne laser beam having a gaussian distribution along the X or Y -axis is given by

$$I = (K/W_D) \exp (- (x/W_D)^2) \qquad : 6.4$$

where K ($= I_o W_D'$) is determined by measuring the maximum intensity (I_o) and the beam diameter at ambient (W_D').

The lensing effect can be represented as $W_D(t)$, while the prismatic effect can be represented as a shift Δx along the X-axis. Taking into account these two processes 6.4 can be written as

$$I(t) = \frac{K}{W_D(t)} \exp \left\{ - \left(\frac{x + \Delta x(t)}{W_D(t)} \right)^2 \right\} \qquad : 6.5$$

The above relation represents the variation of intensity with time on a generical point along the X-axis. If I_1 and I_2 are the intensity values at $x = 0$ and $x = x_o$, then

$$I_1 = (K/W_D(t)) \exp \left\{ - (\Delta x(t)/W_D(t))^2 \right\} \qquad : 6.6$$

$$I_2 = (K/W_D(t)) \exp \left\{ - \left((x_o + \Delta x(t))/W_D(t) \right)^2 \right\} \qquad : 6.7$$

Combination of 6.6 and 6.7 leads to, at generical time t,

$$\frac{K}{W_D} \exp \left[- \left\{ (\ln K/W_D I_2)^{\frac{1}{2}} - x_o/W_D \right\}^2 \right] - I_1 = 0 \qquad : 6.8$$

Or

$$\frac{K}{W_D} \exp \left[- \left\{ (\ln K/W_D I_1)^{\frac{1}{2}} + x_o/W_D \right\}^2 \right] - I_2 = 0 \qquad : 6.9$$

Thus, starting from the measurement of x_o and the intensities I_1 and I_2 at any generical time, W_D can be computed using either 6.8

or 6.9 depending on whether I_2 is positive or negative at that instant and the computer program for the evaluation of W_D is given in Appendix B.

6.22 THE THERMAL TIME CONSTANT.

The thermal time constant of a repetitively pumped laser rod is defined as the time taken by the centre of the rod to return to the ambient temperature and is given by[19]

$$T_o = r_o^2 \, C \, d/K \qquad : 6.10$$

where r_o - radius of the rod

C - Specific heat

d - mass density

K - thermal conductivity

The time taken by the temperature at the centre of the rod to come down to 1/e of the initial maximum value is known as the thermal relaxation time and is given as[19] $t = T_o/4$. These equations are valid only under ideal conditions where the surface temperature of the rod is constant and the cooling as well as the heat dissipated by the rod throughout the volume is uniform.

6.3 EXPERIMENT.

The experimental set up for the measurement of thermal effects is shown in Fig. 6.2. The pumping chamber was double circular in geometry with the flashlamp and the laser rod close-coupled (Figs. 5.4A and 5.4B). In close-coupled pumping chambers direct radiation from the flashlamp plays an important role in creating thermal distortions inside the rod.

FIG. 6.2 EXPERIMENTAL SETUP FOR STUDYING THERMAL EFFECTS

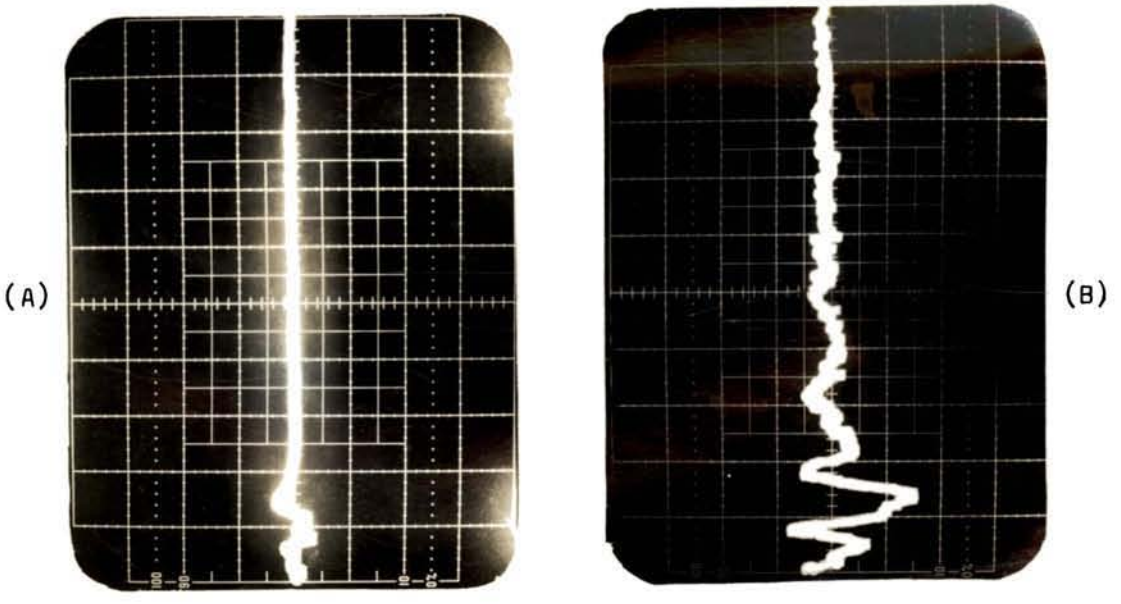

FIG. 6.3 PROBE BEAM INTENSITY VARIATION IN THE SINGLE SHOT MODE

A,B – SWEEP SPEED : 0.2 SEC./DIV., GAIN : 5 mV/DIV.

(C)

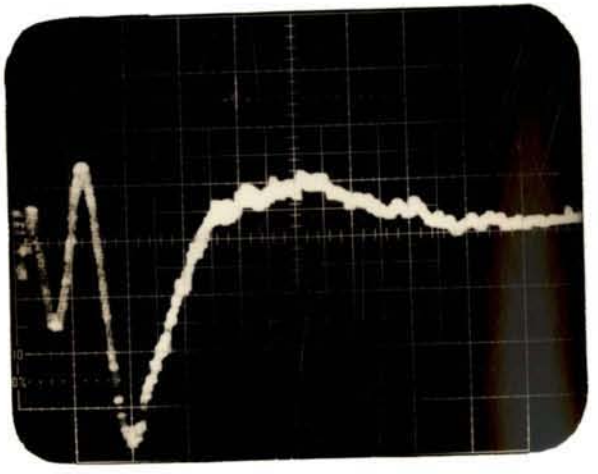

(D)

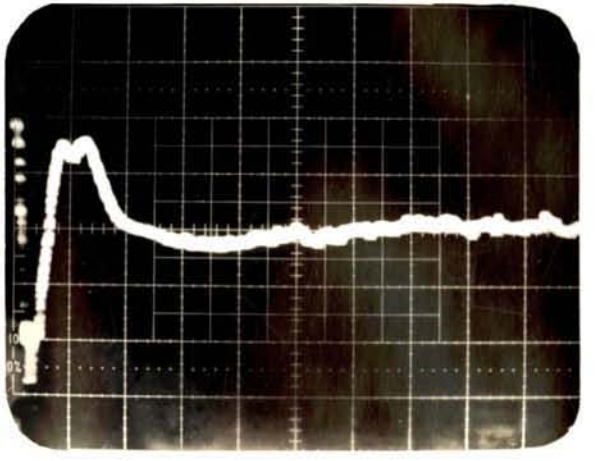

(E)

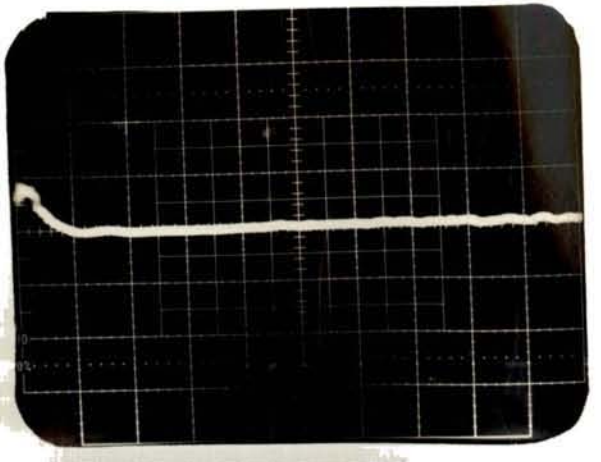

(F)

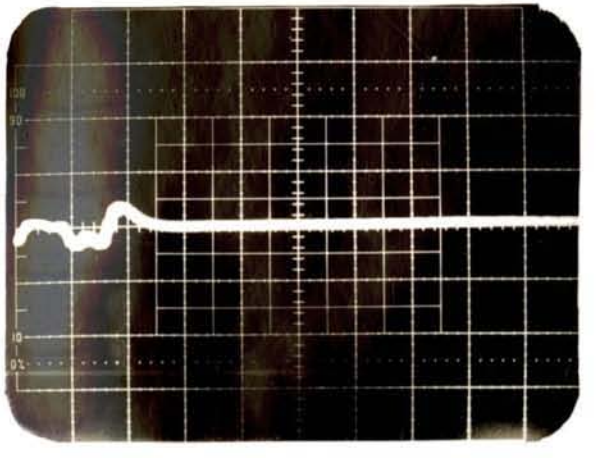

FIG. 6.3 PROBE BEAM INTENSITY VARIATION IN THE SINGLE SHOT MODE

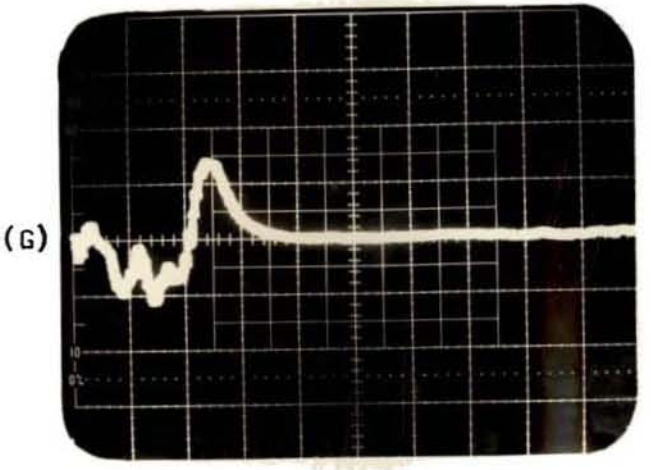

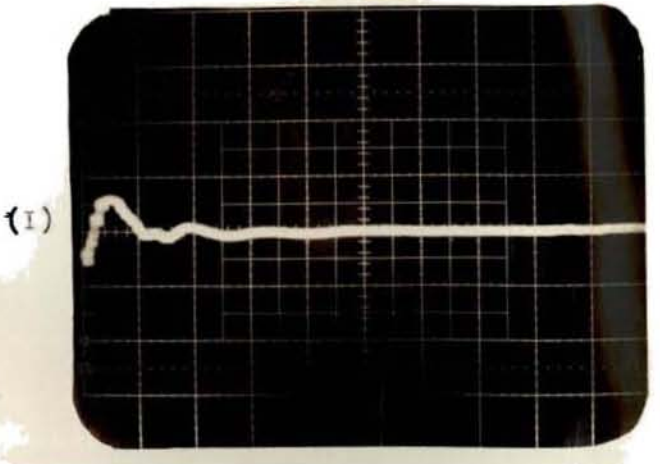

FIG. 6.3 PROBE BEAM INTENSITY VARIATION IN THE SINGLE SHOT MODE

G,H,I - SWEEP SPEED: 0.2 SEC./DIV., GAIN: 5 mV/DIV.

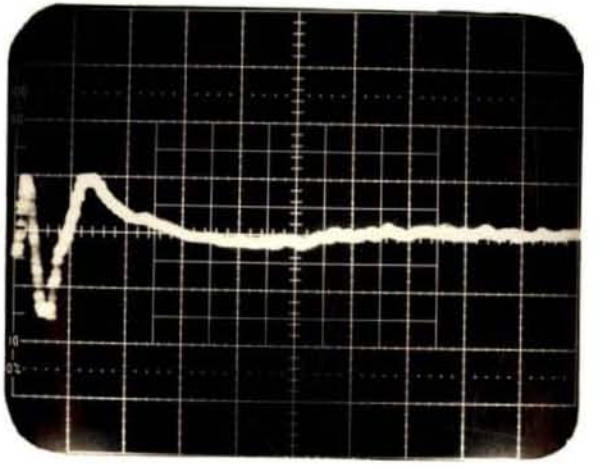

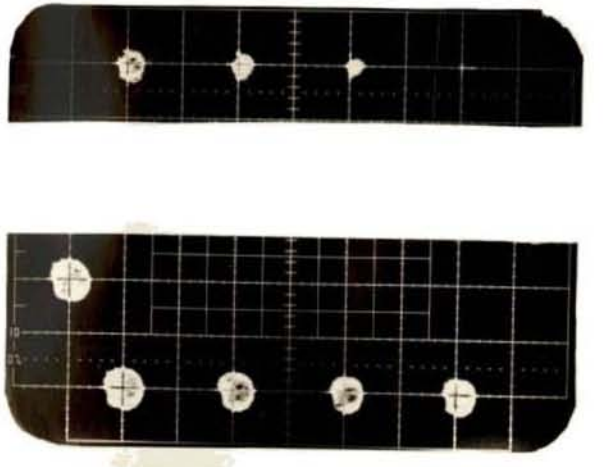

FIG. 6.8 LASING TEST RESULTS

The 152.4 mm x 6 mm HOYA LSG 91H Nd^{3+} doped silicate glass rod was pumped using two 6F6G (ILC Technology, U.S.A) linear flashlamps. These flashlamps had an arc length of 152.4 mm and bore diameter of 6 mm. The He-Ne laser beam emerging from the laser rod was focussed with a biconvex lens of focal length 49 cm on to a detector kept out of focus. A 170 μm pinhole was fitted on top of the Hewlett Packard hp2 - 4207 photodiode and the whole assembly was mounted on a micrometer sledge that had provision for movement along the X and Y directions. The photodiode was operated in the reverse bias at 27 Volts and gave a rise time of 5 μs when a 1 M resistor was used as the load. The photodiode output was fed on to a Tektronix Oscilloscope, Model - 466 DM44. In the present investigation optical distortions induced by a single shot and by a sequence of shots were studied.

6.4 RESULTS AND DISCUSSIONS.

For studying the distortions produced by a single flashlamp pulse, the intensity variation at nine different positions (Fig. 6.3) along the rod cross section were measured with an input energy of 100 Joules into the lamp. The flashlamp output was about 200 μs in duration. Figs. 6.3A-I show variation in the He-Ne laser beam intensity observed respectively at these nine positions. In the present arrangement an upward swing of the trace corresponds to a decrease in intensity which indicates a broadening of the probe beam, while a downward swing of the trace represents an increase in intensity indicative of the probe beam convergence.

In the present study, the intensity variation did not show any initial converging and then diverging feature as reported by Marchetti et al.[18] Instead at position C, the intensity pattern was found to swing from a diverging to a converging one and vise-versa upto about 3-4 times in 2 seconds after the pump pulse. However, apart from the initial transient lensing behaviour observed at C, the nature of the lensing pattern is similar to the earlier report.[18] It was observed that at the rod edges the thermal effect lasts only for 0.2 to 0.5 seconds while at the centre it lasts for 2 to 2.5 seconds. This shows that the cavity is concentrating the energy into the centre of the rod. The lack of symmetry between Figs. 6.3A and 6.3E and Figs. 6.3F and 6.3I may be due to a slightly larger amount of energy being discharged into the flashlamp that is triggered first or due to a positioning error of the rod or the lamp. The symmetry between Figs. 6.3E and 6.3I and Figs. 6.3A and 6.3F further confirms the above assumption. The result is thus a prismatic behaviour of the laser rod.

The induced focal length in the single shot mode was determined by measuring the intensity values corresponding to any two positions of the pinhole at any particular instant from Figs.6.3A-I and using 6.8, 6.9, 6.3 and 6.2. The values obtained for typical positions are plotted in Figs. 6.4A and 6.4B.

For studying the cumulative effects, 50 shots were made at a repetition rate of 30 pulses per minute with a fixed input energy into the flashlamp. Horizontal scanning of the laser rod

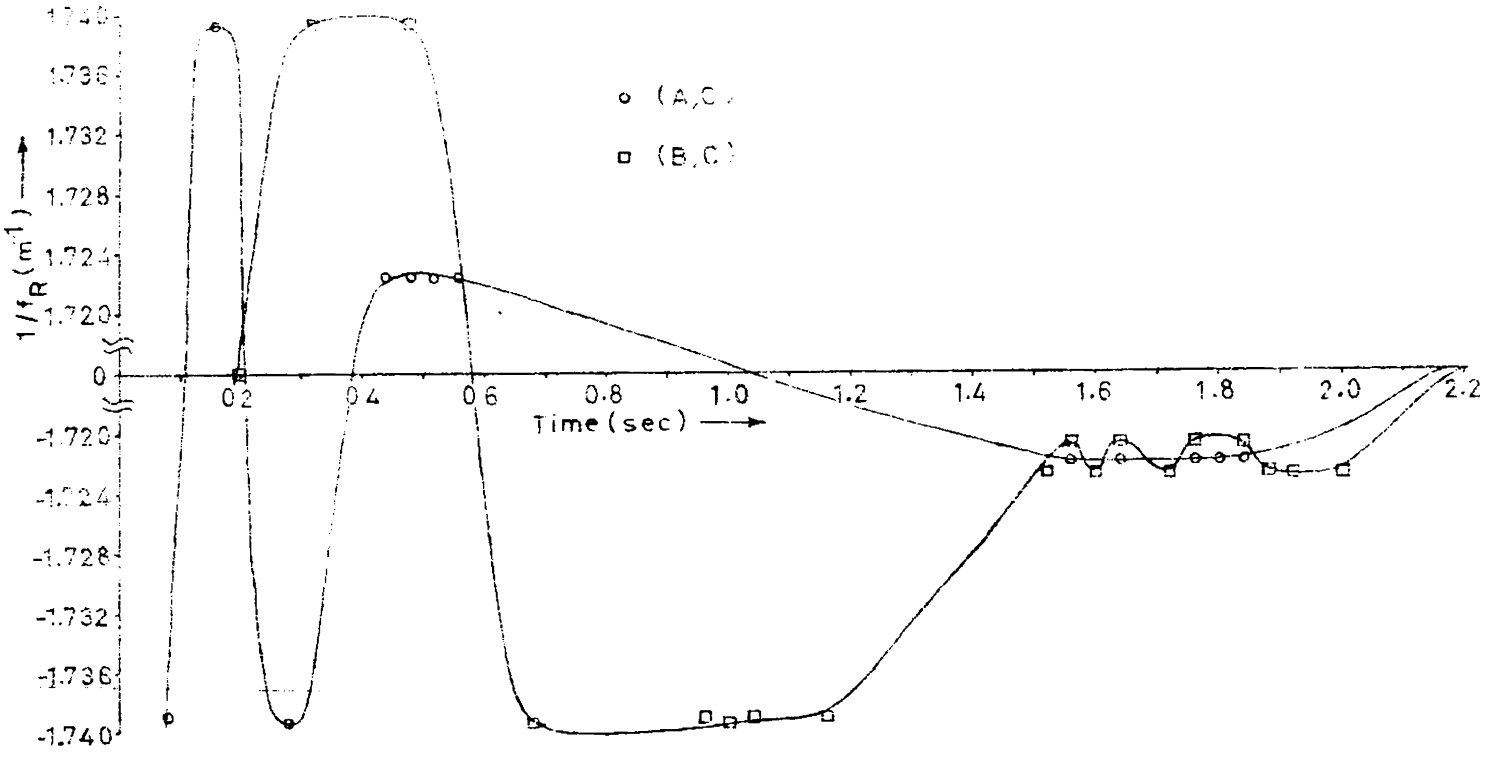

FIG. 6.48 INDUCED FOCAL LENGTH VARIATION WITH TIME

profile was made using the pinhole photodiode setup before and after test shots. The intensity profiles obtained for input energies of 25J, 50J and 75J are shown in Fig. 6.5. The low intensity peaks that appear on either side of the central one are due to the spherical aberration of the focussing lens.

As the geometrical dimensions were unaltered throughout the entire experiment, the observed broadening of the probe beam profile, with reduction in the peak intensity value, can be attributed to a negative lens effect in the laser rod. The induced focal length (f_R) computed from the W_D values measured at the $1/e^2$ points using 6.3 and 6.2 are plotted in Fig.6.6. It may appear that the focal length computed (-55 cm) is too small compared to the results (40-60 m) reported by Marchetti et al.[18] But for assessing the extent of the induced focal length one has to take into account the flashlamp input power.[19] As the input powers were quite high (50-150 kW) in the present study, the values obtained are sufficiently reliable. It may also be noted that there is a shift in the position of the maxima due to the prism effect. The displacement of the peak position Δx with input energy is plotted in Fig. 6.7.

In order to substantiate the observed lensing behaviour lasing was tested in the conventional pulsed mode with an output mirror of 50 % reflectivity. The laser output was made to impinge on an exposed photographic plate. Fig.6.8 show the burn patterns obtained when the laser was operated with the 100 μF bank capacitor

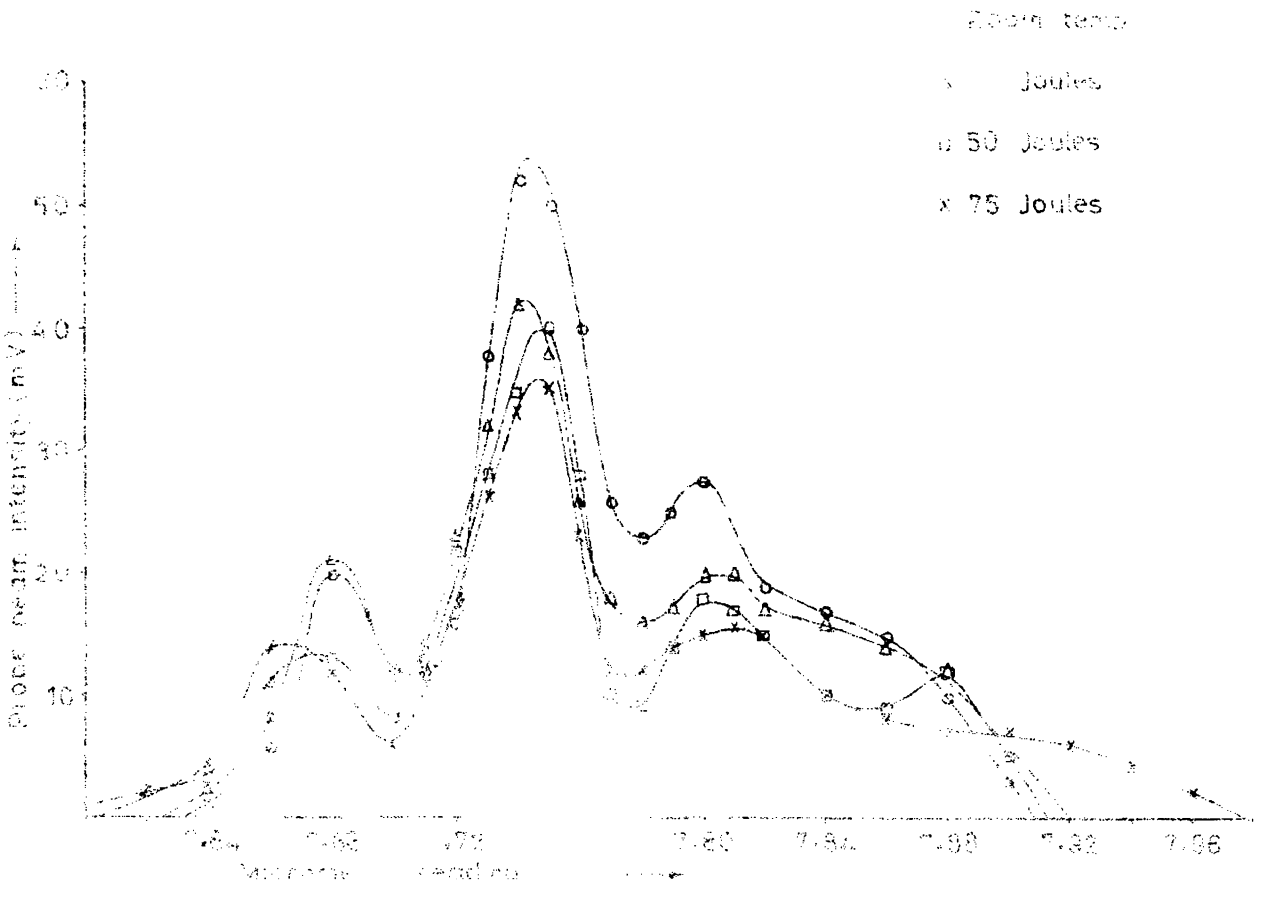
Room temp
Joules
50 Joules
75 Joules

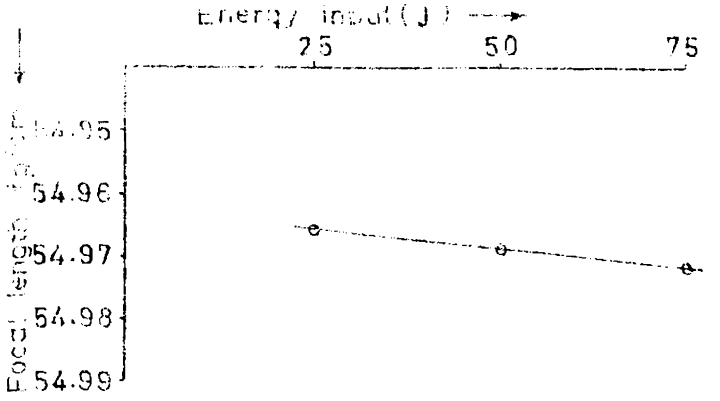
Energy input (J) ⟶
25
50
75
54.95
54.96
54.97
54.98
54.99

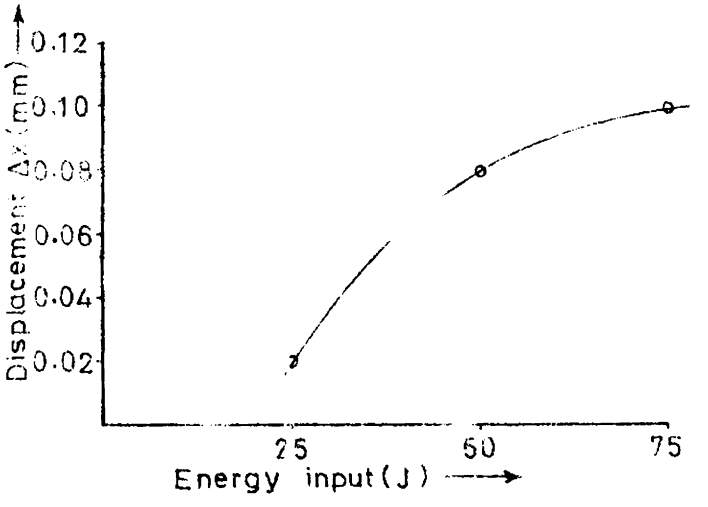
Displacement Δx (mm)
0.12
0.10
0.08
0.06
0.04
0.02
25
50
75
Energy input (J) ⟶

charged to voltage of 1.4, 1.8, 2.0, 2.2, 2.4, 2.6, 2.8 and 3.0kV. Before every test shot, the He-Ne laser beam used for alignment was made to fall exactly at the centre of the cross on the photo-plate. In all these tests the damaged site was seen shifted towards the side where the flashlamp that fires first was located. This accounts for the observed prism effect. Moreover, it was observed that at low pump energies, the rod lases in the central region and as the pump energy is increased, the pumped area also increases radially with the whole rod volume contributing to laser action at about 3 kV charging voltage. This is similar to the result expected from a steady-state analysis which assumes that the axis of the rod is hotter than the outer surface[1] and contrary to what happens under conventional pumping configurations, where an initially positive and then negative temporal evolution is observed with a better illumination of the rod's outer surface than the center.[16]

REFERENCES.

1. J.D. Foster and L.M. Osternik, J. Appl. Phys., 41, 3656 (1970)
2. T.J. Gleason et al., Appl. Opt., 12, 2942 (1972)
3. M.K. Chun, IEEE J. Quantum Electron., QE-7, 220 (1971)
4. D.C. Burnham, Appl. Opt., 9, 1727 (1970)
5. G.D. Baldwin and E.P. Riedel, J. Appl. Phys., 38, 2726 (1967)
6. W. Koechner, Appl. Opt., 9, 2548 (1970)
7. L.M. Osternik and J.D. Foster, Appl. Phys. Lett., 12, 128 (1968)
8. H. Kogelnik, Bell Syst. Tech. J., 44, 455 (1965)

9. J. Steffen et al., IEEE J. Quantum Electron., QE-8, 239 (1972)

10. C.M. Stickley, IEEE J.Quantum Electron., QE-2, 511 (1966)

11. H. Welling and C.J. Bickart, J. Opt. Soc. Amer., 56, 611 (1966)

12. J.N.Bradford and R.C. Eckardt, Appl. Opt., 7, 2418 (1968)

13. G.A. Ermakov and A.V. Lukin, Sov. Phys. Techn. Phys., 15, 1097 (1971)

14. G. Benedetti Michelangeli and S. Martellucci, Appl. Opt., 8, 1447 (1969)

15. B.K. Sinha and N. Gopi, IEEE J. Quantum Electron., QE-16, 433 (1980)

16. M.K. Chun and J.T. Bischoff, IEEE J.Quantum Electron., QE-7, 200 (1971)

17. R.F. Hotz, Appl. Opt., 12, 1834 (1973)

18. R. Marchetti et. al., Optics Commun., 29, 347 (1979)

19. W. Koechner, Solid-state Laser Engineering, New York: Springer - Verlag, 344 (1976)

20. W.G. Driscoll (Ed.), Handbook of Optics., Mc Graw - Hill Book Co., 2 - 10 (1978)

CHAPTER VII.

LASER-INDUCED DAMAGE TO TRANSPARENT CONDUCTING SnO_2 FILMS AT 1062 nm.

7.1 INTRODUCTION.

Laser-induced damage to transparent optical materials is a process by which it suffers an observable change upon the passage of a laser beam.[1-2] Laser-induced damages can be classified into four temporal regions: damage involving picosecond pulses,[3-8] pulses from a few to hundred nanoseconds,[9-11] pulses from a few to about 20 microseconds and cw laser beams. In the nanoseconds and picoseconds regime, the onset of damage is similar to the exponential growth of ionization and resultant plasma formation associated with electrical breakdown.[2] Over longer periods, damage is characterised by the cumulative effect of the laser beam absorption and subsequent distorsions or heating of the material to its melting point. The other factors that influence the damage threshold are the focussing conditions, beam quality, material properties, surface roughness and the experimental technique.[11-18] All these factors are to be considered if an effort is to be made to interpret a given laser damage experiment.

Laser-induced damage threshold values are usually specified in terms of incident energy density or power density. However in an elegant, simple description, Crisp et al.[19] have shown that the correct quantity in specifying the damage threshold in

the short pulse regime is the electric field associated with the laser pulse. This was confirmed later by De Shazer et al.[20] and Newman and De Shazer.[21] The electric field at the surface of an uncoated material with refractive index n_g or for a $\lambda/2$ thick film deposited on it is given by[10]

$$E\ (V/m) = \frac{38.8}{n_g + 1} \sqrt{S}\ (W/m^2) \qquad -- \quad 7.1$$

For $\lambda/4$ or 3 $\lambda/4$ thick films of refractive index n_f, the electric field at the film surface is

$$E\ (V/m) = \frac{38.8\ n_g}{n_g + n_f^2} \sqrt{S}\ (W/m^2) \qquad -- \quad 7.2$$

As n_f approaches n_g, the expressions given by 7.1 and 7.2 coalesce and if the field is indeed the threshold quantity one would expect the variation in threshold power density with film thickness to vanish.

Damage threshold dependence on the material refractive index was studied by many groups. Turner[22] and Austin et al.[23] found an inverse dependence of refractive index on threshold. A similar trend was later observed by De Shazer et al.[20] and Newman and De Shazer[21] on thin films and by Boling et al.[24] on uncoated optics. Recently Bettis et al.[25] have shown an (n^2-1) dependence for refractive index on threshold optical electric field for several transparent material and thin films using 40 ns 1.06 μm laser pulses.

The surface damage thresholds were always found to be 0.3 to 0.5 times less than the bulk values because of the

presence of surface roughness, impurities and imperfections. By using static field theory to calculate the expected field enhancement, Bloembergen[26] recently showed that surface features with characteristic dimensions less than 10 nm would be unimportant in laser-induced damage. De Shazer et al.[27] observed the damage thresholds of coatings to decrease with increasing beam spot sizes beyond 150 μm because of a larger probability of the beam impinging a defect site.

Typical threshold values reported by Bliss et al.[28] for multilayer dielectric films with a Ruby laser focussed to 0.1 to 0.2 mm spot size varied from 0.6 J/cm^2 to 2.9 J/cm^2 for 20 ps pulses and from 16 J/cm^2 to 58 J/cm^2 for 20 ns pulses. For anti-reflection films studied using 30 ns Nd: Glass laser pulses[29], the damage threshold was within the 20 J/cm^2 to 38 J/cm^2 range depending on the layer structure and the percentage of reflectivity.

In high-power laser systems many optical surfaces intercept the beam before the output is utilized. Usually most of these surfaces are either reflective or anti-reflective coated to reduce the transfer losses. So the survivability of thin film coatings to laser beams is of great importance in the reliable and efficient operation of high power laser systems. Thus the laser-induced damage measurements of the optical elements and the thin film coatings assume importance.[30-31]

In longitudinal E-O shutters based on Pockels effect, the electric field on the crystal is maintained parallel to the lasing axis by applying a suitable voltage on the circular ring electrodes kept on either side of the crystal. To achieve adequate electric field uniformity over the aperture a crystal length-to-diameter ratio of $\geq 1:1$ is required.[32] Though crystals with apertures upto 5 cm are available, they are very expensive and are difficult to grow. To overcome the field non-uniformity associated with such structures, cylindrical band electrodes are applied to the end of the crystals[32] or transparent conductive coatings are deposited on the crystal faces or they are kept in contact with transparent conductive coatings deposited on glass substrates. E-O modulators with similar coatings are commercially available. Because of the high field uniformities attainable, the length to diameter constraint is reduced or eliminated. Thin disc crystals can now be used, thereby reducing the cost and other scattering and absorption losses due to the material present in the beam path.

The films that are usually used on E-O modulators at 1.06 μm are stanic oxide or its composite (doped) films. These films have relatively high damage thresholds and high transmission at 1.06 μm. But at still higher power densities these films get damaged and the system thus is rendered useless. To date only very little information is available on the damage thresholds of such films. Pawlewicz et al.[33] have measured the damage threshold of $In_{1.9}\ Sn_{0.1}\ O_3$ films deposited on fused silica by reactive RF

sputtering and obtained a value of 2.3 and 3.1 J/cm^2 for 0.15 and 1 ns pulses respectively at 1.06 μm.

Though RF deposition can always yield better results, the chemical vapour deposition technique[34,35] can be more convenient at times, especially when one builds his own E-O system. To facilitate the use of such films in Q-switches and in similar other devices, the transmission, refractive index and other properties of chemical vapour deposited stanic oxide films were studied along with the measurement of damage threshold using 1062 nm, 15 ns pulses.

7.2 METHOD OF PREPARATION OF $Sn\ O_2$ FILMS.

Transparent conducting films are usually prepared by chemical vapour deposition, sputtering (reactive sputtering of the metal/H.F sputtering of the oxide) and Evaporation techniques[35]. The $Sn\ O_2$ films used in the present study were prepared by Fegade and Karekar[36] by chemical vapour deposition method. Commercially available $Sn\ Cl_2$ was heated in a glass U-tube to about 500° C and oxygen was passed over it. The $Sn\ Cl_2$ vapour carried by oxygen was directed on to borosilicate glass substrates heated to 400° C. As the stannous chloride used was not ultra-pure, the films cannot be taken as undoped. The films so prepared consist of $Sn\ O_2$ and reduced tin in the form

$$(Sn^{4+}_{1-2x} + Sn^{3+}_{2x}) (O_2^{2-} - xO^{2-})$$

and this stochiometry is thought to be responsible for the conductivity.

7.3 MEASUREMENT OF REFRACTIVE INDEX, THICKNESS, TRANSMITTANCE AND RESISTIVITY OF THE THIN FILMS.

Optical method[37] was used for the determination of the refractive index and thickness of the thin film samples. The experimental set up is shown in Fig. 7.1. It may be noted that the measurements were made at 435.8 nm. The samples were oriented at 45° to the incident beam direction. The R_s and R_p values of the reflected beam intensity were measured at this angle. The refractive index (n) of the films is determined using the relation[37]

$$n = \frac{(1 - R_s)(1-R_p) - (1-R_s)(1-R_p)\cos^4 Q}{2\cos Q\left[(1+R_p)(1-R_s) - (1+R_s)(1-R_p)\cos^2 Q\right]} \quad -- 7.3$$

where Q is the angle of incidence of the beam on the sample.

As direct measurement of the thickness of the thin film samples used in this damage experiment was not possible, it was determined by comparison with similar films of known thickness using the relation[37]

$$X = \exp\left[-j4\Pi\,(d/\lambda)\,(N_1^2 - N_o^2 \sin^2 Q)^{\frac{1}{2}}\right] \quad -- 7.4$$

where d, the film thickness

λ, the wavelength of light used

N_1, the refractive index of the film (real part)

N_o, the refractive index of the ambient

and Q , the angle of incidence.

After properly masking, aluminium was vacuum deposited on top of the films to be used for comparison, The thickness of the films were then measured by multiple beam interferometry.

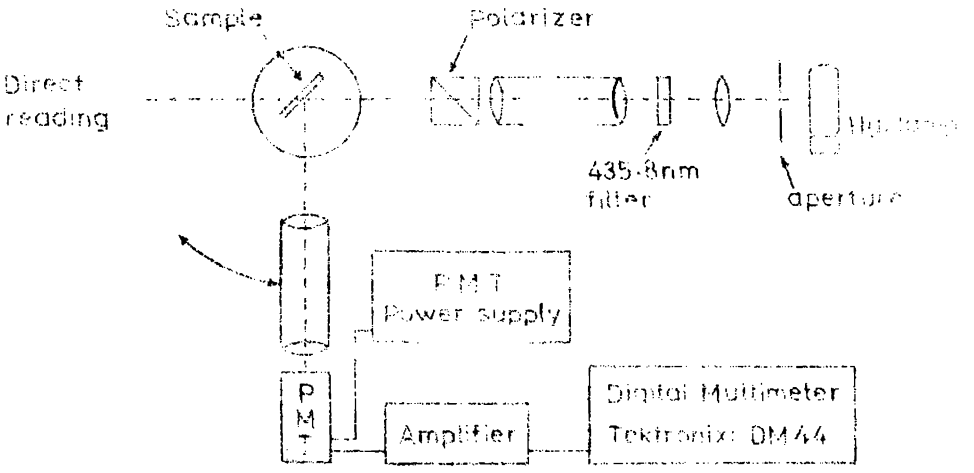

7.1 OPTICAL MEASUREMENT SETUP

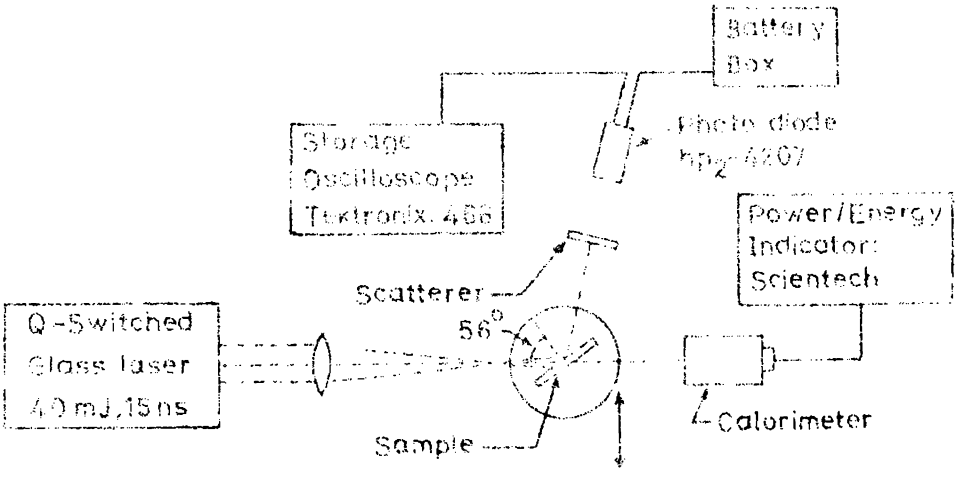

FIG. 7.2 SCHEMATIC [illegible] MEASUREMENT SETUP

The R_s and R_p values were also measured for determining the refractive index of the films using 7.3. The values thus determined were substituted in 7.4 and the exponential term was evaluated. The mean value of the exponential term was now determined for different reference films. This mean value was used for determining the thickness of the films whose refractive indices have already been determined by the optical method.

The transmittance of the films were measured at 435.8 nm by keeping the PMT along the beam direction and noting the multimeter reading with the substrate, with the film sample and without the film sample in the beam path. Care was taken to orient the film samples normal to the beam when the readings were taken.

The in-plane resistance R (Ohms) of the sample films were also measured. The resistivity p (Ohm. cm) was then computed using the relation $p = Rbd/l$, where b, d and l were the breadth, thickness, and length, respectively, of the thin film samples.

7.4 MEASUREMENT OF DAMAGE THRESHOLD.

The general opinion in recent years was that a TEM_{oo} mode laser was essential in the study of laser-induced damage and most of the damage thresholds reported so far have been obtained with such lasers. Though the filamentary hot spots in the beam has higher energy densities compared to the average energy density, recent observation that these filamentary structures are focussed to spot sizes too small to contribute to damage has established that a TEM_{oo} mode laser is not necessary in laser damage studies.[38]

Moreover, one should bear in mind that real-world lasers are not always operated in the TEM_{oo} mode.

Fig. 7.2 is a schematic diagram of the damage experiment, and the experimental setup is shown in Fig. 7.3. The laser used in this study was the E-O Q-switched Glass laser described in Chapter V. The laser output at 1062 nm was about 15 ns at FWHM and was linearly polarized. The beam structure was multimode and was approximately Gaussian in profile with a diameter of about 3 mm at the e^{-1} intensity level. The laser output was focussed, with a biconvex lens of 17 cm focal length, on to the thin film sample kept out of focus. The sample film surface was cleaned using a thin film cleaner (Optical Coating Laboratory, USA) before mounting on the holder fitted on a rotating platform. The film was oriented so that the incident beam makes an angle of 56° with the normal. This large incidence angle was used to avoid multiple beam interference in the borosilicate substrates. The laser pulse width was monitored with a hp2 - 4207 photodiode and the energy incident on the thin film sample by a thermopile (1 inch Scientech Disc Calorimeter, Model 38-0101).

Throughout the entire study the laser output energy was kept constant. For this purpose the 100 uF capacitor bank voltage was set at 3 kV. With an input energy of 450 Joules an output energy of 40 mJ $\pm$ 2 mJ was obtained. The Q-switch was biased at 7.6 kV and was triggered after a delay of 360 μs. With the present set up, accurate measurement of the output energy was not possible

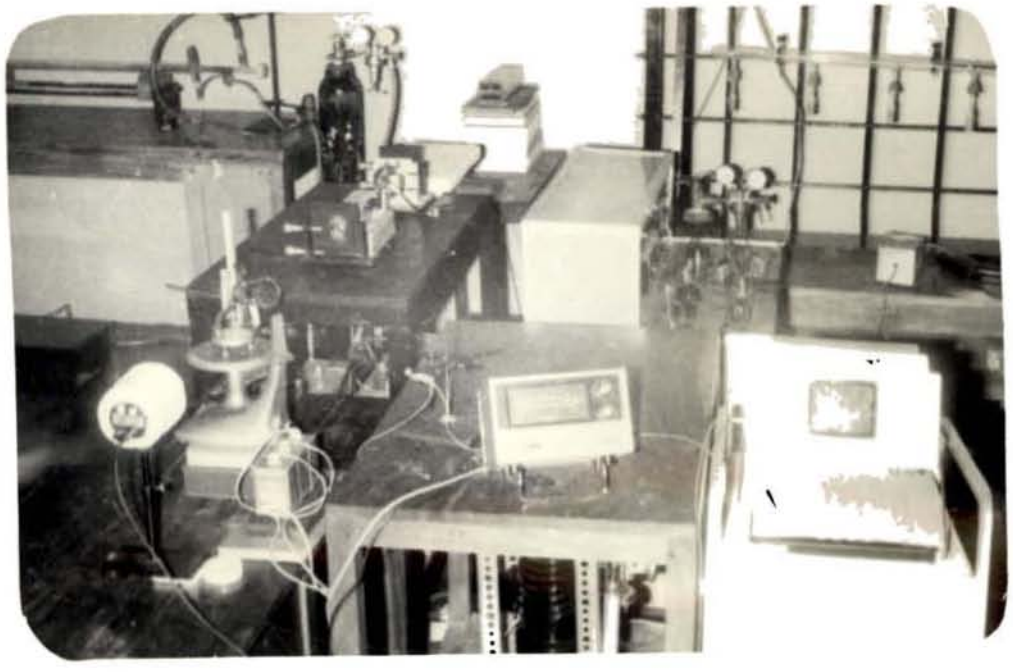

FIG. 7.3 EXPERIMENTAL SETUP FOR LASER - INDUCED DAMAGE THRESHOLD ENERGY MEASUREMENT

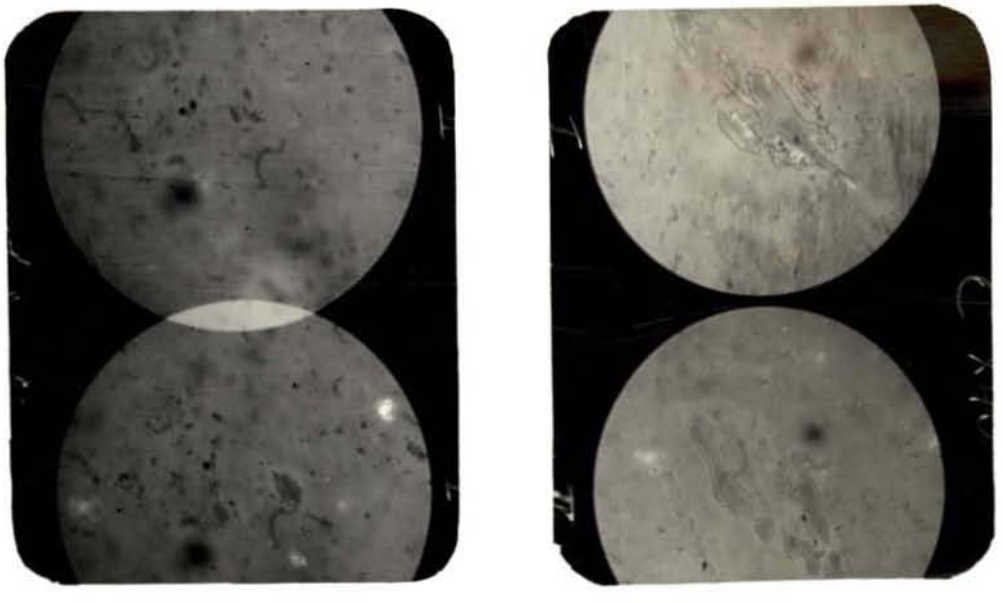

FIG. 7.4 DAMAGED SITES AT THRESHOLD (A) AND AT HIGHER ENERGY DENSITIES (B)

for every damage attempt. However, the energy verification was made before and after a set of damage tests.

Between successive test shots the thin film sample was pushed forward in the direction indicated by the arrow. This enables the next shot to impinge on a site to the left of the previous shot. It may be noted that as the film is pushed forward, it also moves toward the focus of the lens. This increases the incident power density on the sample. Thus as the film is pushed after every test shot, the energy density will slowly increase and the film will get damaged at a particular energy density known as the damage threshold. With subsequent test shots, due to further increase in energy density the sites will get heavily damaged and complete evaporation of the film occurs at the damaged site.

When the test run is complete, the damaged sites are observed on a metallurgical microscope (Carl Zeiss Jena EPY-Type: 2) and photographed. Typical photographs showing the damage sites at threshold damage and at higher densities are shown in Figs.7.4A and 7.4B. As the laser beam cross section can be assumed to be circular and as the half angle subtended at the lens focus is much less than the angle of incidence (56°), the damage sites will be elliptical in shape. By measuring the major and minor axis of the ellipse, the damaged area or the area on which the beam had impinged can be computed. Now, along with the knowledge of the pulse energy and the pulse width the threshold energy densities and the

threshold power densities can be estimated. The values obtained for the sample films tested are shown in Table 7.1.

As the thickness of the films used in the present study was arbitrary, neither 7.1 nor 7.2 could not be used to determine the threshold optical electric field with any good amount of accuracy. Still, as the film thickness was between $\lambda/8$ and $\lambda/4$, 7.2 was used to calculate the threshold fields and reasonably representable values were obtained.

7.5 RESULTS AND DISCUSSION.

Table 7.2 gives the values of the damage threshold energy, threshold field, refractive index, resistivity, absorptance, thickness and threshold power density of the films used in the present study. Also shown are the corresponding values obtained by Pawlewicz et al.[33] for conducting indium tin oxide coatings. It may be noted that the films used in the present study had higher absorptance values because of the film composition and the desposition technique being different. Moreover, the film thickness was also less. These factors can be taken to be responsible for the reduction in the threshold energy values. Another factor that may be noticed is that as the laser beam spot sizes on the film was quite large, there was an increased probability for hitting a defect and causing damage. Thus, for conducting films deposited using chemical and sputter deposition techniques, an exact comparison or correlation is practically impossible, because to the best of author's knowledge, similar damage studies have not

TABLE - 7.1

THRESHOLD ENERGY DETERMINATION.

Coating	Laser Energy E(mJ)	Damaged site dimensions		Microscope magnification M	Area of damaged site $A=\Pi ab/M(cm^2)$	Energy density at 56° angle of incidence $E/A(J/cm^2)$
		Semi minor axis b (cm)	Semi major axis a (cm)			
I	40	0.6	1.5	40	0.0706858	0.56588
II	38	0.5	1.1	40	0.0431969	0.87969

TABLE - 7.2

RESULTS OF THE PRESENT AND PREVIOUS WORK.

Film Parameters	Present Results		Previous Results (Pawlewicz et al.[33])	
	Coating I	Coating II	Coating A	Coating B
Resistivity[(a)] (Ω cm)	0.0188	0.0166	0.017	0.55
VIS/NIR absorptance (%)	10.42[(b)]	14.40[(b)]	≤ 1[(c)]	< 1[(c)]
Refractive index	1.7100[(b)]	1.8122[(b)]	1.75[(d)]	1.79[(d)]
Thickness(nm)	151.028	140.926	344.0	314.2
Damage threshod at normal incidence (J/cm^2)	1.01196	1.57315	5.5	5.5
Power density at threshold(W/cm^2)	6.746×10^7	10.488×10^7	3.1×10^9	3.1×10^9
Measured threshold field.[(e)] (MV/cm)	0.0185	0.1252	0.6920	0.6920
Laser pulse width (ns)	15	15	1.0	1.0
Deposition Technique	Chemical Vapour Deposition[(f)]		Sputter Deposition	
Film composition	$(Sn^{4+}_{1-2x} + Sn^{3+}_{2x})$ $(O^{2-}_2 - xO^{2-})$		$In_{1.9}\ Sn_{0.1}O_3$	
Film Substrate	borosilicate		fused silica	

(a) in-lane component

(b) Measured at 435.8 nm

(c) Measured spectrophotometrically

(d) Measured at 1064 nm

(e) Calculated using 7.2

(f) Films from Dr.Karekar, Poona University.

been attempted so far on sputter deposited films with longer duration (15-20 ns) pulses at 1062 nm.

The threshold field which is a function of the power density and the film refractive index was also calculated for the results reported by Pawlewicz et al.[33] The values obtained in the present experiment is in satisfactory agreement with the previous results, though the field calculation was done using 7.2 in both the cases. To place these threshold fields in perspective, the values obtained by Bettis et al.[25] for half wave dielectric films of Al_2O_3 (n = 1.754) on Saphire and SiO_2 (n = 1.449) on BK - 7 were 0.556 MV/cm and 1.05 MV/cm respectively.

If one can sacrifice the slight increase in the transmission losses while using chemical vapour deposited transparent conducting films, these simple to deposit, less expensive, films can replace RF sputter deposited films in large aperture Pockels cells maintaining the switching speeds and the threshold energy limits.

REFERENCES.

1. N. Bloembergen, Symposium on Laser - solid interactions and laser processing, AIP Conf. Proceedings, No.50, p.1-9 (1978).
2. W. Lee Smith, Opt. Engg., 17, 489 (1978)
3. G. Leppelmeir and M. Finkelstein, Lawrence Livermore Lab. Laser Program Annual Report, UCRL - 50021 - 74, p.162 - 166
4. D. Milam, Lawrence Livermore Lab. Laser Program Annual Report, UCRL - 50021 - 75, p.214 - 218.

5. W.L. Smith et al., Lawrence Livermore Lab. Laser Program Annual Report, UCRL - 50021 - 76, p.278-282.

6. W.H. Lowdermilk et al., Lawrence Livermore Lab. Laser Program Annual Report, UCRL - 50021 - 77, p.197-205.

7. W.H. Lowdermilk et al., Lawrence Livermore Lab. Laser Program Annual Report, UCRL - 50021 - 78, p.88-98.

8. D. Milam, Appl. Opt., 16, 1204 (1977)

9. R.A. House et al., Laser-induced damage to optical materials, NBS Special Publication No.435, p.305-320 (1975)

10. J.R. Bettis, Laser-induced damage as a function of dielectric properties at 1.06 μm Ph.D Dissertation, Report AFWL-TR - 76-61, Kirtland AFB, New Mexico 87117.

11. R.A. House, The effect of surface structural properties on laser-induced damage at 1.06 μm., Ph.D Dissertation, Air Force Institute of Technol., Wright Patterson AFB, Ohio, 1975 (AFWL - TR - 76-62 Report, Kirtland AFB, NM - 877117).

12. J.R. Bettis et al., Proc. of 8th Annual symp. on Optical Materials for High Power lasers (1976) p.338-345.

13. D. Milam, Proc. of Soc. Photo Opt. Instrum. Engineers, 140, Opt. Coatings II (1978)

14. M.D. Crisp, Am. Sci., 65, 435 (1977)

15. R.A. House et al., IEEE J. Quantum Electron., QE-13, 361 (1977).

16. W. Melle and H.Endert, Opt. Commun., 27, 403 (1978)

17. S.S.C. Babu, IEEE J.Quantum Electron., 15, 533 (1979)

18. R.A. House II et al., Appl. Opt., 16, 1130 (1977)

19. M.D. Crisp, et al., Appl. Phys. Letts., 21, 364 (1972).

20. L.G. De Shazer, et al., Study of laser-irradiated thin films, University of Southern California (1973)

21. B.E. Newman and L.G. De Shazer, NBS Special publication 372, p.123 (1972)

22. A.F. Turner, NBS Publication 356 p.119 (1971).

23. R.R. Austin et al., NBS Publication 372, p.135 (1972).

24. N.L. Boling et al., NBS Publication 387, p.69 (1973).

25. J.R. Bettis, et al., Opt. Letts., 4, 256 (1979)

26. N. Bloembergen, Appl Opt., 12, 661 (1973).

27. L.G. De Shazer et al., Appl. Phys. Letts., 23, 607 (1973).

28. E.S. Bliss, et al., Appl. Opt., 12, 677 (1973).

29. R.R. Austin and A.H. Guenther, Appl. Opt., 11, 695 (1972).

30. O.S. Heavens, Thin Solid Films, 50, 157 (1978)

31. R.M. Wood, et al., Optics and Laser Technol., 105 (1975)

32. L.L. Steinmetz, et al., Appl. Opt., 12, 1468 (1973).

33. W.T. Pawlewicz, et al., Appl. Phys. Letts., 34, 196 (1979)

34. G. Haacke, et al., J.Electrochem. Soc., 124, 1923 (1977)

35. E. Ritter, Progress in Electro-Optics, Ezio Camatini (Ed) Plenum Press, New York, 1975.

36. A.M. Fegade and R.N. Karekar, Private communication.

37. R.M.A. Azzam and N.M. Bashara, Ellipsometry and polarised light, North Holland Pub. Co. (1977).

38. N.L. Boling and G. Dube, Damage threshold studies of Glass laser Materials, Owens-Illinois Technical Report (1974).

CHAPTER VIII

CONCLUSIONS.

Taking into consideration the various fabrication and design aspects, a transversely excited portable Nitrogen laser was built. This laser was operated at 337.1 nm, from a few to 50 pulses/sec. with a maximum efficiency of 0.12 %. The maximum output peak power obtained with the present system was 250 kW in 5 ns pulses. The reliability of the laser system was checked by operating it continuously for six hours at 25 pulses/sec. without any observable failure. It may also be noted that the entire system is in good shape without any appreciable degradation in efficiency after having completed more than three years of regular use. With approximately two to three hours of operation per day this amounts to more than 3000 hours of working.

A detailed study of the electrical and optical characteristics of the Nitrogen laser was made. Different configurations of the discharge circuit (Blumlein type) were tested and their electrical characteristics analysed to arrive at a configuration that gives the maximum efficiency. A non-Blumlein type transmission line circuit was found to give maximum output peak power for a fixed line length.

Analysis was made of the Nitrogen laser emission spectra using a 0.5 meter Jarrel Ash monochromator. The output of the Nitrogen laser though assumed to be monochromatic was found to contain various other emission bands of lesser intensity.

Other than the main 337.1 nm band, the laser output was found to contain 331.83 nm, 340.85 nm, 357.69 nm,303.49 nm, 371.05 nm and 315.93 nm bands with relative intensities within a few to about 29 % of the main band. The intensity variation of these bands with pressure and voltage was studied for deriving the optimum conditions for intensity enhancement at these wavelengths. Most of the bands were identified to those belonging to the second positive system of the nitrogen molecule and to the β system of the NO molecule. The transition at 331.83 nm, observed degraded to red could not be identified with the CN (6,4) band belonging to the $B^2\Sigma - X^2\Sigma$ violet system and the N_2 (0,5) Goldstein Kaplan band of the $C' {}^3\Pi_u - B^3\Pi_g$ system that have frequencies in the near vicinity. It is presumed that this spurious band could be a new transition arising out of rotational vibrational levels between which normal transitions with large intensities have not been reported so far. The present observation of laser action in bands other than the 337.1 nm, 355.7 nm and 315.9 nm bands have not been reported earlier in Nitrogen laser discharges.

A versatile laser system built around a 152.4 mm x 6 mm Nd: Glass laser rod was operated at 1062 nm in the conventional pulsed, Electro-Optically Q-switched and Dye Q-switched modes. The electrical, mechanical and optical sub-systems were fully designed and fabricated. Parameters like the pumping coefficient, resonator loss and gain coefficient were evaluated and the lasing characteristics analysed with the laser rod being pumped in an

elliptical and a close-coupled double circular pumping chamber. For an input energy of 450 Joules into the two 6F6G flashlamps, a 2.2 Joule pulse of 400 μs duration at FWHM was emitted in the pulsed mode with a slope efficiency of 0.649 %. In the E-O Q-switched mode, for an input energy of 648 Joules an output pulse of 110 mJ in 15 ns at FWHM was obtained. When the single flashlamp pumped system was Q-switched using Eastman Kodak 9860 Dye Solution, the output energy was 135 mJ in 100 ns at FWHM for an input energy of 272 Joules. The slope efficiencies in the E-O Q-switched and Dye Q-switched modes were 0.034 % and 0.125 % respectively.

Thermal effects in a Nd: doped silicate glass laser rod (LSG 91H) were studied in a close-coupled double circular pumping chamber by passing a probe beam through the rod and observing the changes in the beam profile due to pumping. The thermal relaxation time when operated in the single shot mode was found to be 2 to 2.5 seconds when the input energy into the system was 100 Joules. The thermal lensing behaviour in the repetitively pulsed mode was also studied and analysed. The observed broadening of the probe beam profile with reduction in peak intensity value was attributed to a negative lens effect. In addition to this lensing behaviour a prism effect was also observed where the intensity position shifted laterally with increase in input energy. Lasing tests conducted could prove that this prism effect was due to the uneven distribution of energy into the two flashlamps when the capacitor bank discharged.

With the E-O Q-switched Glass laser operated in the multi-mode structure, the damage threshold of transparent conducting $Sn\ O_2$ films prepared by Chemical Vapour Deposition technique were studied using 15 ns pulses at 1062 nm. The optical electric field associated with the laser-induced damage was also computed. For a film of 140.926 nm thickness, the damage threshold was 1.5 J/cm^2 and the equivalent electric field was 0.1252 MV/cm. These films find application in large aperture Pockels cells and other E-O modulators used for pulse shaping and gating purposes in high power laser amplifiers.

APPENDIX-A

COMPUTER PROGRAM FOR THE DETERMINATION OF ROD FOCAL LENGTH.

```
* FORTRAN
* FORTRAN STARTED *
      PROGRAM CUPH05
      DIMENSION ALPHA (100) ,BETA(100),GAMA(100),DELTA(100),W(100)
      READ(7,10)(W(I),I=1,3)
10    FORMAT (3F5.3)
      I=0
111   I=I+1
      IF (I.EQ.4) GO TO 999
      A=(4.0*0.6328*0.6328*1.0E-08)/(3.141593*3.141593*0.6*0.6)
      B=0.6*0.6*(1.0-15.917/(49.0-15.917))-W(I)*W(I)
      C=-2.0*0.6*B*(80.5+15.917*49.0/(49.0-15.917))
      D=0.6*0.6*(80.5+15.917*49.0/(49.0-15.917))
      ALPHA (1)=0
      BETA(1)=(B/A)*1.0E-04
      GAMA (1)=(C/A)*1.0E-06
      DELTA(1)=(D/A)*1.0E-08
      DO 20 K=1,4
      ALPHA(K+1)=ALPHA(K)*ALPHA(K)-2*BETA(K)
      BETA(K+1)=BETA(K)*BETA(K)-2*ALPHA(K)*GAMA(K)+2*DELTA(K)
      GAMA(K+1)=GAMA(K)*GAMA(K)-2*BETA(K)*DELTA(K)
```

```
      DELTA(K+1)=DELTA(K)*DELTA(K)
20    CONTINUE
      P=ALPHA(5)-ALPHA(4)*ALPHA(4)
      Q=BETA(5)-BETA(4)*BETA(4)
      R=GAMA(5)-GAMA(4)*GAMA(4)
      IF(P.NE.1.0E-5) GO TO 40
      IF(Q.NE.1.0E-5) GO TO 50
      IF(R.NE.1.0E-5) GO TO 60
      X1=ALPHA(5)
      X2=BETA(5)/ALPHA(5)
      X3=GAMA(5)/BETA(5)
      X4=DELTA(5)/GAMA(5)
      R1=X1**0.0625
      R2=X2**0.0625
      R3=X3**0.0625
      R4=X4**0.0625
      GO TO 70
40    X1=BETA(5)
      X2=GAMA(5)/BETA(5)
      X3=DELTA(5)/GAMA(5)
      R1=X1**0.03125
      R2=R1
      R3=X2**0.0625
      R4=X3**0.0625
      GO TO 70
```

```
50    X1=ALPHA(5)
      X2=GAMA(5)/ALPHA(5)
      X3=DELTA(5)/GAMA(5)
      R1=X1**0.0625
      R2=X2**0.03125
      R3=R2
      R4=X3**0.0625
      GO TO 70
60    X1=ALPHA(5)
      X2=BETA(5)/ALPHA(5)
      X3=DELTA(5)/GAMA(5)
      R1=X1**0.0625
      R2=X2**0.0625
      R3=X3**0.03125
      R4=R3
70    FUN1=R1*R1*R1*R1+BETA(1)*R1*R1+GAMA(1)*R1+DELTA(1)
      FUN2=R2*R2*R2*R2+BETA(1)*R2*R2+GAMA(1)*R2+DELTA(1)
      FUN3=R3*R3*R3*R3+BETA(1)*R3*R3+GAMA(1)*R3+DELTA(1)
      FUN4=R4*R4*R4*R4+BETA(1)*R4*R4+GAMA(1)*R4+DELTA(1)
      FR1=0.49*R1*(0.49-0.15917)/((0.49-R1)*0.49)
      FR2=0.49*R2*(0.49-0.15917)/((0.49-R2)*0.49)
      FR3=0.49*R3*(0.49-0.15917)/((0.49-R3)*0.49)
      FR4=0.49*R4*(0.49-0.15917)/((0.49-R4)*0.49)
      WRITE(8,80)ALPHA(K),BETA(K),GAMA(K),DELTA(K),W(I)
```

```
30    FORMAT (10X,E15.5,10X,E15.5,10X,E15.5,10X,E15.5,10X,F10.5)
      WRITE(8,81)R1,R2,R3,R4
81    FORMAT(10X,F10.5,10X,F10.5,10X,F10.5,10X,F10.5)
      WRITE(8,82)FUN1,FUN2,FUN3,FUN4
82    FORMAT(10X,F10.5,10X,F10.5,10X,F10.5,10X,F10.5)
      WRITE(8,83)FR1,FR2,FR3,FR4
83    FORMAT(10X,F10.5,10X,F10.5,10X,F10.5,10X,F10.5)
      GO TO 111
999   STOP
      END
```

APPENDIX - B.

COMPUTER PROGRAM FOR THE DETERMINATION OF W_D IN THE SINGLE SHOT MODE.

```
* FORTRAN
* FORTRAN STARTED *
      PROGRAM CUPHO5
      DIMENSION P (10,60),X(20),Q(10,60)
      READ(7,100)(X(I),I=1,10)
100   FORMAT(10F5.3)
      WRITE(8,701(X(J),J=1,10)
701   FORMAT(4X,10F7.3)
      READ(7,110),((Q(I,J), (J=1,51),I=1,10)
110   FORMAT(16F5.1)
      WRITE(8,702)((Q(J,K),K=1,51),J=1,10)
702   FORMAT (4X,16F7.1)
      AL= -0.01
      AH= +0.01
      I = 1
120   K = I+1
130   J = 1
      TIME = 0.0
135   P(I,J)=Q(I,J)
      P(K,J)=Q(K,J)
      IF(ABS(P(K,J)).LT.1.0E-5)GO TO 190
      XD=ABS(X(I)-X(K))
```

```
170   WRITE(8,180)P(I,J),P(K,J),XD,TIME,I,J,K
180   FORMAT(10X,F6.2,10X,F6.2,10X,F6.4,10X,F4.2,3I4)
      IF(P(I,J).LT.1.0E-5 AND.P(K,J).LT.1.0E-5)GO TO 136
      IF(P(K,J).LT.1.0E-5) GO TO 137
      GO TO 139
136   P(I,J)=ABS(P(I,J))
      P(K,J)=ABS(P(K,J))
      GO TO 139
137   XD= -XD
      TEMP=P(I,J)
      P(I,J)=P(K,J)
      P(K,J)=TEMP
139   W=5.0
140   W=W-0.02
      IF(ABS(W).LT.0.01)GO TO 190
      ATRAF=4.294/W*(2.718 2818**(-(((1.4572187/(W*P(K,J)))**0.5
      -XD/W)**2))
      IF(ATRAF.LT.1.0E-10) GO TO 190
      TRAF=ATRAF-P(I,J)
      IF(TRAF.LT.AH.AND.TRAF.GT.AL) GO TO 150
      IF(W.GT.0.01) GO TO 140
      GO TO 190
150   WRITE(8,160)W,TRAF
160   FORMAT(15X,F5.3,10X,E15.5)
      IF(W.LE.0.01) GO TO 190
```

```
190   J=J+1
      TIME =TIME+0.04
      IF(J.LE.51) GO TO 135
      K=K+1
      IF(K.LE.5) GO TO 130
      IF(K.GE.8.AND.K.LE.10) GO TO 130
      I=I+1
      IF (I.LE.4) GO TO 120
      IF(I.EQ.5) I=6
      IF(I.LE.9) GO TO 120
      STOP
      END
```